CHEMICAL DURABILITY OF MULTICOMPONENT SILICATE GLASSES

By

MORRIS FRANKLIN DILMORE

A DISSERTATION PRESENTED TO THE GRADUATE SCHOOL
OF THE UNIVERSITY OF FLORIDA
IN PARTIAL FULFILLMENT OF THE REQUIREMENTS FOR THE
DEGREE OF DOCTOR OF PHILOSOPHY

UNIVERSITY OF FLORIDA

1977

Dedicated to the fond and enduring memories of my mother and father, Rena Mae and Charlie Clarrie Dilmore (both deceased), and especially to my kind, loving and understanding wife, Katrina Yvonne Goodwin Dilmore, forever!

ACKNOWLEDGMENTS

The author wishes to express appreciation to his committee members and especially to his extremely capable committee chairman, Dr. Larry L. Hench. He also wishes to thank John T. Healey, Edwin C. Ethridge, Carlo G. Pantano, and special thanks to David E. Clark for their particular assistance in data interpretation and preparation.

In addition, thanks are extended to Helen Brasfield, Helen Heverling, and Carl Miles for their solution analysis testing and kind patience over the past three years. Also, special thanks are due to Mrs. Vicki Turner and Miss Alice Holt for their typing of the dissertation.

TABLE OF CONTENTS

Table of Contents - continued.

Table of Contents - continued.

LIST OF TABLES

LIST OF FIGURES

List of Figures - continued.

List of Figures - continued.

List of Figures - continued.

List of Figures - continued.

List of Figures - continued.

List of Figures - continued.

List of Figures - continued.

List of Figures - continued.

List of Figures - continued.

Abstract of Dissertation Presented to the Graduate Council of the University of Florida in Partial Fulfillment of the Requirements for the Degree of Doctor of Philosophy

CHEMICAL DURABILITY OF MULTICOMPONENT SILICATE GLASSES

By

Morris Franklin Dilmore

March, 1977

Chairman: Larry L. Hench
Department: Materials Science and Engineering

The very nature of commercial glass compositions, i.e., in excess of six components, complicates the investigation of their corrosion behavior. As with many industrial products, glass formulations have been developed and altered over a longer period of time in order to achieve optimal properties for various applications.

The importance of various common corrosion parameters such as time and temperature has been discussed in the literature for numerous glass systems. However, in this investigation well defined glass systems are used to illustrate all of the important parameters that affect glass corrosion. These include time, temperature composition, pH, SA,V, and soluble ion inhibitors.

Although the importance of the corrosion behavior for commercial glass compositions is known in practice, the basic principles governing the corrosion processes are not well understood. For instance, K_2O silicate glasses corrode at a much faster rate than Na_2O silicate glasses. However, commercial glasses with certain ratios of Na_2O/K_2O exhibit a corrosion rate that is much less than that for Na_2O silicate glasses. This is commonly referred to as the mixed alkali effect.

Of even greater importance, is the presence of small percentages of alumina in commercial glasses. Most commercial glass container compositions are composed of 14%-17% Na_2O, 10% CaO, and the remainder of SiO_2. By replacing some of the SiO_2 with as little as 2% Al_2O_3 in the glass, the corrosion rate can be significantly decreased. Furthermore, the presence of soluble Al^{+3} ions in the corrosion solution itself improves the corrosion resistance of the glass.

Simple two, three, and four component glass systems were used to study details of these effects of mixed alkali and alumina on glass corrosion reactions. Corrosion solution evaluation in conjunction with recently developed dissolution equations was employed as the

standard evaluation technique. However when required, more sophisticated surface analytical tools such as AES, IRRS, and SEM were used to compliment the corrosion solution results.

The Mixed-Alkali Effect (MAE) has been evaluated for both powder and bulk glasses. It has been established that the magnitude of the MAE is dependent upon the pH of the corrosion solution. In addition the pH has been observed to be a function of corrosion time and temperature, glass composition and the ratio of glass surface area (SA) to corrosion solution volume (V). For pH $\leq$ 9, the MAE is present, but for pH > 9, the MAE diminishes.

The effects of Al_2O_3 additions to binary lithia-silicate glasses on corrosion behavior has been investigated. The first 2.5 mole % Al_2O_3 addition has the greatest effect on increasing durability of Li_2O-Al_2O_3-SiO_2 glasses. Larger Al_2O_3 additions also increase durability but to a lesser extent than the first 2.5%.

The effect of pH on glass durability does not appear to be as important for glasses containing alumina as it is for the binary lithia-silicate glasses. This is thought to occur because of the formation of an alumina-silicate rich surface film that is resistant to corrosion solutions of high pH.

The effects of soluble aluminum ions on the corrosion behavior of a binary lithia-disilicate glass have been investigated. In general, the presence of Al^{+3} in the corrosion solution decreases the total dissolution process but has relatively little effect on the selective leaching processes. This data suggest that the increase in chemical durability is a result of surface passivation by the presence of alumina-silicate sites as opposed to the formation of a thick surface film acting as a physical barrier to alkali diffusion.

In the appendix, the effects of various SO_2 treatments on glass durability have been investigated. The increase in durability of the SO_2 treated surfaces has been attributed to the dealkalization of the glass surface, and the resultant formation of a high silica surface film.

CHAPTER I
INTRODUCTION

Glass is among the most chemically resistant of common materials,[1] and for that reason it has found wide use as food, beverage, and pharmaceutical containers, windows, light bulbs, and scientific apparatus. It is the high resistance to corrosion that has led a number of authors to assume that glasses do not react at all with their environments and thus they can be described as inert materials.[2] This ever increasing use of glass in modern society has resulted in a significant surge in research and development of glass durability.

The phrase "Chemical Durability" as used in this dissertation refers to the ability of glasses to resist partial or total reaction with aqueous and atmospheric environments. A glass of high durability reacts only slightly, if at all, with its environment, while glasses of low durability react very readily. This reactivity results in the formation of dissolution products as surface films and the occurrence of general surface deterioration as evidenced by a decrease in glass transparency.

The reactions associated with glass corrosion processes are very complex in nature and therefore are often difficult to identify and explain. They are influenced by a large number of possible external variables, sample environmental conditions, and sample states which must be considered in any investigation of glass durability (listed in Table I). Also inhibiting the explanation of glass durability is the wide range of experimental methods and theoretical analyses that have been utilized in earlier studies to discuss the reactions that occur.

Reviews by Bacon,[1] Holland,[2] Weyl,[3] Das,[4] Doremus,[5] Volf[6] and Morey[7] describe the various experimental techniques utilized and corrosion parameters investigated over the past 75 years. These reviews show that, in general, each individual investigation was approached from a different standpoint and yielded results specific to a particular problem. Each investigative team generally used different experimental methods, analysis techniques and presentations, and studied different corrosion parameters.

The objective of the present work was to make the first comprehensive systematic study of a group of glasses

Table I

Factors Affecting Glass Durability

I. External Variable Conditions

1. Temperature
2. Time
3. Pressure
4. Prior surface treatments, i.e., SO_2, $SnCl_4$, etc.

II. Sample Environmental Conditions

1. Aqueous environment
2. Relative humidity environment
3. Buffered corrosion solutions
4. Soluble ion corrosion solutions
5. pH of the initial corrosion solution
6. Static solution environment
7. Dynamic solution environment
8. Replenishing solution environment

III. Sample State Condition

1. Glass composition
2. Phase separation
3. Crystallization
4. Inherent heterogeneities occurring from the glass melt
5. Surface roughness
6. Glass surface area to corrosion solution volume, SA/V ratio
7. Extent of prior corrosion
8. Stresses present in the glass sample from the forming process
9. Stresses present in the glass sample from external forces
10. Powder glass surfaces
11. Bulk glass surfaces

with simple yet closely related compositions while carefully controlling the essential experimental variables. A variety of experimental techniques were used to facilitate cross comparisons of the results. The investigations undertaken were the following: (i) verification of the experimental techniques associated with the major parameters affecting glass corrosion and their interactions has been obtained in several standard glass systems. Strong emphasis was placed on standardization of experimental methods, analysis techniques and analysis presentations in an effort to understand and interrelate the many parameters observed in glass corrosion. This work is described in the Appendix. (ii) The Mixed-Alkali Effect (MAE) has been evaluated for both powder and bulk glasses. The relative role of structural and corrosion solution ion effects in the MAE has been determined. (iii) The effect of Al_2O_3 additions on the corrosion of binary lithia-silicate glasses has been investigated. Strong emphasis was placed upon the effect of various mole % Al_2O_3 additions to a binary lithia-silicate glass and the subsequent effect on chemical durability. (iv) The effect of soluble aluminum ions on the corrosion behavior of a binary lithia-disilicate glass has been determined by adding various concentrations of $AlCl_3$ to the corrosion solution.

Glass Durability Overview

Although glass durability is a complex phenomenon, generalized reactions and equations have been developed that are applicable or adaptable to most glasses.

Glass corrosion processes may be generalized by the following two reactions:[8-12] Stage I reaction - selective leaching due to ion-exchange, pH $\leq$ 9. This reaction is characterized by H^+ ions in the corrosion solution ion-exchanging for alkali ions in the glass structure thereby releasing the alkali ions into the solution by the following reaction:

Stage I reaction, selective leaching (ion exchange), pH $\leq$ 9.

$$\begin{array}{c} | \\ -Si-O-R \\ | \end{array} + H_2O \rightarrow \begin{array}{c} | \\ -Si-OH \\ | \end{array} + R^+ + OH^- \quad (1)$$

The stage II reaction with total dissolution on pH > 9 is characterized by the OH^- ion attack of the Si-O-Si network, thereby leading to total glass structural breakdown as shown by the following reactions:

$$\begin{array}{c} | \\ -Si-O- \\ | \end{array} \begin{array}{c} | \\ -Si- \\ | \end{array} + OH^- \rightarrow \begin{array}{c} | \\ -Si-OH \\ | \end{array} + \begin{array}{c} | \\ -Si-O^- \\ | \end{array} \quad (2)$$

$$\begin{array}{c} | \\ -Si-O^- \\ | \end{array} + H^+ \rightarrow \begin{array}{c} | \\ -Si-OH \\ | \end{array} \quad (3)$$

Douglas and El-Shamy[11] have developed an equation for describing the kinetics of both the selective leaching (ion-exchange) mechanism (pH $\leq$ 9) and the total dissolution mechanism (pH > 9) for constant temperatures.

$$Q = K \cdot t^{\gamma} \tag{4}$$

where: Q = quantity of alkali ions removed from the glass

t = time of the corrosion experiment

K = reaction rate constant assuming a constant glass surface area

γ = 1/2 for the selective leaching (ion-exchange) reaction

γ = 1 for the total dissolution reaction

A dissolution parameter, α,[12-14] is very useful for investigating the relative leaching/ion-exchange and total dissolution discussed in the previous paragraphs. A generalized equation is shown below for any two to four component glasses; different species may be included or excluded where applicable.

$$\alpha = \frac{\frac{\text{ppm Si}}{\text{AW Si}}}{\frac{\text{ppm Li}}{2\text{AW Li}} + \frac{\text{ppm Na}}{2\text{AW Na}} + \frac{\text{ppm K}}{2\text{AW K}} + \frac{\text{ppm Ca}}{\text{AW Ca}} + \frac{\text{ppm Al}}{2\text{AW Al}}} \times \frac{1 - P_{SiO_2}}{P_{SiO_2}} \tag{5}$$

$PSiO_2$ = mole fraction of SiO_2 in glass composition

AW = atomic weight

ppm Si = concentration of Si in the corrosion solution

ppm Li = concentration of Li in the corrosion solution

ppm Na = concentration of Na in the corrosion solution

ppm K = concentration of K in the corrosion solution

ppm Ca = concentration of Ca in the corrosion solution

ppm Al = concentration of Al in the corrosion solution

For $\alpha = 0$ (pH $\leq$ 9), selective leaching due to ion-exchange is the dominant corrosion mechanism; when $\alpha = 1$ (pH > 9), total dissolution is the dominant corrosion mechanism.

Experimental Procedure Techniques

I. Bulk Corrosion - The schematic experimental arrangement for bulk corrosion is shown in Figure 1. The corrosion cell was made from a 1 in^3 Teflon(R) cube with a 3/8" diameter, 3/8" deep cavity for containment of the corrosion solution, yielding a glass surface area to corrosion solution volume (SA/V) ratio of 0.77 cm^{-1}. Various bulk samples were polished with 120-600 grit SiC paper and attached to the corrosion cells for various times and temperatures (±1°C).

(R) E. I. du Pont de Nemours & Co., Inc., Wilmington, Del.

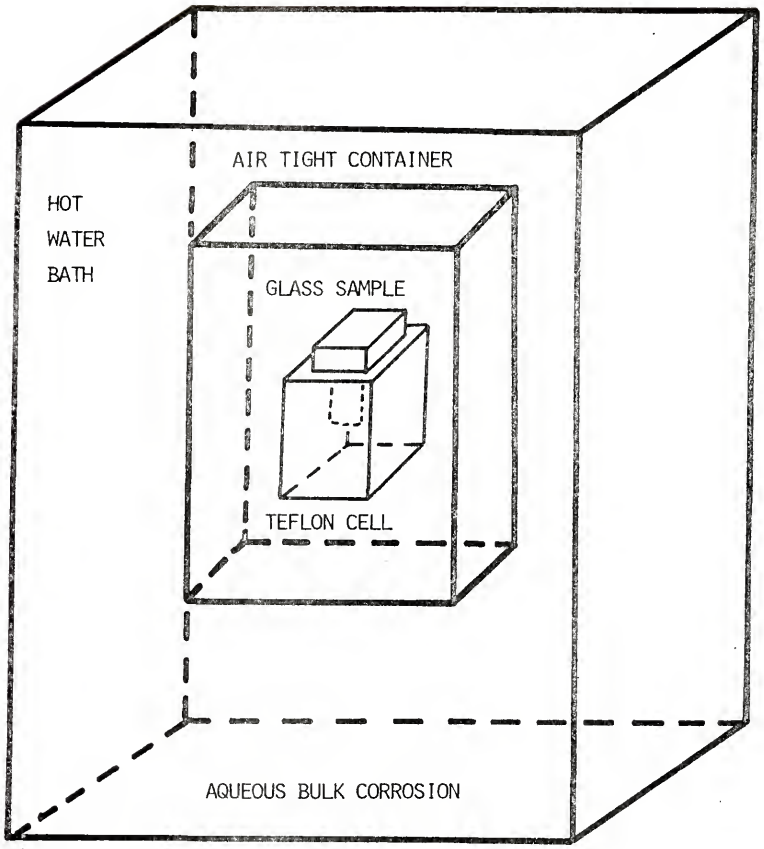

Figure 1. Schematic of the bulk experimental arrangement for aqueous corrosion.

II. Powder Corrosion - The schematic experimental setups for studying powders is shown in Figure 2. Glass powders were produced by pulverizing bulk glasses with an alumina mortar and pestle. The powders were then placed through appropriate sieve screens to yield the desired particle size ranges.

From these particle size ranges, specific surface area (SA) to volume of solution (V) ratios were maintained by adding certain weights of glass particles to known volumes of corrosion solutions in polyethylene containers. For corrosion testing, the containers were placed in a hot water bath for various times and temperatures (±1°C).

III. Relative Humidity Weathering - The schematic arrangement for weathering is shown in Figure 3. Bulk surfaces were polished with 600 grit SiC paper and placed in the relative humidity weathering environment for various corrosion times at 25°C (±1°C).

Compositional Analysis

Solution Analysis

Atomic emission* and absorption** spectroscopy were utilized to determine the lithium, sodium, potassium and

*Beckman B. Spectrometer, Beckman Instruments, Inc., Fullerton, California
**Perkin-Elmer 303 Spectrometer, Perkin-Elmer Corp., Norwalk, Connecticut

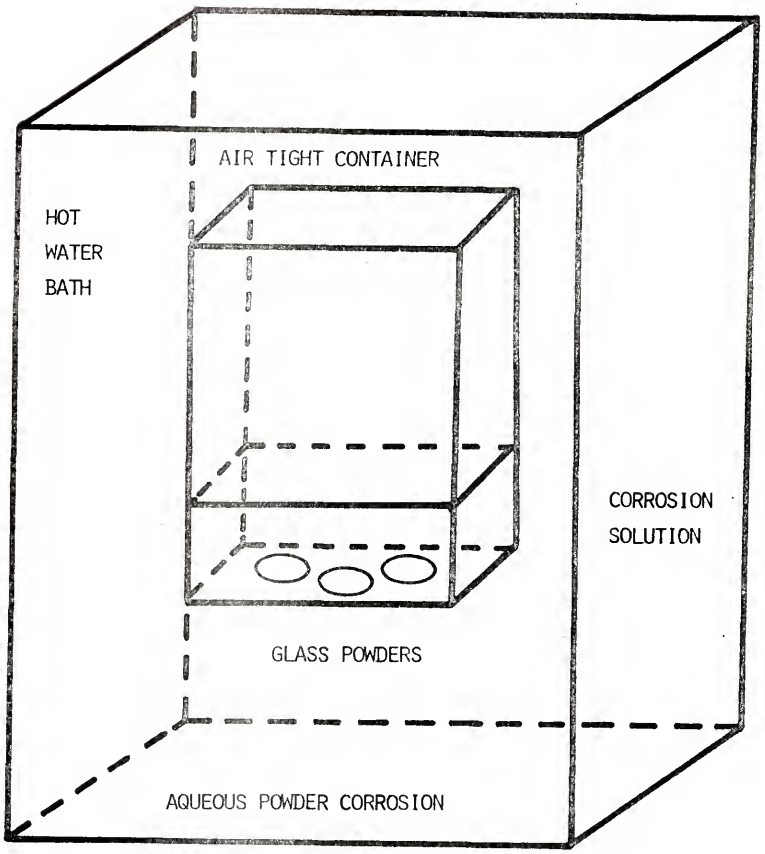

Figure 2. Schematic of the powder experimental arrangement for aqueous corrosion.

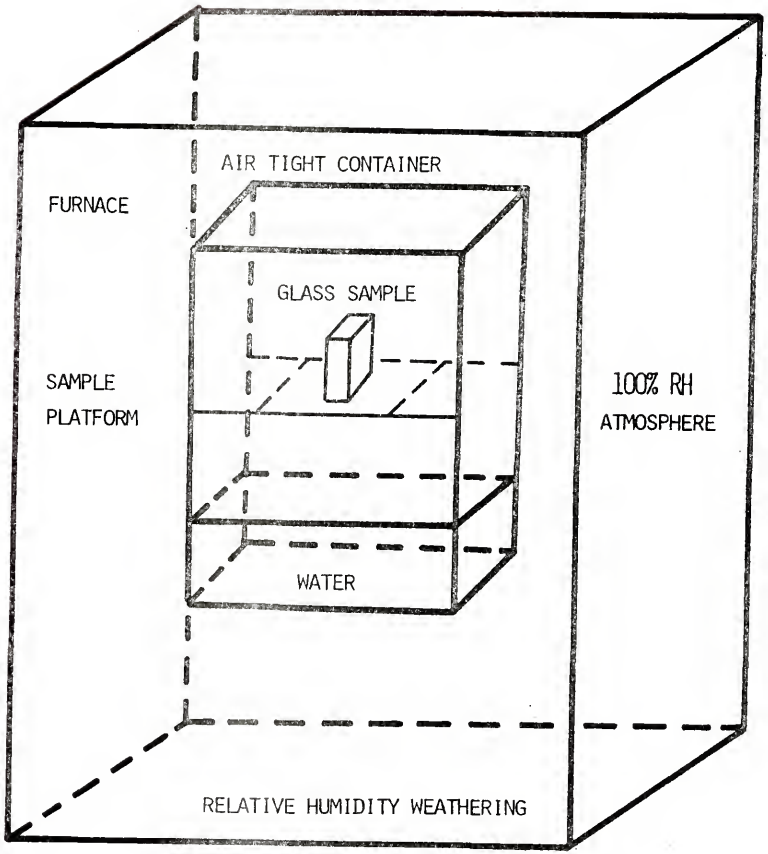

Figure 3. Schematic of the bulk experimental arrangement for 100% relative humidity weathering.

calcium, silicon, zinc, copper and aluminum concentrations in the corrosion solution.

In some instances, the silicon concentration was determined by the molybdenum blue colorimetric method.*

Also, the pH of the corrosion solution is a very important parameter for characterizing the extent of corrosion. Indicator paper** was used to check the pH of these solutions.

The resolution of the various solution analysis techniques described above are shown in Table III.

Surface Analysis

Infrared reflection spectroscopy (IRRS)*** is an invaluable tool for investigating structural and chemical changes occurring in glass surfaces exposed to either aqueous or relative humidity environments. The IRRS methods and procedures employed in this investigation were established by Sanders.[15]

Auger electron spectroscopy (AES)**** is one of the newest methods used in investigating glass corrosion. Since

*Hach "Direct Reading" Colorimeter, Hach Chemical Co., Ames, Iowa.
**Gallard-Schlesinger Chemical Mfg. Corp., Carle Place, New York.
***Perkin-Elmer 467 IRRS, Perkin-Elmer Corp., Norwalk, Connecticut.
****Physical Electronics Ind., Model 10-150 Spectrometer, Edina, Minn.

Table II

Resolution of Solution Analysis Parameters

	Method	Solution Parameter	Resolution
1.	Colorimetric Spectroscopy	Si^{+4}	±0.05 ppm
2.	Atomic Emission Spectroscopy	Li^{+}	±0.02 ppm
3.	Atomic Absorption Spectroscopy	Si^{+4}	±1.6 ppm
4.	Atomic Absorption Spectroscopy	Al^{+3}	±0.8 ppm
5.	(a) pH paper 2.5-4.0 range	pH	±0.10 ppm
	(b) pH paper 4.0-7.0 range	pH	±0.15 ppm
	(c) pH paper 6.5-10.0 range	pH	±0.10 ppm
	(d) pH paper 7.5-14.0 range	pH	±0.25 ppm
	(e) pH paper 11.0-13.0 range	pH	±0.15 ppm

AES can only yield information concerning the surface (5-10 Å), this can lead to analysis limitations. This analytical limitation has been solved through the combined use of AES and ion-beam milling processes. By utilizing both AES and ion-beam milling methods, depth reaction profiles may be established for corroded glass specimens under investigation. The AES methods and procedures employed in this investigation were established by Pantano.[16]

In addition to the surface analysis methods discussed above, scanning electron microscopy (SEM)* of corroded and uncorroded glass surfaces was performed to evaluate changes in surface topography. The SEM methods and procedures employed in this investigation were performed in accordance with standardized techniques developed over the years.

Solution analysis allows a determination of whether the glass surface is undergoing selective leaching or total dissolution. The corrosion results observed from

*Cambridge Stereoscan, Kent Cambridge Scientific, Inc., Morton Grove, Ill.

solution analysis may be verified by the use of infrared reflection spectroscopy (IRRS). From the IRRS spectra, if the glass surface has experienced only selective leaching, the alkali peak (silicon-nonbridging oxygen peak, NSL) will be greatly reduced, if present at all, and the Si-O-Si stretch peak intensity will be substantially increased over the freshly abraded glass surface. If total dissolution is the primary process, the overall IRRS spectra will be similar to that observed for the freshly abraded surface but the spectral intensity will be decreased moderately due to surface roughness. Because of the large sampling depth of the IRRS beam, 0.5 μm, information concerning the outer surface (0-20 Å) and the near surface (20-2000 Å) will not be apparent.

By using Auger electron spectroscopy (AES) with the previous techniques, fine surface and near surface chemical detail can be obtained. Greater analysis depths may be obtained by using ion-milling techniques with the AES technique, thereby giving a detailed chemical analysis profile for the corroded glass surface. Finally, although the SEM yields no direct chemical analysis in the emissive mode, visual observations of the corrosion processes at

the surface can be made, i.e., the surface film formation, crystal formation and growth, and surface roughening which is necessary to confirm the mechanisms occurring.

Thus, in combination, the above analytical methods provide a powerful procedure for studying glass durability giving considerably more information than any one method used alone.

CHAPTER II
AQUEOUS CORROSION OF MIXED-ALKALI SILICATE AND MIXED-ALKALI LIME SILICATE GLASSES

Introduction

The chemical durability of mixed-alkali oxide glasses has been reported to be superior to that of similar single oxide glasses.[17-22] Previous investigators have suggested that this Mixed-Alkali Effect (MAE) is due entirely to the structural modifications in the glass resulting in decreased alkali mobility. There are several theories on how the structure is modified when there are mixed-alkalis present in the glass. (a) According to Weyl and Marboe[17] the simultaneous presence of two kinds of alkali ions results in a "tightening-up" of the electron clouds of the non-bridging oxygen ions, causing a decrease in alkali mobility. This in turn is proposed to decrease the probability of the ion exchange reaction. (b) In his review Isard[22] describes a mixed-alkali theory in which there is a mutual blocking of diffusion paths of alkali ions of one type by the presence of alkali ions of another type. This theory assumes that mixed-alkali glasses are homogeneous solutions with a random distribution of the two

alkali ions. (c) Other mixed-alkali theories have been proposed by Isard[22] and Charles[23] on the assumption of separated small atomic regions of high and low alkali groupings, or even separate phases in a nominally homogeneous glass. The hindering diffusion mechanism in this theory is the high silica regions with the tighter structure in combination with the reduced diffusion rates due to the presence of mixed alkali ions. Since all three theories are based on reduced diffusion rates for mixed-alkali glasses, an investigation of glass durability will not establish which of the theories are correct, only that reduced diffusion rates exist.

The extent of the MAE should be more apparent in the early stage of corrosion (pH $\leq$ 9) since ion-exchange and diffusion is the rate controlling reaction.[11,24] During the later stage of corrosion, i.e., total glass dissolution, the effect should be diminished since total glass dissolution is not diffusion-controlled.

Yastrebova and Antonova[18] have examined the only ternary mixed-alkali glass system, $X(Na_2O)\cdot(0.20-X)K_2O\cdot(0.80)\cdot SiO_2$, studied to date for durability. They found that these glasses exhibited a maximum in chemical durability (hence MAE) in a 2N water solution of HCl at a Na_2O/K_2O molar ratio of 9.

Other investigators have studied the MAE in various quaternary glass systems. Peddle[19] found in the mixed-alkali lead oxide silicate glasses, that maximum durability occurred at a K_2O/Na_2O weight ratio of 2.33 (1.53 molar ratio). Peddle[20] also found that when PbO was replaced with BaO, a much less noticeable effect was produced. In a similar study, Sen and Tooley[21] found that the MAE was lessened when CaO was substituted for PbO.

To the present time, little effort has been made to understand the effect of alkaline earth ions on mixed-alkali durability behavior. Also, previous studies have not considered possible consequences of such variables as: pH, ratio of glass surface area to corrosion solution volume (SA/V), bulk surfaces versus powder surfaces, or the influence of reaction on the Mixed-Alkali Effect (MAE). All of the above variables should be important if the MAE is a diffusion-controlled phenomenon. Furthermore, the contribution of the corrosion solution ions to the overall MAE have not been examined independently from the structural effects. In other words the effects of the various ions released into the corrosion solution may interact in solution and affect the diffusion rate at which other ions come out of a glass. This possibility has not been previously considered.

The objectives of this investigation are to: (a) demonstrate that a Mixed-Alkali Effect is observed even when there is not a minimum in total alkali extraction from the two end member compositions. When a minimum is observed, this is normally referred to as the "Classical" Mixed-Alkali Effect, CMAE, (b) demonstrate that the extent of the Mixed-Alkali Effect is dependent on corrosion time, SA/V ratio, the range and system of glass composition, and solution pH, (c) separate the glass structural contributions to the MAE from those due to the mixed-alkali ions being present in the corrosion solution. This is obtained from chemical-mixing, mechanical-mixing, and non-mixing experiments, and (d) present physical evidence other than solution analysis for the "Classical" Mixed-Alkali Effect.

Experimental Procedure

The glasses described in Table III were prepared from reagent grade Na_2CO_3, K_2CO_3, $CaCO_3$, and 5 μm SiO_2 powder.* Glass batches were melted in closed Pt crucibles for 24 hours in an electric muffle furnace between 1325-1425°C depending on the glass composition. The molten glass was cast between graphite blocks and given a 4 hour annealing period at 500°C.

*Min-U-Sil from Pennsylvania Glass Sand Corp., Pittsburg, Pennsylvania

Table III

Mixed-Alkali Glass Compositions Investigated, Mole %

Code	Li_2O	Na_2O	K_2O	CaO	SiO_2
LNS-3300	33.0				67.0
LNS-2508	25.0	8.0			67.0
LNS-16.516.5	16.5	16.5			67.0
LNS-0825	8.0	25.0			67.0
LNS-0033		33.0			67.0
LNS-2500	25.0				75.0
LNS-2005	20.0	5.0			75.0
LNS-12.512.5	12.5	12.5			75.0
LNS-0520	5.0	20.0			75.0
LNS-0025		25.0			75.00
LKS-2500	25.0				75.00
LKS-2005	20.0		5.0		75.0
LKS-12.512.5	12.5		12.5		75.0
LKS-0520	5.0		20.0		75.0
LKS-0025			25.0		75.0
NKS-2500		25.0			75.0
NKS-2500		20.0	5.0		75.0
NKS-12.512.5		12.5	12.5		75.0
NKS-0520		5.0	20.0		75.0
NKS-0025			25.0		75.0

Table III - continued.

Code	Li_2O	Na_2O	K_2O	CaO	SiO_2
NKS-2000		20.0			80.0
NKS-1802		18.0	2.0		80.0
NKS-1406		14.0	6.0		80.0
NKS-1010		10.0	10.0		80.0
NKS-0614		6.0	14.0		80.0
NKS-0218		2.0	18.0		80.0
NKS-0020			20.0		80.0
NKCS-200010		20.0		10.0	70.0
NKCS-150510		15.0	5.0	10.0	70.0
NKCS-101010		10.0	10.0	10.0	70.0
NKCS-051510		5.0	15.0	10.0	70.0
NKCS-150010		15.0		10.0	75.0
NKCS-120310		12.0	3.0	10.0	75.0
NKCS-090610		9.0	6.0	10.0	75.0
NKCS-060910		6.0	9.0	10.0	75.0
NKCS-031210		3.0	12.0	10.0	75.0
NKCS-001510			15.0	10.0	75.0

Specimens ∿3/4" x 3/4" x 1/4" were sectioned from glass plates, polished through 600 grit SiC paper, and stored in a desiccator. Prior to testing, the specimens were given a final abrasion with 600 grit dry SiC paper to eliminate environmental effects.

Powders were prepared by pulverizing bulk glass compositions with an alumina mortar and pestle and sieving through appropriate screens to yield a particle size range of -45+60 mesh (250-354 μm) and -60+100 mesh (149-250 μm).

Static bulk corrosion tests were performed using Teflon(R) cubes with a 3/8" diameter, 3/8" deep cavity filled with triple distilled (3D) H_2O as described in previous papers.[25,26] The specimen cells were placed in a water tight container and submerged in a hot water bath for various times at 100°C. The ratio of glass surface area to corrosion solution volume was maintained at 0.77 cm^2/cm^3 (cm^{-1}).

Testing of glass powders was similar to the American Ceramic Society tentative method No. 1.[27] Sufficient quantities (weights) of glass powders (-45+60, -60+100

(R)E. I. de Pont de Nemours & Co., Inc. Wilmington, Del.

mesh) to give initial glass surface area to corrosion solution volume ratios of 0.077, 0.77, 4.30, and 7.70 cm^{-1} were digested in 3D-H_2O (initial pH = 6.5) at 100°C for various times. Most powder-corrosion experiments were performed for each of the following: (1) chemical-mixtures of alkali glasses in which both alkali ions were homogenized in the same glass melt, (2) mechanical-mixtures of alkali glasses prepared by combining sufficent quantities of 150010 and 001510 glass powders (Table III) to give the same Na_2O/K_2O ratio as in the chemical-mixtures, (3) non-mixtures of single alkali glasses. In order to evaluate the effects of non-mixing, quantities of 150010 and 001510 glasses yielding the same Na_2O/K_2O ratio as for the chemical- and mechanical-mixtures were corroded in separate containers, while maintaining their respective individual constant SA/V ratios (Table IV). Two SA/V ratios (0.77, 7.7 cm^{-1}) were examined for each of the three experimental cases.

The corrosion solutions were filtered with No. 40 filter paper* before performing solution analysis. The quantity of dissolved silica was determined by the

* W & R Balston, LTD, England

Table IV

Glass Surface Area (SA) to Corrosion Solution Volume (V) Ratio, cm^{-1}

Glass	Chemical Mixtures (one solution)	Mechanical Mixtures (one solution)	Non-mixtures (two solutions)
150010		150010 (0.77 cm^{-1})	Soln.I-150010 (0.77 cm^{-1})
		001510 (0.00 cm^{-1})	Soln.II-001510 (0.00 cm^{-1})
	150010 (0.77 cm^{-1})	150010 (0.77 cm^{-1})	
120310		150010 (0.62 cm^{-1})	Soln.I-150010 (0.62 cm^{-1})
		001510 (0.15 cm^{-1})	Soln.II-001510 (0.15 cm^{-1})
	120310 (0.77 cm^{-1})	120310 (0.77 cm^{-1})	
090610		150010 (0.46 cm^{-1})	Soln.I-150010 (0.46 cm^{-1})
		001510 (0.31 cm^{-1})	Soln.II-001510 (0.31 cm^{-1})
	090610 (0.77 cm^{-1})	090610 (0.77 cm^{-1})	
060910		150010 (0.31 cm^{-1})	Soln.I-150010 (0.31 cm^{-1})
		001510 (0.46 cm^{-1})	Soln.II-001510 (0.46 cm^{-1})
	060910 (0.77 cm^{-1})	060910 (0.77 cm^{-1})	

Table IV - continued.

Glass	Chemical Mixtures (one solution)	Mechanical Mixtures (one solution)	Non-mixtures (two solutions)
031210		150010 (0.15 cm^{-1})	Soln.I-150010 (0.15 cm^{-1})
		001510 (0.62 cm^{-1})	Soln.II-001510 (0.62 cm^{-1})
	031210 (0.77 cm^{-1})	031210 (0.77 cm^{-1})	
001510		150010 (0.00 cm^{-1})	Soln.I-150010 (0.00 cm^{-1})
		001510 (0.77 cm^{-1})	Soln.II-001510 (0.77 cm^{-1})
	001510 (0.77 cm^{-1})	001510 (0.77 cm^{-1})	

molybdenum blue colorimetric method.* Na^+, K^+ and Ca^{+2} solution concentrations were determined by atomic emission** and atomic adsorption*** spectroscopy, respectively. The pH of the corrosion solutions were checked with pH indicator paper.**** The resolution of the various solution analysis techniques described above are shown in Table III.

The surfaces of bulk samples were analyzed using infrared reflection spectroscopy (IRRS)***** by scanning at a medium rate from 1400 cm^{-1} to 600 cm^{-1}.[15,28] The spectra of the corroded samples were compared with the spectra of freshly abraded glass surfaces.

Scanning electron microscope (SEM)****** specimens (bulk) were vacuum coated with 150 Å of Au-Pd.

Results: Quaternary Glasses

Individual Na^+ and K^+ molarity corrosion curves versus glass composition for the $(X)Na_2O\cdot(0.15-X)\ K_2O\cdot(0.10)\ CaO\cdot(0.75)$

*Hach "Direct Reading" Colorimeter, Hach Chemical Co., Ames, Iowa
**Beckman B. Spectrometer, Beckman Instruments, Inc., Fullerton, Calif.
***Perkin-Elmer Model 303 Spectrometer, Perkin-Elmer Corp., Norwalk, Conn.
****Gallard-Schlesinger Chemical Mfg., Corp., Carle Place, New York
*****Perkin-Elmer Model 467 IRRS, Perkin-Elmer Corp., Norwalk, Conn.
******Cambridge Stereoscan, Kent Cambridge Scientific, Inc., Morton Grove, Ill.

SiO_2 glass system are shown in Figure 4. This figure presents data obtained by corroding glass powders (-60+100 mesh), for 12 hours at 100°C under the following conditions: 1) chemical mixing, 2) mechanical mixing, and 3) non-mixing. The glass surface area to corrosion solution volume (SA/V) ratio was maintained at 0.77 cm^{-1} (Table IV).

The sum of the Na^+ and K^+ molarity curves of Figure 4 is shown in Figure 5 for each of the three experimental conditions. Also shown in this figure are the total (Na^+ + K^+) molarity curves for the 7.7 cm^{-1} SA/V ratio.

The chemical-mixed glasses for the different SA/V ratios yielded curves exhibiting minima in corrosion rates (maximum durability) at the 120310 glass composition. This minimum in corrosion is traditionally referred to as the Classical Mixed-Alkali Effect (CMAE).[18-21]

The mechanical-mixed glasses yielded nearly a straight line for SA/V=0.77 cm^{-1}. When the SA/V was increased to 7.7 cm^{-1}, the line deviated from linearity.

The results of the non-mixtures reveal the corrosion solution ion effects on mixed-alkali glass corrosion. The total alkali molarity was found to be greater for the non-mixed corroded alkali glasses than for the equivalent mechanical-mixed glasses (Figure 5).

Figure 4. Na^+ and K^+ solution results for powder corrosion in the $(X)Na_2O\cdot(0.15-X)K_2O\cdot(0.10)CaO\cdot(0.75)SiO_2$ glass system.

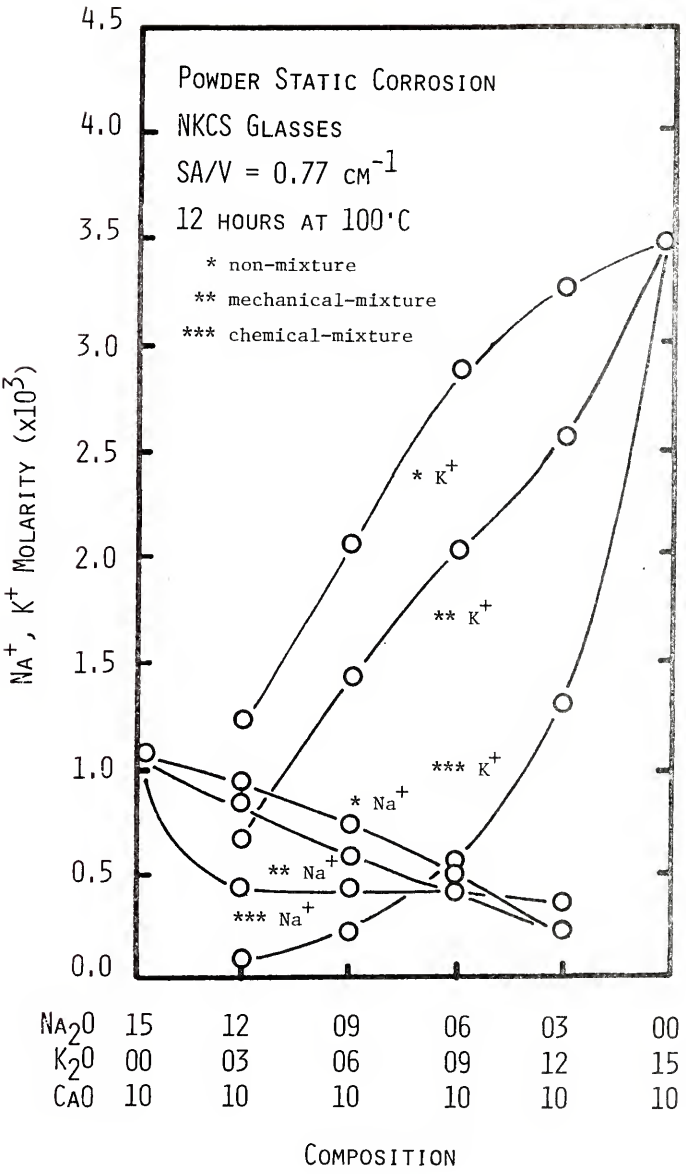
Powder Static Corrosion
NKCS Glasses
SA/V = 0.77 cm-1
12 hours at 100°C
* non-mixture
** mechanical-mixture
*** chemical-mixture
* K+
** K+
*** K+
* Na+
** Na+
*** Na+
Na+, K+ Molarity (x10-3)
4.5
4.0
3.5
3.0
2.5
2.0
1.5
1.0
0.5
0.0
Na2O 15 12 09 06 03 00
K2O 00 03 06 09 12 15
CaO 10 10 10 10 10 10
Composition

Figure 5. $N^+ + K^+$ solution results for powder corrosion in the $(X)Na_2O\cdot(0.15-X)K_2O\cdot(0.o0CaO\cdot(0.75)SiO_2$ glass system.

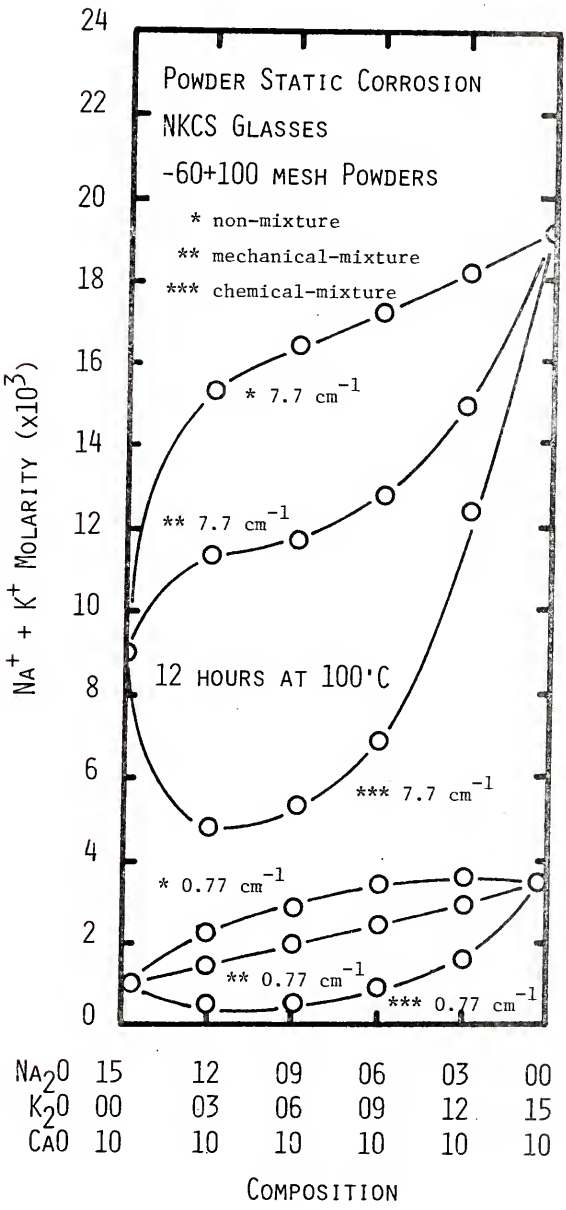
POWDER STATIC CORROSION
NKCS GLASSES
-60+100 MESH POWDERS
* non-mixture
** mechanical-mixture
*** chemical-mixture
* 7.7 cm-1
** 7.7 cm-1
12 HOURS AT 100°C
*** 7.7 cm-1
* 0.77 cm-1
** 0.77 cm-1
*** 0.77 cm-1
Na+ + K+ MOLARITY (x10-3)
24
22
20
18
16
14
12
10
8
6
4
2
0
Na2O 15 12 09 06 03 00
K2O 00 03 06 09 12 15
CaO 10 10 10 10 10 10
COMPOSITION

Figure 6 further illustrates the MAE by plotting pH versus glass composition for both the mechanical- and chemical-mixed glasses. These data are presented for the same SA/V ratios as shown in Figure 5. The important feature of this figure is that for the chemical-mixed curves, minimum values in pH occur at the same glass composition (120310) as was observed for molarity (Na^+ + K^+) in Figure 5.

The Si^{+4} and Ca^{+2} molarities corresponding to the alkali molarities (chemical-mixtures) of Figure 5 are shown in Figure 7. Again, a maximum durability is shown for the 120310 glass.

Na^+ and K^+ alkali concentration curves are shown in Figure 8 for the $(X)Na_2O\cdot(0.15-X)K_2O\cdot(0.10)CaO\cdot(0.75)SiO_2$ glass system for bulk experiments. Bulk corrosion tests were performed at 100 °C and at a SA/V ratio of 0.77 cm^{-1}. Also shown in this figure are the total alkali (Na^+ + K^+) concentration curves. The small minima observed for bulk corrosion in the 120310 composition corresponds to the same location of the minima observed for powder corrosion.

Similar results (Na^+ and K^+ alkali concentration curves) are shown in Figure 9 for the $(X)Na_2O\cdot(0.20-X)K_2O\cdot(0.10)CaO\cdot(0.70)SiO_2$ glass system. Bulk corrosion

Figure 6. pH solution data for powder corrosion in the $(X)Na_2O\cdot(0.15-X)K_2O\cdot(0.10)CaO\cdot(0.75)SiO_2$ glass system.

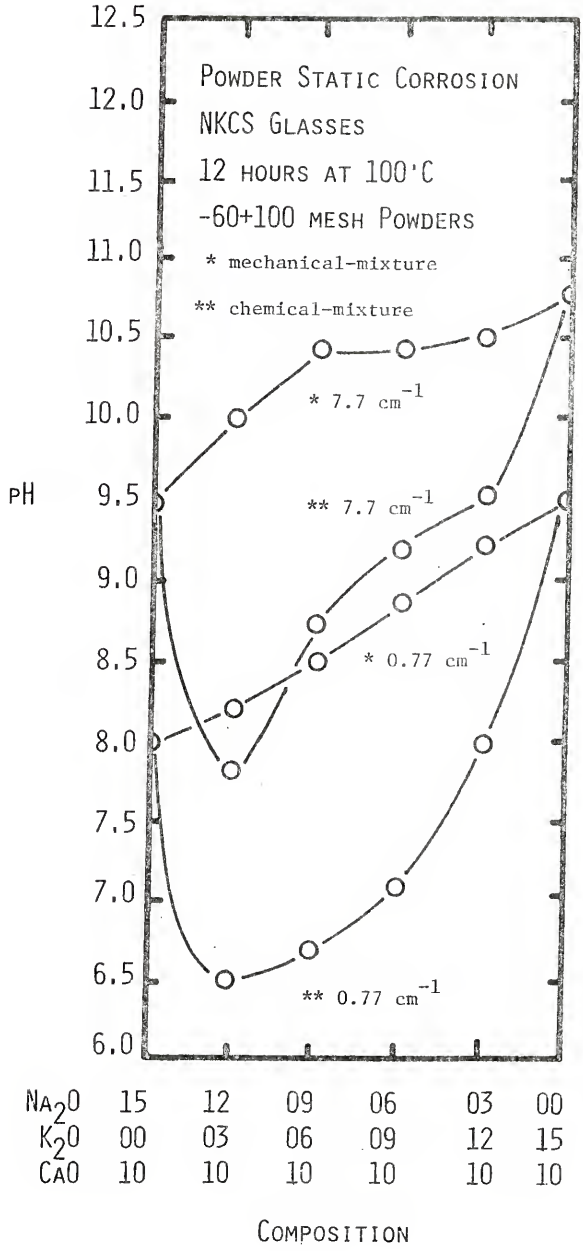
POWDER STATIC CORROSION
NKCS GLASSES
12 HOURS AT 100°C
-60+100 MESH POWDERS
* mechanical-mixture
** chemical-mixture
* 7.7 cm-1
** 7.7 cm-1
* 0.77 cm-1
** 0.77 cm-1
pH
12.5
12.0
11.5
11.0
10.5
10.0
9.5
9.0
8.5
8.0
7.5
7.0
6.5
6.0
Na2O 15 12 09 06 03 00
K2O 00 03 06 09 12 15
CaO 10 10 10 10 10 10
COMPOSITION

Figure 7. Ca^{+2} and Si^{+4} solution data for powder corrosion in the $(X)Na_2O\cdot(0.15-X)K_2O\cdot(0.10)CaO\cdot(0.75)SiO_2$ glass system.

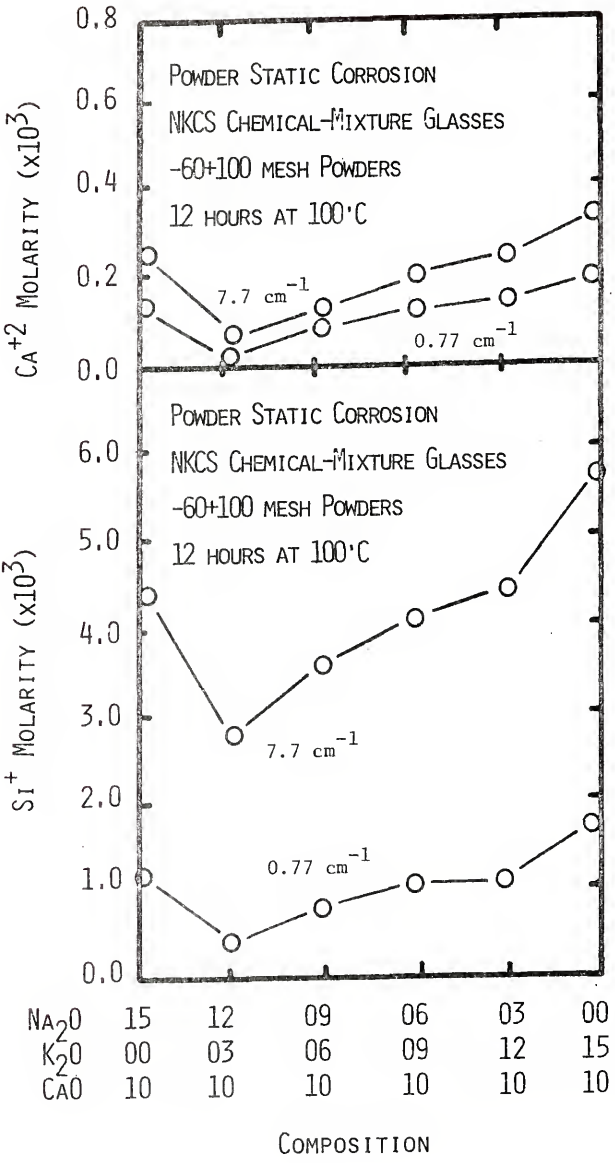
POWDER STATIC CORROSION
NKCS CHEMICAL-MIXTURE GLASSES
-60+100 MESH POWDERS
12 HOURS AT 100°C
7.7 cm-1
0.77 cm-1
CA+2 MOLARITY (x10-3)
0.0
0.2
0.4
0.6
0.8
POWDER STATIC CORROSION
NKCS CHEMICAL-MIXTURE GLASSES
-60+100 MESH POWDERS
12 HOURS AT 100°C
7.7 cm-1
0.77 cm-1
SI+ MOLARITY (x10-3)
0.0
1.0
2.0
3.0
4.0
5.0
6.0
Na2O 15 12 09 06 03 00
K2O 00 03 06 09 12 15
CaO 10 10 10 10 10 10
COMPOSITION

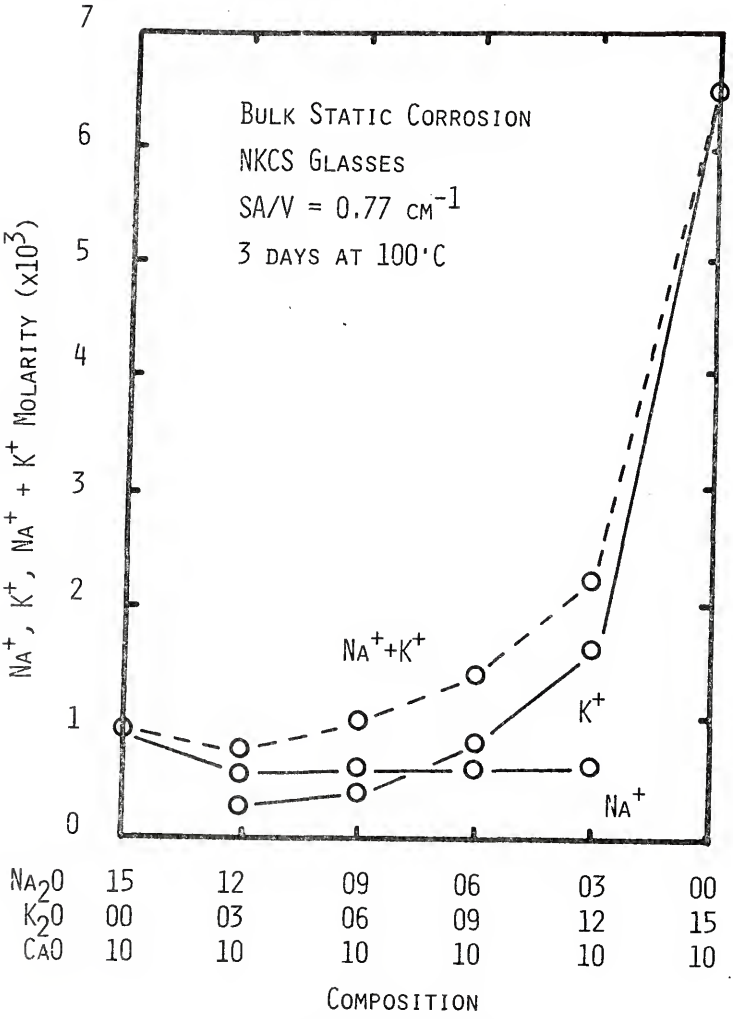

Figure 8. N^+, K^+ and $Na^+ + K^+$ solution data for bulk corrosion in the $(X)Na_2O\cdot(0.15-X)K_2O\cdot(0.10)CaO\cdot(0.75)SiO_2$ glass system.

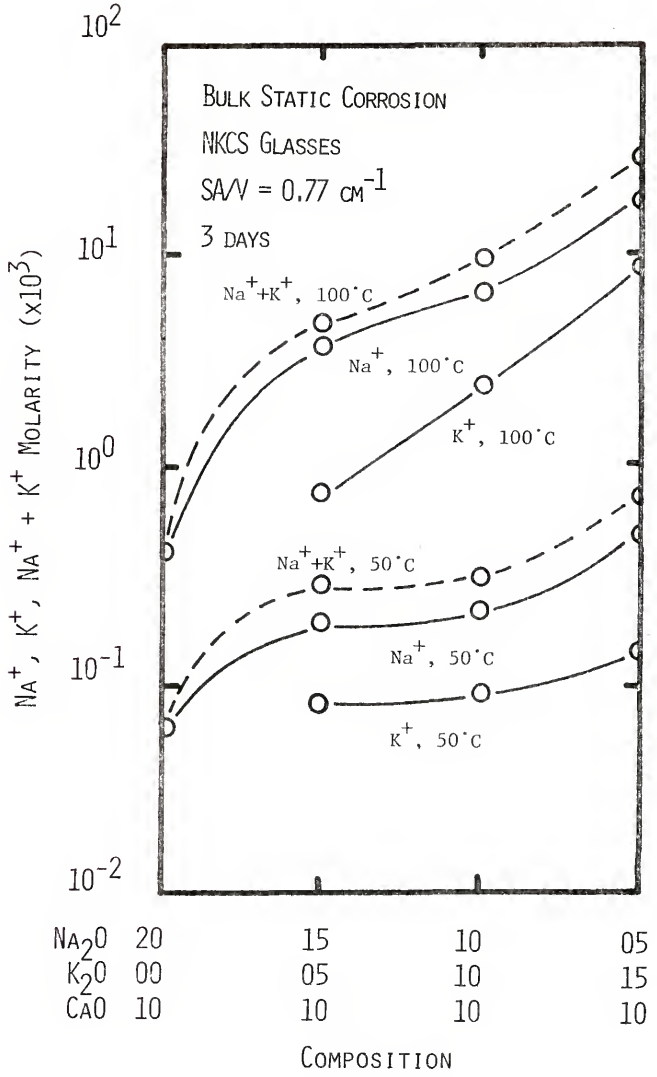

Figure 9. Na^+, K^+ and Na^+ + K^+ solution data for bulk corrosion in the $(X)Na_2O\cdot(0.20-X)K_2O\cdot(0.10)CaO\cdot(0.70)SiO_2$ glass system.

tests were performed at 50° and 100°C and at a SA/V ratio of 0.77 cm^{-1}. Also shown in this figure are the total alkali ($Na^+ + K^+$) concentration curves. At the 20 mole % total alkali level, no minima in the total alkali solution concentration is observed, in contrast to glasses with 15 mole % total alkali.

Figure 10 shows the extent of the Mixed-Alkali Effect (in terms of Na^+ and K^+ molarity) for chemical-mixtures as a function of corrosion time for the 150010 and 120310 glass compositions. The slope of the molarity-composition curve, determined by the difference between the molarity of the 150010 glass and the molarity of the 120310 glass, is a measure of the extent of the MAE. The MAE is more obvious in the 0.77 cm^{-1} (powder) than for the 0.077 cm^{-1} (powder) and appears to go through a maximum at 1 day. After 3 days, the MAE has begun to diminish, and has almost completely disappeared after 7 days (i.e., the slope is equal to that obtained for the equivalent mechanical mixture). It should be noted that the pH of the 7 day (0.77 cm^{-1}, powder) corrosion solution was >9, (from Figure 12) corresponding to the pH regime where total glass dissolution is usually significant. Also shown in Figure 10 is the MAE for bulk glasses with SA/V = 0.77 cm^{-1}.

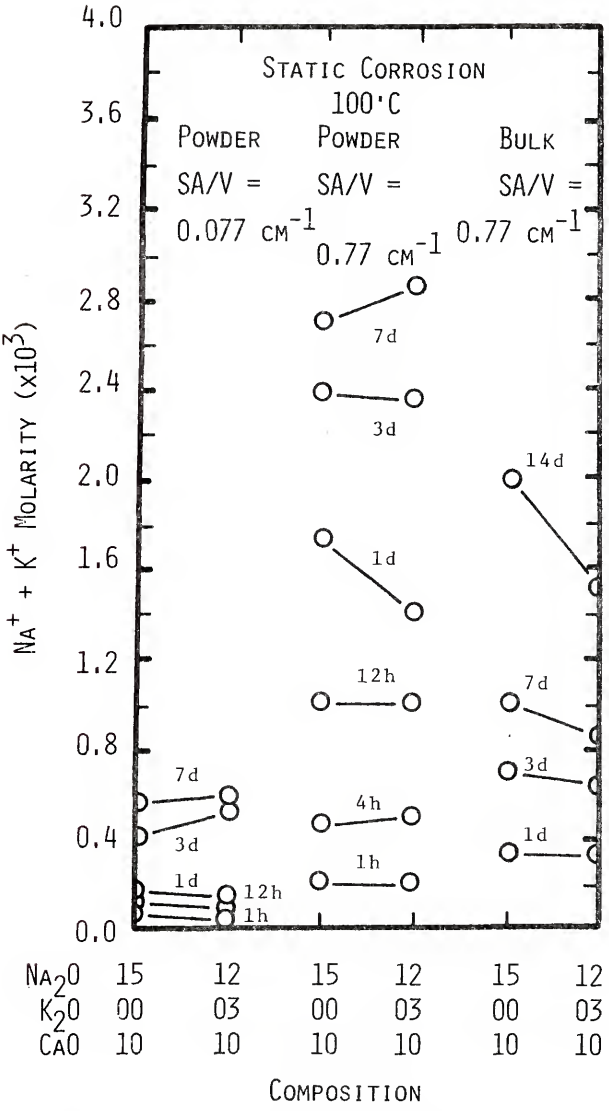

Figure 10. $Na^+ + K^+$ solution data for bulk and powder corrosion of the NKCS - 150010 and NKCS - 120310 glass compositions.

A strong MAE still exists after 14 days for bulk glass corrosion. However, the molarity ($Na^+ + K^+$) range in which the MAE appears to be a maximum is approximately the same for both the powder and bulk glasses at the 0.77 cm^{-1} ratio even though the rates for the two cases are different.

Figure 11 presents molarity ($Na^+ + K^+$) versus corrosion time for the 150010 and 120310 glass powders corroded for the 0.77 cm^{-1} ratio. The total alkali ion concentration in solution is greater for the former up to $\sim$3.5 days, after which time the 120310 glass yields a higher alkali concentration up to 7 days

The solution pH as a function of corrosion time is shown in Figure 12 for the glasses and conditions presented in Figure 11. The pH values of the corrosion solutions were significantly different during the first 3 days of corrosion but obtained equal values for longer corrosion times.

A parameter useful in discussing the relative leaching and total dissolution tendency of glasses is α (equation 5).

Figure 13 illustrates α (degree of selective alkali leaching or total dissolution) dependence upon time for the 150010 and 120310 glass powders for a 0.77 cm^{-1} SA/V ratio.

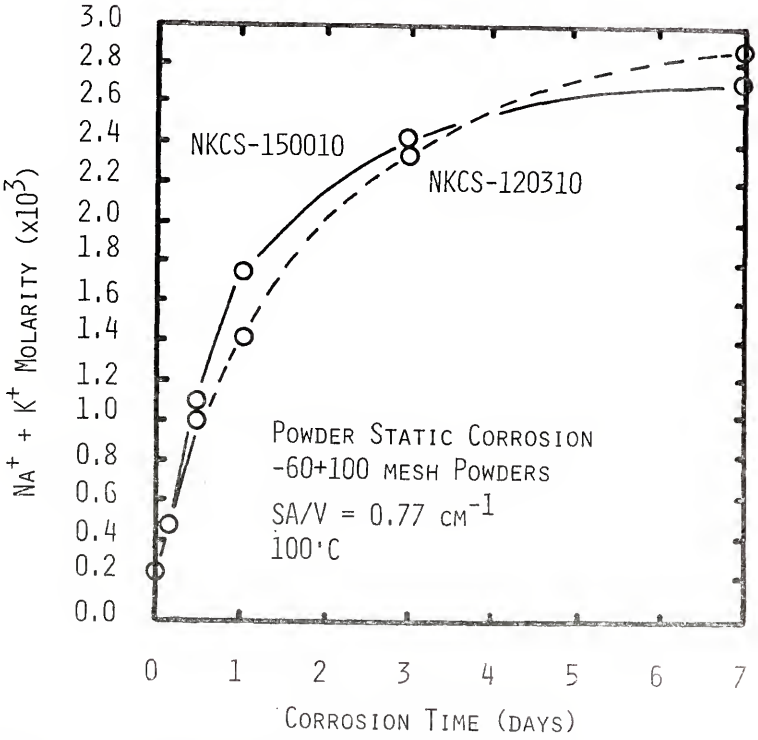

Figure 11. $Na^+ + K^+$ solution data for powder corrosion of the NKCS - 150010 and NKCS - 120310 glass compositions.

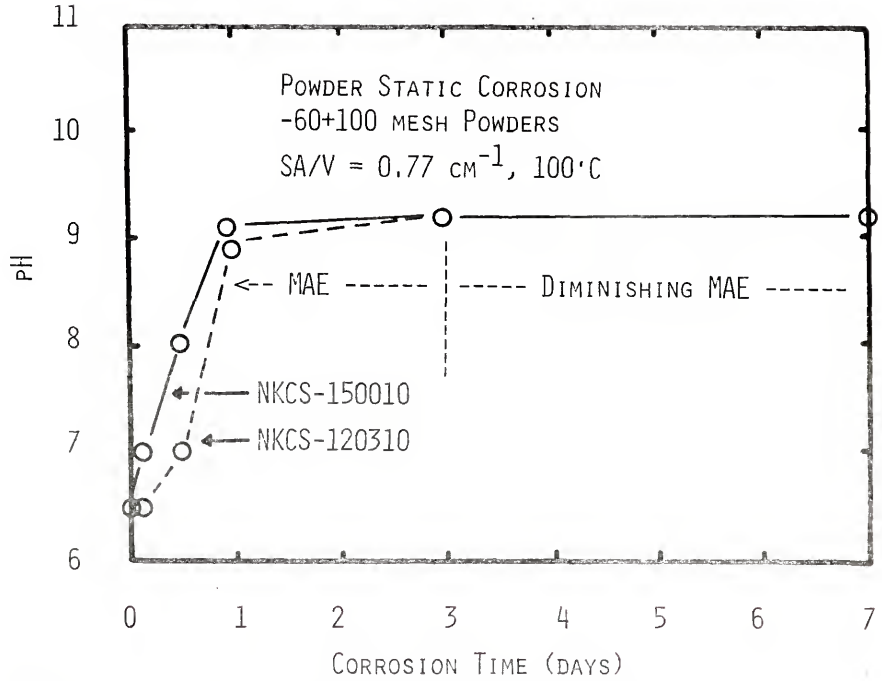

Figure 12. pH solution data for powder corrosion of the NKCS - 150010 and KNCS - 120310 glass compositions.

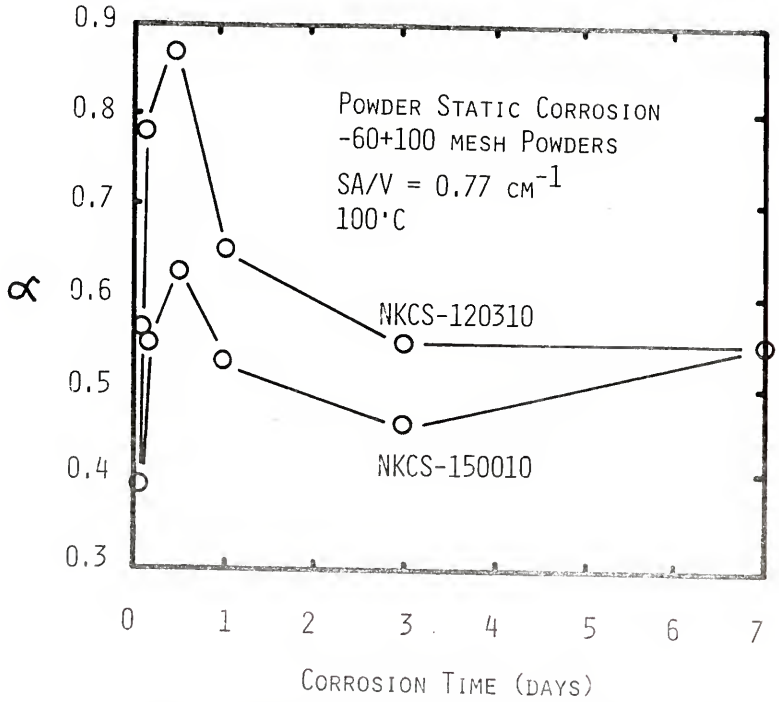

Figure 13. Alpha values for powder corrosion of the NKCS - 150010 and NKCS - 120310 glass compositions.

The α values are low for short periods (<1 h) indicating extensive selective alkali leaching. As corrosion time increases, the α values go through maxima before finally reaching a semiequilibrium condition. The α values of the 120310 glass are higher than those for the 150010 glass for <7 days indicating that the former has a greater tendency to selectively leach than does the 120310 glass. At 7 days the α values for both glasses are approximately equal and are showing a tendency to increase suggesting that total glass dissolution is becoming an important corrosion mechanism as time increases.

The infrared reflection (IR) spectra of the 150010, 120310 and 001510 bulk glasses are represented in Figure 14. The NSL peak (alkali) for the 001510 glass was completely gone after 1 day while 14 days were required for the disappearance of the same peak for the 150010 glass. However, the 120310 glass exhibited a distinctive NSL peak even after 14 days of corrosion.

IRRS spectra of the 200010, 150510, 101010, and 051510 glass compositions are shown in Figure 15. The presence of a NSL peak (alkali) for the 3 days 50°C and 100°C test is inversely proportional to the percent of K_2O present in the glass composition, i.e., high Na_2O/no

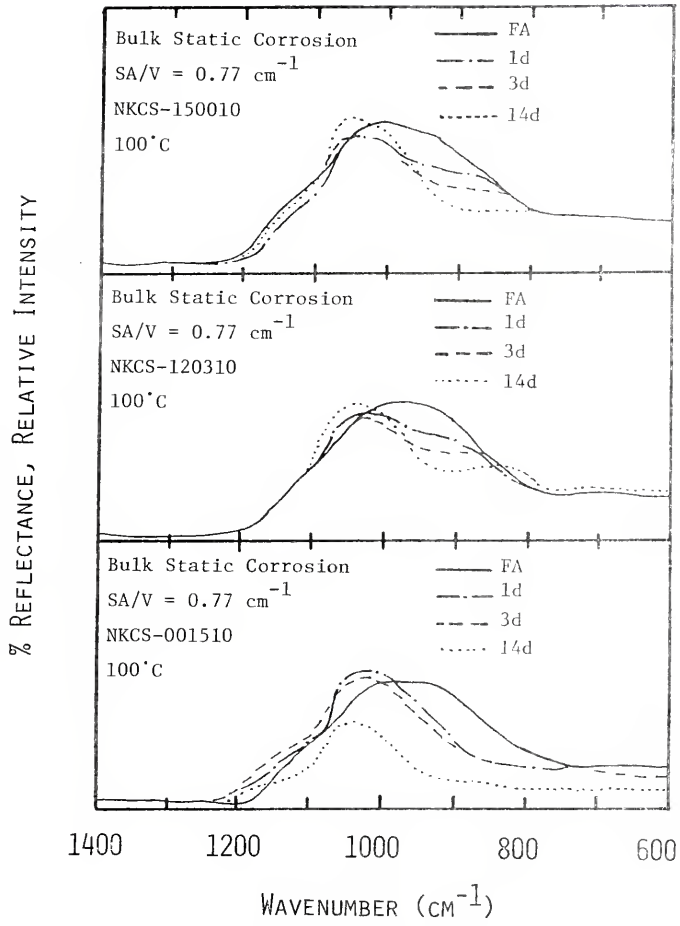

Figure 14. Infrared reflection spectra for bulk corrosion of the NKCS - 150010, NKCS - 120310 and NKCS - 001510 glass compositions.

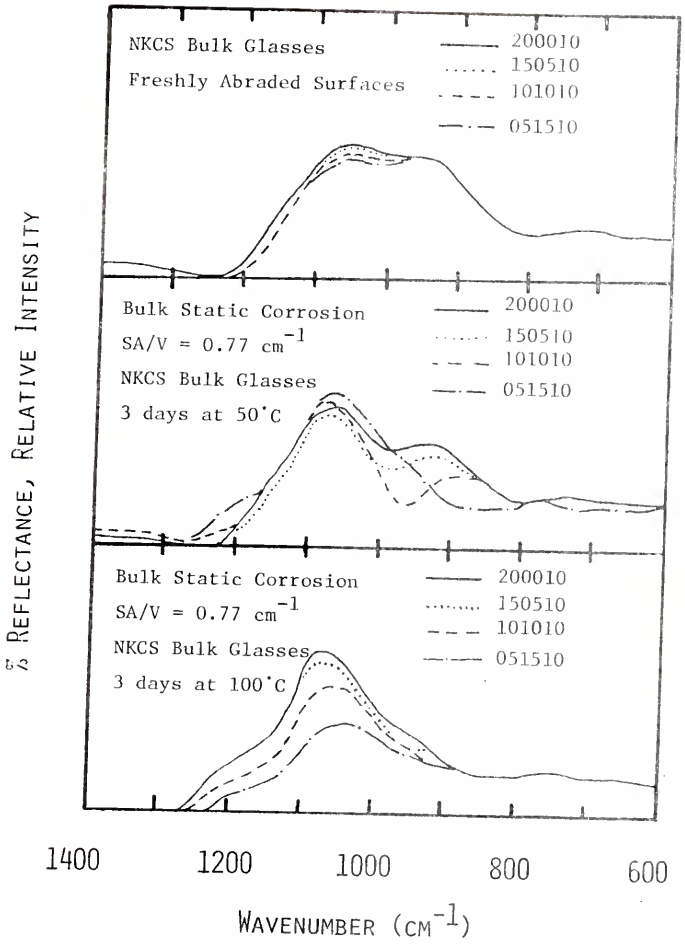

Figure 15. Infrared reflection spectra for bulk corrosion of the NKCS - 200010, NKCS - 150510, NKCS - 101010 and NKCS - 051510 glass compositions.

K_2O, a large NSF peak is observed; a low Na_2O/high K_2O no NSL peak is observed.

Scanning electron micrographs of the three bulk glasses discussed in Figure 14 corroded for 14 days are shown in Figure 16, along with a non-corroded (freshly abraded) glass surface. The SEMs show that the 120310 glass is corroded to a smaller extent than the 150010 or 001510 glasses.

Discussion: Quaternary Glasses

Lower electrical condutivities and lower ionic diffusion (alkali mobility) rates are characteristic of mixed alkali glasses.[5,17-23,29-35] The decrease in alkali mobility is thought to be responsible for the increase in chemical durability in these glasses.[22]

The separation of the mechanical- and chemical-mixture curves in Figure 5 is due to the structural contributions of the Mixed-Alkali Effect. The data for both the 0.77 and 7.7 cm^{-1} SA/V ratios indicate that the 120310 glass is the most durable composition, i.e., a minima is observed. These results suggest that the 120310 glass is selectively leached at a smaller rate than all the other glasses over the compositional range investigated.

Figure 16. Scanning electron micrographs for bulk glasses under the following conditions: (a) NKCS - 150010 freshly abraded surface (2500X), (b) NKCS - 150010 corroded for 14 days at 100°C (2500X), (c) NKCS - 120310 corroded for 14 days at 100°C (2500X) and (d) NKCS - 001510 corroded for 14 days at 100°C (2500X).

(a)

(b)

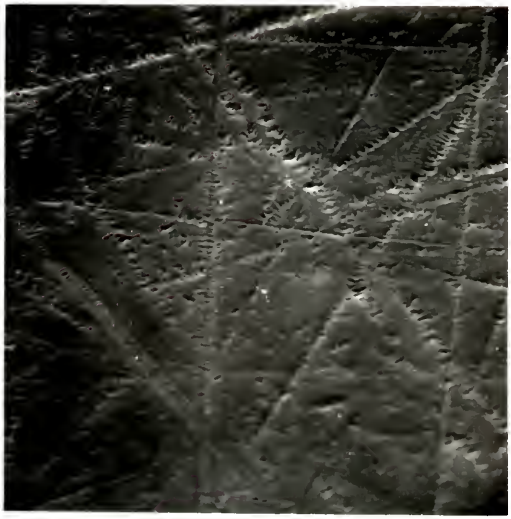

(c)

(d)

The presence of a minimum in the total alkali (Na^+ + K^+) concentration curves as compared with the single alkali end members corresponds to the "Classical" Mixed-Alkali Effect (CMAE). Even if there was no minimum in the total alkali concentration curve, as long as the chemical-mixture curve is below the mechanical-mixture curve, a Mixed-Alkali Effect (MAE) is present. Therefore, in this chapter, whenever a minimum is observed, it will be described as a Classical Mixed-Alkali Effect (CMAE) and when a minimum is not observed but the chemical-mixture curve is below the ideality concentration curve (mechanical-mixtures), it will be described as a Mixed-Alkali Effect (MAE).

The straight line obtained for the mechanical-mixed glasses at SA/V = 0.77 cm^{-1} (Figure 5) represents expected "ideal" corrosion behavior when only the contribution of a single mechanism is significant. The non-linear line for the 7.7 cm^{-1} mechanical-mixtures suggests that the corrosion process is more complicated than the ideal behavior found for the 0.77 cm^{-1} SA/V ratio. This non-ideal behavior could be due to the presence of high concentrations of alkali ions (hence high pH) in the corrosion solution of the high potassia glasses. The leaching of alkali ions from glasses at high pH is probably decreased due to the lower alkali-hydrogen exchange

ratio.[11,24] This competition between several corrosion mechanisms due to solution pH differences results in non-linear corrosion behavior for the compositions investigated. For pH < 9 the complications are not observed. Figure 6 illustrates that for SA/V = 0.77 cm^{-1}, the pH values are ≤ 9 for all compositions. This corresponds to the pH regime where ion exchange is the primary mechanism of corrosion. However, for SA/V = 7.7 cm^{-1}, the pH values are ≥ 9 and several corrosion reactions are possible in this pH range.

Figure 5 shows that the total alkali concentration is greater for the non-mixtures than for the equivalent mechanical-mixture glasses. The difference between these two curves illustrate that the presence of mixed-alkali ions in solution yields lower corrosion rates than for the comparable single alkali glasses. This decrease in corrosion due to the presence of mixed-alkali ions in the corrosion solution is the corrosion solution ion contribution to the overall Mixed-Alkali Effect

The molarities of Si^{+4} and Ca^{+2} shown in Figure 7 also reveal the presence of the Classical Mixed-Alkali Effect for both the 0.77 and 7.7 cm^{-1} SA/V ratios. The presence of these two ions in solution usually requires

total glass dissolution. Thus, the glasses which correspond to the low pH values (Figure 6) also show less total dissolution.[11]

The CMAE observed for bulk corrosion in Figure 8 is found to be present at the same location (120310 composition) as that of powder corrosion. However, for bulk corrosion, the CMAE is not as large after 3 days of corrosion as that observed for powders after 1 day even with equivalent SA/V ratios. This difference can be explained by the fact that powder corrosion rates and kinetics are greater than those observed for bulk planar surfaces (refer to Appendix, Section III). After 14 days of corrosion, the CMAE for the bulk is approximately equal to the CMAE for powders corroded for 1 day (see Figure 10).

Although from electrical properties the Classical Mixed-Alkali Effect is observed for total alkali concentrations of 20-33%, according to Peddle,[19] no CMAE for chemical durability is observed at these total alkali levels in the mixed-R_2O-RO-SiO_2 glasses.

In Figure 9, no Classical Mixed-Alkali Effect is observed for the 20 mole % alkali level for either the 50°C or 100°C corrosion tests in contrast to that (CMAE) observed for the 15 mole % alkali level at 100°C. However, if these chemical-mixture concentration curves are compared

with the projected idealized concentration curves, a Mixed-Alkali Effect is observed.

A measure of the extent of the CMAE/MAE can be seen from the slope of the dissolution molarity curve (Figure 10) determined by the difference between the molarity of the 150010 glass and the molarity of the 120310 glass. A large negative slope indicates a strong CMAE due to glass structural contributions. At short times, very little selective leaching has occurred in either glass and hence the magnitude of the CMAE is small. As time proceeds, the difference in selective leaching between the two glasses increases resulting in a large CMAE. For pH > 9, total dissolution becomes important and the CMAE/MAE diminishes.

Figure 11 illustrates that the CMAE is dependent upon corrosion time. The molarity of the 120310 glass increases above the molarity of the 150010 glass after 3 days suggesting a decrease in the CMAE. It is significant that the solution pH for both glasses is >9 (Figure 12) after 3 days. This is the pH range where total glass dissolution is important and hence the CMAE, which is a diffusion controlled phenomenon, should diminish.

The leaching tendencies discussed up to this point have not taken the amount of Si^{+4} in the corrosion solutions into consideration, only the quantities of alkali

ions. In order to view the overall corrosion process, the Si^{+4} and Ca^{++} concentrations must be taken into account. This is done in Figure 13 where the α values confirm that the 150010 glass has a higher tendency to be selectively leached than does the 120310 glass. The rapid initial increase in α for both glass can be attributed to the dissolving of extremely fine particles adhering to the larger particles. After 2 days, the glasses have settled into an α range where selective leaching and total dissolution are occurring in equilibrium. Although the α for the 120310 glass remains relatively constant the 150010 glass tends more toward total dissolution after 3 days and closely approaches the 120310 α value at 7 days. As stated previously, the presence of a Mixed-Alkali Effect is dependent upon lower alkali diffusion rates for mixed alkali glasses than for single alkali glasses. After 7 days of corrosion, the 150010 and 120310 glasses have equal α values, as shown in Figure 13. Common α values for the two glasses is indicative of a decreasing Mixed-Alkali Effect. Since the selective leaching rates are equal, there must be approximately equal alkali diffusion rates.

Figure 14 illustrates the infrared reflection spectra (IRRS) of the 150010, 120310 and 001510 bulk glasses. The

shift in the non-bridging oxygen-silicon (NSL) peak[36] to higher wavenumbers is indicative of the dealkalization of the glasses. The 001510 glass was completely dealkalized after 1 day within the depth of IRRS penetration ($\sim$0.5 μm). The rate of dealkalization for the 150010 glass is much slower than for the 001510 glass, the former requiring 14 days for the Na^+ to be leached from the same depth. Moreover, the intensity of the NSL peak is still strong in the 120310 glass after 14 days, suggesting an even slower dealkalization process for this mixed-alkali glass as compared to the single alkali glasses.

The IRRS results shown in Figure 15 confirm the solution results of Figure 9, i.e., the absence of a Classical Mixed-Alkali Effect. From IRRS results, the presence of the NSL peak (alkali) after 3 days corrosion at both 50°C and 100°C is found to be inversely proportional to the percent of K_2O in the glass. In fact, the 100°C IRRS spectra reveal that extreme selective leaching has occurred for the 20 mole % alkali glasses with the probability that total glass dissolution is already an important corrosion mode for these glasses after 3 days. This again could be due to the corrosion kinetics. Glasses containing $\geq$20 mole % alkali corrode faster and have a greater tendency for total dissolution than do glasses containing $\leq$15 mole

% alkali. At very small corrosion times (i.e., before total dissolution becomes important), the CMAE may be observed for the 20 mole % alkali glasses. Evidence for this can be seen by comparing the 50°C and 100°C curves in Figure 9. It is obvious that the 50°C curve, where total dissolution is expected to be less, also exhibits a greater tendency towards a CMAE.

Solution data presented in Figure 10 and IRRS spectra shown in Figure 14 confirm the presence of a CMAE after 14 days for bulk glasses in the $(X)Na_2O\cdot(0.15-X)K_2O\cdot(0.10)CaO\cdot(0.75)SiO_2$ system. Further evidence can be seen from scanning electron micrographs (SEMs) shown in Figure 16. The SEMs show that the 120310 glass is corroded to a smaller extent than either of the other two glasses. The corrosion pits are more pronounced for the 001510 glass than for the 120310 or 150010 glasses suggesting more of a total network breakdown for the former.

Results: Ternary Glasses

Figure 17 shows Na^+ and K^+ molarity concentrations as a function of Na_2O/K_2O ratios for $(X)Na_2O\cdot(0.20)K_2O\cdot(0.80)SiO_2$ glass powders (-45+60 mesh) corroded at 50°C for 6 hours and 1 day ($SA/V = 4.3\ cm^{-1}$). The rate of dissolution of the K^+ end member is a factor of 10^2 or

Figure 17. Na^+, K^+ and $Na^+ + K^+$ solution data for powder corrosion in the $(X)Na_2O\cdot(1-X)K_2O\cdot(0.80)SiO_2$ glass system.

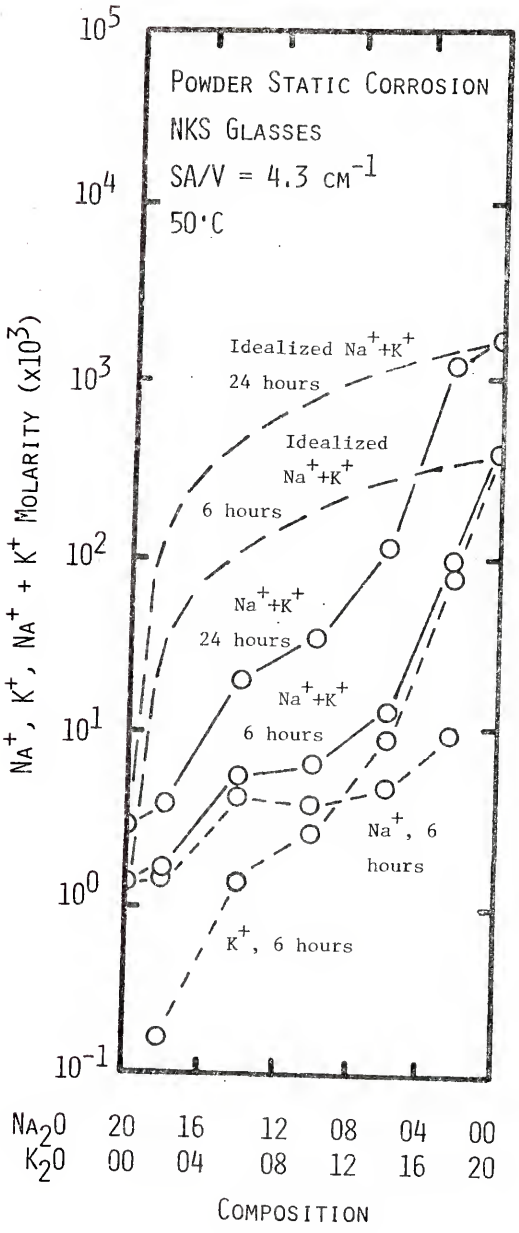
POWDER STATIC CORROSION
NKS GLASSES
SA/V = 4.3 CM^{-1}
50°C
Idealized $Na^+ + K^+$
24 hours
Idealized
$Na^+ + K^+$
6 hours
$Na^+ + K^+$
24 hours
$Na^+ + K^+$
6 hours
Na^+, 6
hours
K^+, 6 hours
Na^+, K^+, $Na^+ + K^+$ MOLARITY ($x10^3$)
10^5
10^4
10^3
10^2
10^1
10^0
10^{-1}
Na_2O 20 16 12 08 04 00
K_2O 00 04 08 12 16 20
COMPOSITION

more greater than the Na^+ end member. Also shown in Figure 17 are the linear "ideal" alkali molarity curves which should result from a simple additive compositional change. As discussed previously the behavior of the mechanical-mixtures closely approximates "ideal" molarity behavior. From Figure 17, replacing K_2O with Na_2O greatly decreases the measured total rate of dissolution of the glasses as compared to the idealized cases. Furthermore, increasing the corrosion time from 6 hours to 1 day gives a corresponding increase in both Na^+ and K^+ ions in solution for all compositions investigated.

Bulk planar surface data for the $(X)Na_2O\cdot(0.25-X)K_2O\cdot(0.75)SiO_2$ glass series is shown in Figure 18 for 25° and 50°C corrosion tests. These curves illustrate the degree to which the measured Na^+ and K^+ lines deviated from their idealized values. The surface to volume ratio for these glasses was 0.77 cm^{-1}.

The effect of Na_2O or K_2O in a Li_2O glass system is shown in Figures 19 and 20, respectively. From previous investigations, as the size of the alkali ions increases, the rate of dissolution of the glass increases.[37-39] For Li_2O-SiO_2 glasses containing 5 mole % Na_2O or K_2O, the Li^+ (smaller ion) dissolution decreases from the Li_2O end member, indicating a tendency toward a Classical Mixed-

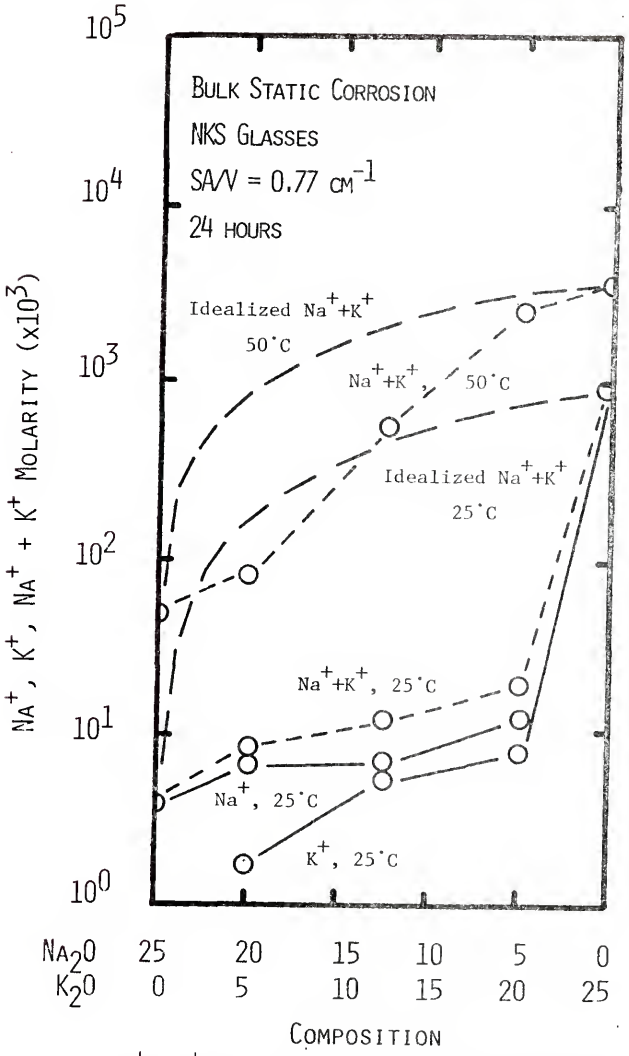

Figure 18. Na^+, K^+ and $Na^+ + K^+$ solution data for bulk corrosion in the $(X)Na_2O\cdot(1-X)K_2O\cdot(0.75)SiO_2$ glass system.

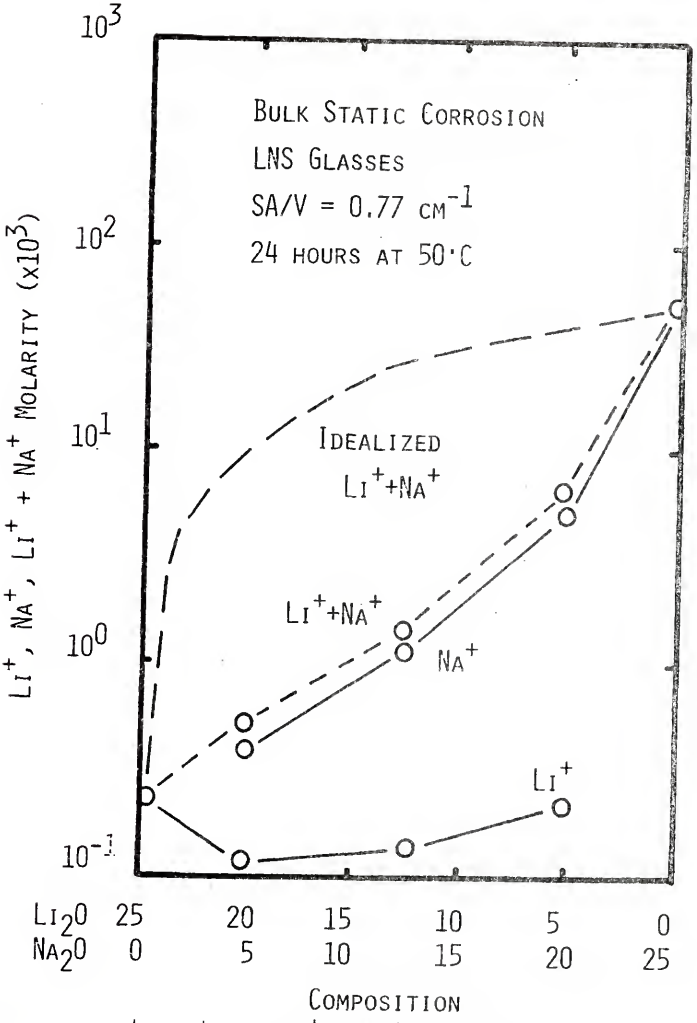

Figure 19. Li^+, Na^+ and $Li^+ + Na^+$ solution data for bulk corrosion in the $(X)Li_2O\cdot(1-X)Na_2O\cdot(0.75)SiO_2$ glass system.

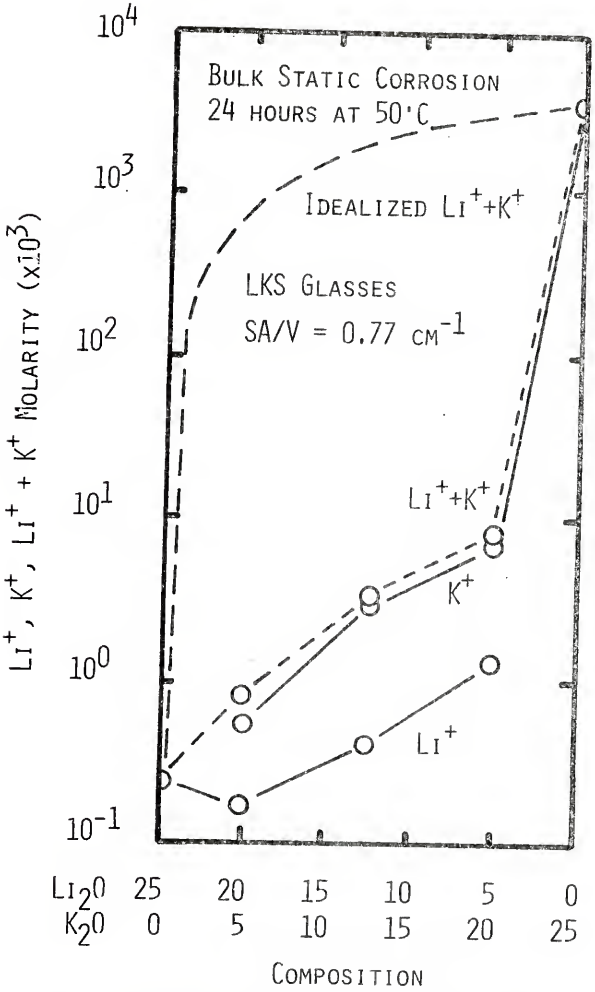

Figure 20. Li^+, K^+ and $Li^+ + K^+$ solution data for bulk corrosion in the $(X)Li_2O\cdot(1-X)K_2O\cdot(0.75)SiO_2$ glass system.

Alkali Effect. However, both the Na^+ and K^+ dissolution concentrations compensate for the decreased Li^+ concentration and therefore eliminate a Classical Mixed-Alkali Effect. However, since a significant departure from the idealized behavior exists, a Mixed-Alkali Effect does occur, although it is not classical.

Li^+ and Na^+ alkali ion dissolution results for the $(X)Li_2O\cdot(0.33-X)Na_2O\cdot(0.67)SiO_2$ glass system are shown in Figure 21. It is of interest that the rate of Li^+ dissolution after 240 hours (10 days) is comparable with the rate of Na^+ dissolution after 6 hours (1/4 day), indicating that Na^+ ions are extracted from the glasses at a much faster rate than are the Li^+ ions.

Si^{+4} dissolution concentrations corresponding to the alkali dissolution results of Figure 21 are shown in Figure 22.

Using infrared reflection spectroscopy (IRRS), the formation of surface films from degradation of the mixed-alkali glasses can be monitored.[36,40] Figures 23a-d illustrate the dominant mode of corrosion for the mixed-alkali ternary $(X)Li_2O\cdot(0.33-X)\cdot Na_2O\cdot(0.67)SiO_2$ glass system. The 33 mole % Na_2O glass exhibits a greater tendency towards total dissolution after 1 day, 50°C as evidenced by the presence of both the Si-O-Si stretch peak and the NSL (alkali) peak than does the corresponding

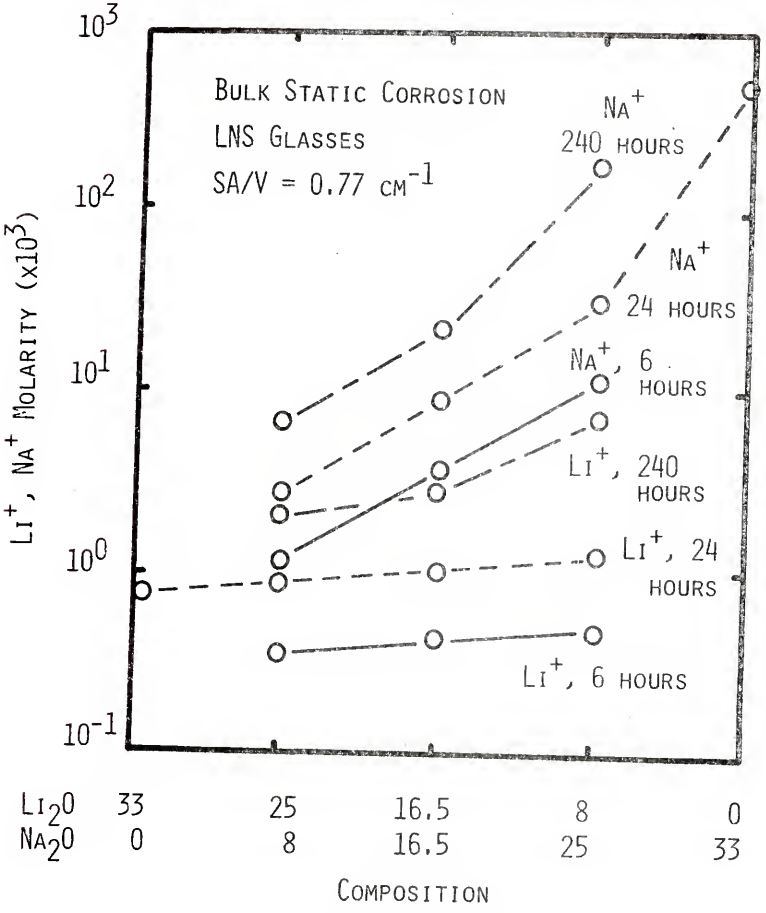

Figure 21. Li^+ and Na^+ solution data for bulk corrosion in the $(X)Li_2O\cdot(1-X)Na_2O\cdot(0.67)SiO_2$ glass system.

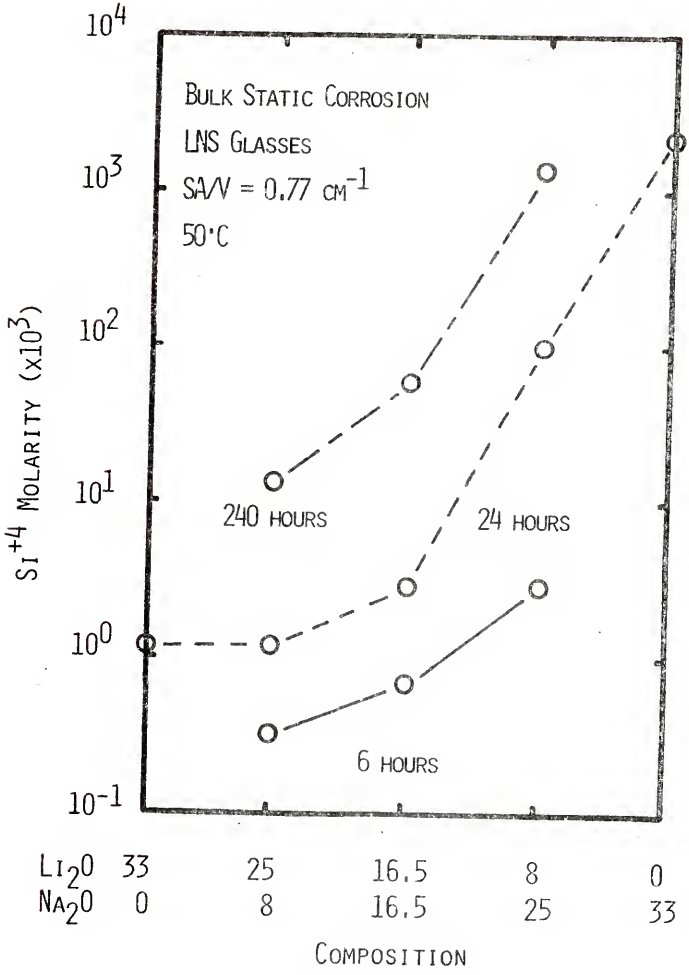

Figure 22. Si^{+4} solution data for bulk corrosion in the $(X)Li_2O \cdot (1-X)Na_2O \cdot (0.67)SiO_2$ glass system.

Figure 23. Infrared reflection spectra for bulk corrosion of the LNS-3300, LNS-16.516.5, LNS-0825 and LNS-0033 glass compositions.

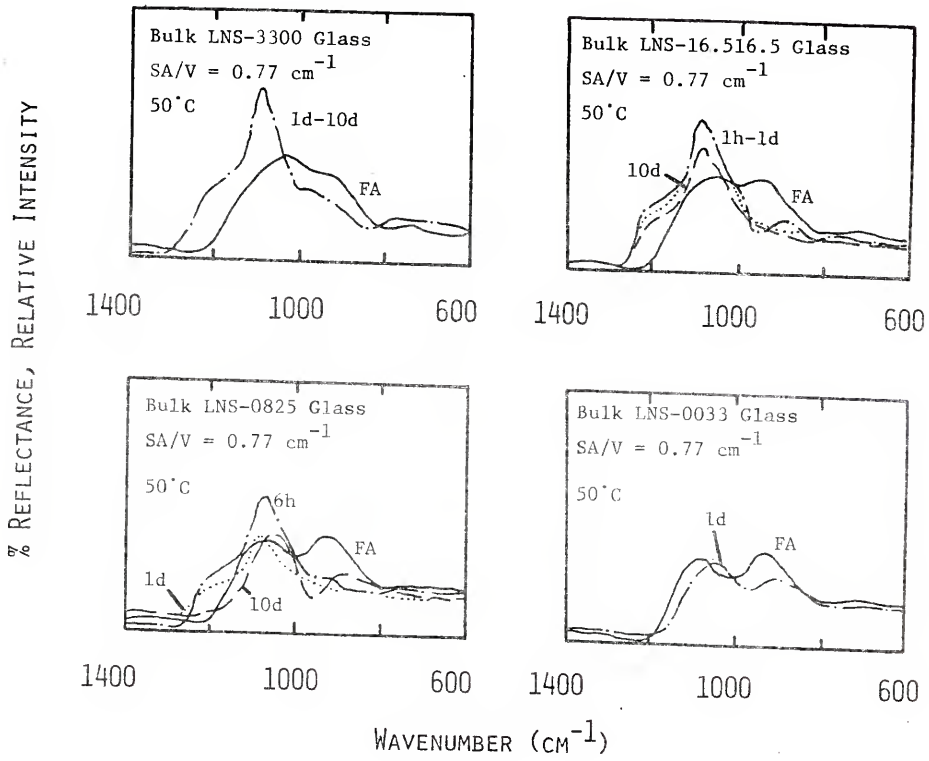
Bulk LNS-3300 Glass
SA/V = 0.77 cm^{-1}
50°C
1d-10d
FA
Bulk LNS-16.516.5 Glass
SA/V = 0.77 cm^{-1}
50°C
1h-1d
10d
FA
Bulk LNS-0825 Glass
SA/V = 0.77 cm^{-1}
50°C
6h
FA
1d
10d
Bulk LNS-0033 Glass
SA/V = 0.77 cm^{-1}
50°C
1d
FA
1400
1000
600
% Reflectance, Relative Intensity
Wavenumber (cm^{-1})

Li_2O glass, i.e., there is no NSL peak present. For the mixed-alkali glasses, as the % Na_2O increases the tendency towards total dissolution also increases. Again, this is determined by the presence of both the Si-O-Si stretch peak and the NSL peak.

Discussion: Ternary Glasses

From the definition of the Classical Mixed-Alkali Effect (CMAE) reduced diffusion rates occur for mixed-alkali glasses over those rates observed for both single alkali glasses.[5,17-23,29-35]

Experiments performed by Yastrebova and Antonova[18] indicate that a Classical Mixed-Alkali Effect is observed in the $(X)Na_2O\cdot(0.20)K_2O\cdot(0.80)SiO_2$ glass series corroded in 2N HCl-H_2O solution of pH = -0.03. The CMAE is expected in solutions where pH $\leq$ 9, since this is the pH range where alkali diffusion affects the corrosion process. However, for pH > 9, the CMAE will not be observed because total dissolution is the dominant corrosion mechanism in this pH range and alkali diffusion is not important in total dissolution.

From the previous discussion of quaternary glasses, ideal, linear corrosion behavior is represented by mechanical-mixtures of single alkali glasses. In Figure

17, no Classical Mixed-Alkali Effect is observed for the $(X)Na_2O\cdot(0.20-X)K_2O\cdot(0.80)SiO_2$ glass powders corroded in 3D-H_2O. These experiments may be contrasted with the 2N HCl-H_2O solution corrosion experiments conducted by Yastrebova and Antonova.[18] In the 3D-H_2O experiments, the pH is not sufficiently low (initial pH = 6.5) to maintain the corrosion process in the selective leaching mode and hence, the total dissolution mode rapidly becomes important. Hence, no Classical Mixed-Alkali Effect is observed. Although no CMAE is evident in Figure 17, for the 6 hour or 1 day corrosion tests, a Mixed-Alkali Effect (MAE) is evident when the measured $Na^+ + K^+$ concentration curves of the chemical mixtures are compared with the projected idealized $Na^+ + K^+$ concentration curves.

Alkali solution results for the $(X)Li_2O\cdot(0.25-X)Na_2O\cdot(0.75)SiO_2$ and $(X)Li_2O\cdot(0.25-X)K_2O\cdot(0.75)SiO_2$ glass series are shown in Figures 19 and 20 respectively. Although there is a minimum in Li^+ ion concentrations in both curves of Figures 19 and 20, no minima in the total alkali concentration levels ($Li^+ + Na^+$, $Li^+ + K^+$) are observed and thus no CMAE is observed. However, as was the case in Figures 17 and 18, a MAE is observed.

Li^+ and Na^+ results in Figure 21 for the $(X)Li_2O\cdot(0.30-X)Na_2O\cdot(0.67)SiO_2$ glass series confirm the results

of previous figures, i.e., the absence of a CMAE and the presence of a MAE. It is of interest to note that this alkali composition range is often the range investigated in the Mixed-Alkali Effects in electrical properties.[19,23,29]

It was observed from Figure 18 that temperature in general does not directly affect the presence of the CMAE. From Figures 18 and 21 it is seen that the alkali composition range does not appear to affect the absence of the CMAE. Likewise, the Si^{+4} results of Figure 22 confirm that no CMAE is observed.

IRRS spectral results of Figure 23 confirm the solution results of Figures 21 and 22, i.e., the absence of the CMAE. From Figures 21-23, it is seen that the chemical durability decreases progressively from the Li_2O end member to the Na_2O end member. In Figure 23, the Li_2O-Na_2O-SiO_2 mixed-alkali glasses are classified according to their corrosion modes, i.e., selective leaching and total dissolution: (a) LNS-3300, selective leaching is the primary mode of corrosion. This is evidenced by the increase in the Si-O-Si stretch peak and the decreased NSL peak for long periods of time. (b) LNS-16.516.5, selective leaching is the dominant corrosion mode with total dissolution in a minor role. The Si-O-Si stretch peak is not as durable as that observed for the 3300 composition, while the

minor role of total dissolution is shown by the overall decrease in the IR spectra. (c) LNS-0325, total dissolution is the dominant corrosion mode with selective leaching in a minor capacity. The rapid increase in the Si-O-Si peak occurs because of the selective leaching process; however, the rapid decrease in this peak and the presence of the NSL peak for long periods of time indicates total dissolution is in control of the corrosion process. (d) LNS - 0033, total dissolution is the primary mode of corrosion. It is apparent that total dissolution is the mode of corrosion because the spectra after corrosion is similar to the freshly abraded surface, with the exception that the magnitude is slightly decreased.

Conclusions

I. The Mixed-Alkali Effect may be placed into two categories: (a) a Classical Mixed-Alkali Effect (CMAE) is present when a minimum in the total alkali ion concentration curve is observed in relationship to the single alkali end members and (b) a Mixed-Alkali Effect (MAE) is present when the chemical-mixture curve is below the idealized total alkali concentration curve (mechanical-mixtures).

II. Both CMAE and MAE appear to consist of two contributions: (a) structural effects in which the mixed-alkali ions present in the glass structure result in a decrease in the corrosion rate, and (b) corrosion ion effects in which mixed-alkali ions are present together in the same corrosion solution and cause a lowering of the ion-exchange rate at the glass-solution interface.

III. The magnitude of the CMAE appears to go through a maximum for glass powders and is not very extensive in either the early-stage of corrosion (short times) or in later-stage corrosion where total dissolution occurs (long times and pH > 9).

IV. The presence of the CMAE or MAE is a function of corrosion solution pH. For pH $\leq$ 9, selective leaching is the dominant mode of corrosion and a CMAE or MAE may be present because selective leaching is dependent upon alkali diffusion. For pH > 9, total dissolution is the dominant mode of corrosion. In this pH range, a CMAE or MAE is not present as expected because total dissolution is not dependent upon alkali diffusion.

V. The magnitude of the CMAE or MAE is dependent upon the following factors: (a) corrosion time--for

short periods of time and pH $\leq$ 9, a small CMAE or MAE is present, for intermediate times and pH $\leq$ 9, the CMAE or MAE increases. When pH > 9 after long periods of time, the CMAE or MAE is not present or is diminishing. (b) corrosion temperature--the CMAE or MAE is more likely and lasts longer for low temperatures. This is because the reaction kinetics are slower at lower temperatures, and hence result in lower pH values. For higher temperatures, the CMAE or MAE is observed for only short times, for longer times the reaction will switch to total dissolution and the CMAE or MAE diminishes. (c) glass composition--in general, the more durable mixed-alkali glasses exhibit the CMAE, while the less durable mixed-alkali glasses exhibit the MAE. (d) SA/V--in general, an increase in the SA/V ratio results in an increase in the CMAE or MAE, however, as was the case in the other factors, the pH of the corrosion solution determines the extent and magnitude of the effect.

VI. Structural contributions to the total CMAE or MAE can be seen when the chemical- and mechanical-mixture curves are compared. This is probably due to the lower alkali diffusion rates in the chemical-mixture glasses as compared to the single alkali glasses.

VII. Solution ion contributions to the total MAE can be seen when the mechanical- and non-mixture curves are compared. Combining of both single alkali soda and potassia glasses in the same corrosion solution by mechanical-mixing appears to retard the corrosion process.

VIII. The molarities of sodium, potassium, calcium, and silicon and pH are solution variables used in establishing the presence of a CMAE/MAE.

IX. Physical evidence for the Classical Mixed-Alkali Effect independent of solution ion analysis has been shown with infrared reflection spectroscopy (IRRS) and with scanning electron microscopy (SEMs). Both techniques demonstrate that the 120310 glass composition is the most durable glass of the compositional range investigated in the $(X)Na_2O\cdot(0.15-X)K_2O\cdot(0.10)CaO\cdot(0.75)SiO_2$ glass system.

CHAPTER III
AQUEOUS CORROSION OF LITHIA-ALUMINA-SILICATE GLASSES

Introduction

The relative abundance of Al_2O_3 and its positive influence on glass durability makes it a commercially desirable glass additive. The importance of Al_2O_3 on glass durability has been known for many years.[1,5,6,41-45] Previous investigators have concluded that small additions of alumina (~3%) yield relatively higher increases in chemical durability than do larger additions (>5%).[1,6,41,45] However, these earlier studies were carried out in complex glass systems (usually Na_2O-CaO-Al_2O_3-SiO_2) instead of a simple alkali-alumina-silicate ternary glass system. In order to evaluate the effect of Al_2O_3 on glass durability, it is necessary to eliminate other additions (i.e., CaO) from the glass composition that may also improve glass durability. Comparison of ternary glass corrosion behavior with that of binary glasses without alumina should elucidate the role of alumina in glass durability.

The relative percentage of non-bridging oxygen ions present in a glass structure determines its chemical durability.[46,47] Usually, if a glass has a high percentage

of non-bridging oxygens present (number of non-bridging oxygens ≈ number of alkali ions), the glass will exhibit poor durability. If however, the percentage of non-bridging oxygens is low (low alkali, high silica), the glass will have less tendency to corrode.

The behavior of alkali-alumina-silicate glasses is determined by the principle that equivalent percentages of alkali (R_2O) and alumina (Al_2O_3) addded to a silicate glass do not produce any non-bridging oxygens.[17,47-49] This situation occurs because aluminum ions added to an alkali-silicate glass with an alkali/aluminum ratio >1 are in 4-fold coordination (i.e., AlO_4^-) and require a positively charged alkali ion (R^+) for electrical neutrality (Figure 24).[49-52] Since all four oxygens are ionic-covalently bonded to the Al^{+3} ion, and the alkali ion associates with the AlO_4^- tetrahedral group, no non-bridging oxygens are produced. Thus, the addition of alumina proves to be an effective means to increase the chemical durability of a glass, since the Al^{+3} ions change the high reactive non-bridging oxygens which are highly polarized into less reactive Al-O-Si bridging oxygens which are less polarized.

The ionic radius of the alkali ions present in an alkali-alumina-silicate glass also affects the chemical

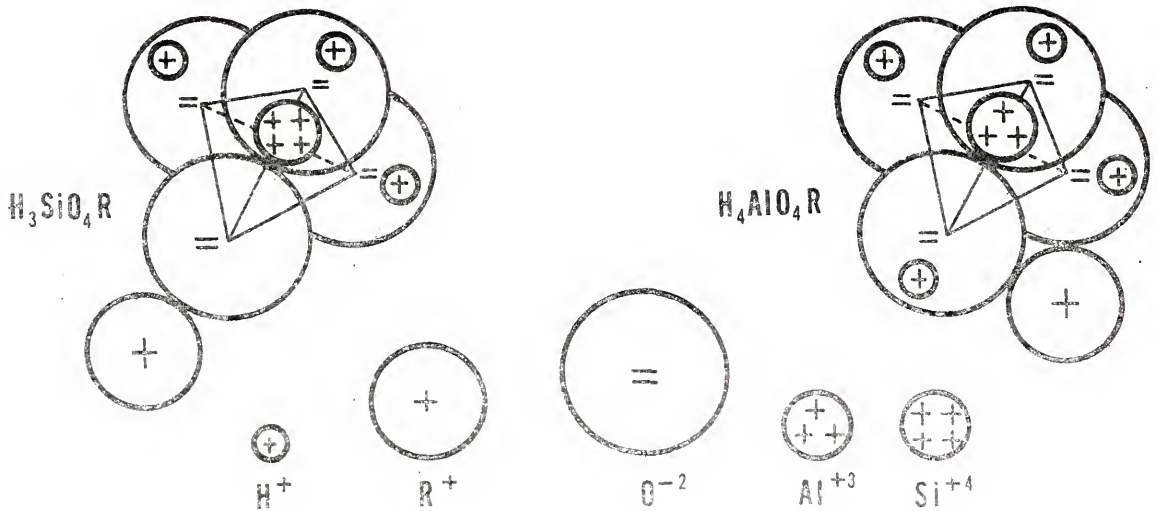

Figure 24. Schematic of the H_3SiO_4R and H_4AlO_4R tetrahedra, illustrating the difference in location of the alkali ion, R.

durability.[53,38,39] Large radius alkali-alumina-silicate glasses (i.e., $K_2O \cdot Al_2O_3 \cdot SiO_2$) have oxygen ions of relatively higher polarization and reactivity than do smaller alkali-alumina-silicate glasses ($Li_2O \cdot Al_2O_3 \cdot SiO_2$).[17]

The most significant feature of alkali-alumina-silicate glasses is that hydrogen ion (H^+) permeation (hence ion-exchange and corrosion) is kept at a minimum for glasses containing oxygen ions of lowest polarizability and reactivity.[17] Since Li^+ ions impart the lowest polarizability to oxygen ions, lithia-alumina-silicate glasses are the most durable of the alkali-alumina-silicate glasses.[17,54]

In a simple binary alkali-silicate glass, the non-bridging, highly polarized (reactive) oxygen ions represent the strongest bond between the alkali ions and the silicate network. When the highly polarized non-bridging oxygens are changed into less polarized oxygens associated with AlO_4^- groups, the alkali ions are no longer associated with a single highly polarized non-bridging oxygen, but with a large AlO_4^- slightly polarized complex as shown in Figure 24.[47,49,55] Hence, the addition of Al_2O_3 not only weakens the bonds of the alkali ions, but also changes their distribution toward one which is more favorable toward ionic diffusion.

Although conditions are more favorable for ionic diffusion in alkali-alumina-silicate glasses,[5,17,56] conditions are not favorable for hydrogen ion (H^+) permeation, i.e., ion-exchange, because of the low polarization of the oxygen ions.[17] The oxygen ions in glasses containing alumina are less polarized than those in binary glasses, with the same being true of the alkali ions. This means that the associated alkali ions in the ternary glasses have a higher diffusivity and hence lower polarization (i.e., ionic conductivity) than the highly polarized alkali ions in the binary glasses. Therefore, according to Weyl,[17] less polarized alkali ions (low polarized oxygen ions are associated with low polarized alkali ions) of ternary glasses have less tendency to ion-exchange with hydrogen ions in the corrosion solution than the alkali ions in binary glasses. Hence, hydrogen ion permeation is less favored in a lithia-silicate glass than in a potassia-silicate glass, with or without equivalent additions of Al_2O_3.

Corrosion of alumina containing glasses is not generally favored in the ion-exchange region of $pH > 7 \leq 9$. In this pH region, the pH is not sufficiently low to cause a high degree of ion-exchange and/or of a total breakdown due to the aluminum dissolving out of the glass leaving

a high porous silica network. Corrosion in solutions >9 (high basic solutions) also is not extensive. According to Doremus,[5] solubility studies have shown that the Al-O-Si bond is more stable than the Si-O-Si bond in aqueous basic solutions. However, in acidic solutions where pH << 7, the hydrated Al_2O_3 behaves as a weak base and thus is more soluble. This leads to a total breakdown of the glass structure.[5,49,57]

The objectives of this investigation were to (a) establish the relative effects of various percentages of alumina on Li_2O-Al_2O_3-SiO_2 glass corrosion, (b) investigate the effect of constant Li^+/Al^{+3} ratios upon glass corrosion, (c) determine the influence of pH upon glass dissolution in alumina glasses, (d) investigate the compositional dissolution path of various lithia-alumina-silicate glasses, and (e) establish a series of isochronal Si^{+4} corrosion curves for a set of specific time periods.

The answers to the above questions will provide information concerning the compositional path of corrosion allowing one to predict the total dissolution behavior of the lithia-alumina-silicate glass system. Furthermore, by comparison of the isochronal corrosion curves (Si^{+4}) with other critical processing variables (i.e., melting temperature), an optimum glass composition with respect

to corrosion behavior and practicality can be tailor-made for any specialized application.

Experimental Procedure

The glasses shown in Table V and Figure 25 were prepared from reagent grade Li_2CO_3, Al_2O_3, and 5 μm SiO_2 powder.* Glass batches were melted in closed Pt crucibles for 24 hours in an electric muffle furnace between 1300-1500°C, depending on the glass composition (refer to Table V). The molten glass was cast between graphite blocks and given a 4 hour annealing period between 475-525°C, again depending on the glass composition (refer to Table V).

Specimens 3/4" x 3/4" x 1/4" were sectioned from glass plates, polished through 600 grit SiC paper, and stored in a desiccator. Prior to the testing procedure, the specimens were given a final abrasion with 600 grit dry SiC paper to eliminate environmental effects.

Static bulk corrosion tests were performed using methods and procedures described in previous papers.[25,26]

*Min-U-Sil from Pennsylvania Glass Sand Corp., Pittsburg Pa.

Table V

Alumina Glass Compositions Investigated, Mole %

Glass Code	% Li_2O	% Al_2O_3	% SiO_2	Melting Point (°C)	Annealing Point (°C)
LAS-20L5A	20.0	5.0	75.0	1500	525
LAS-33L2.5A	33.0	2.5	64.5	1350	500
LAS-33L5A	33.0	5.0	62.0	1375	500
LAS-33L11A	33.0	11.0	56.0	1450	525
LAS-46L5A	46.0	5.0	49.0	1300	475

Triple distilled H_2O (pH = 6.5) was used as the corrosion solution and corrosion tests were carried out for various times up to 41 days. The ratio of glass surface area to corrosion solution volume was 0.77 cm^2/cm^3 (cm^{-1}).

The quantity of dissolved silicon in the corrosion solution was determined by the molybdenum blue colorimeteric method.* Li^+ and Al^{+3} solution concentrations were determined by atomic emission** and atomic adsorption*** spectroscopy, respectively. The pH of the corrosion solutions was checked with pH indicator paper.**** The resolution of the various solution analysis techniques described above are shown in Table II.

Bulk samples were vacuum coated with ~150 Å of Au-Pd and analyzed with the scanning electron microscope (SEM).***** Bulk samples not coated were analyzed using Auger electron spectroscopy[16] (AES)****** and by infrared

*Hach "Direct Reading" Colorimeter, Hach Chemical Co., Ames, Iowa.
**Beckman B Spectrometer, Beckman Instruments Inc., Fullerton, Calif.
***Perkin-Elmer Model 303 spectrometer, Perkin-Elmer Corp., Norwalk, Conn.
****Gallard-Schlesinger Chemical Mfg. Corp., Carle Place, New York.
*****Cambridge Stereoscan, Kent Cambridge Scientific, Inc., Morton Grove, Ill.
******Physical Electronics Ind., Model 10-150 spectrometer

reflection spectroscopy[15] (IRRS).* IRRS scans were run at a medium rate from 1400 cm^{-1} to 600 cm^{-1}. The spectra of the corroded samples were compared to the spectra of the freshly abraded glasses.

Results

The range of glass compositions investigated is shown in Figure 25. Major emphasis on evaluating the corrosion behavior of this matrix of compositions was confined (glasses listed in Table V) to the following glass series: a) $(X)Li_2O\cdot(0.15)Al_2O_3\cdot(0.95-X)SiO_2$; and, b) $(0.33)Li_2O\cdot(X)Al_2O_3\cdot(0.67-X)SiO_2$.

Lithium ion concentrations measured as a function of corrosion time for the two glass series described above. are shown in Figure 26. Approximate linear relations are observed for regions of these plots. As the mole % Li_2O increases in the glass, the rate of Li^+ going into solution also increases for a constant 5 mole % Al_2O_3 (Figure 26a). As the Al_2O_3 composition level decreases (maintaining a constant 33 mole % Li_2O), the rate of Li^+ dissolution increases (Figure 26b).

*Perkin-Elmer Model 467 IRRS, Perkin-Elmer Corp., Norwalk, Conn.

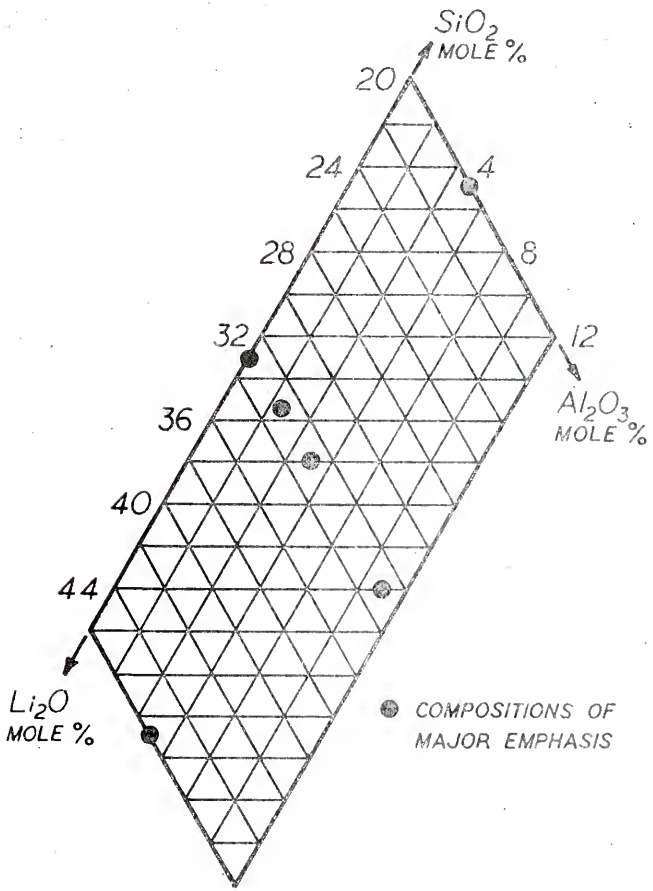

Figure 25. Ternary diagram illustrating the range of glass compositions investigated and in particular, compositions of major emphasis.

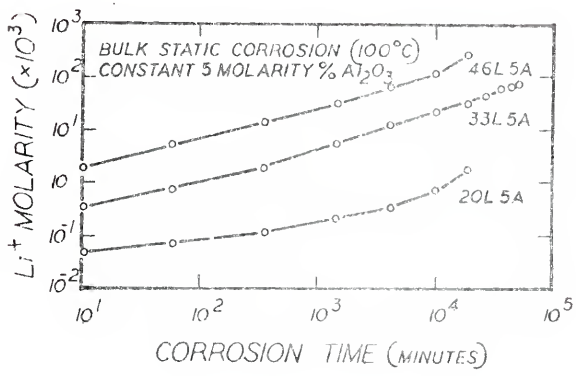

(a)

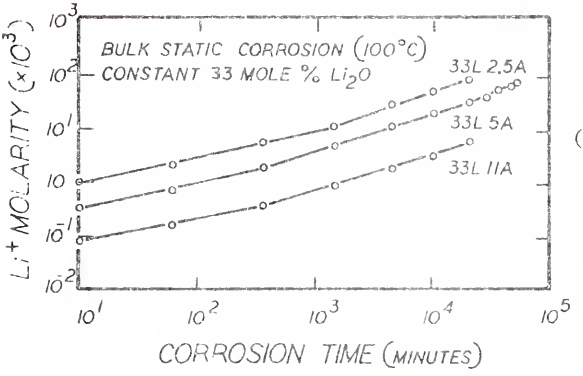

(b)

Figure 26. Li^+ solution data for bulk corrosion in the following glass series:
(a) $(X)Li_2O\cdot(0.05)Al_2O_3\cdot(1-X)SiO_2$ glasses and
(b) $(0.33)Li_2O\cdot(X)Al_2O_3\cdot(1-X)SiO_2$ glasses.

A parameter that is related to Li^+ solution concentration is the pH of the corrosion solution. In Figure 27, the pH of the corrosion solution measured as a function of corrosion time is shown for these glasses. Dramatic changes in pH were observed during the first 6 hours of corrosion for the glasses containing 5 mole % Al_2O_3 and $\geq$ 33 mole % Li_2O. In contrast, the 20 mole % Li_2O glass with the same Al_2O_3 content (5 mole %) showed no significant change even after 14 days of corrision (Figure 27a). Figure 27b illustrates similar results for glasses containing a constant 33 mole % Li_2O and various Al_2O_3 content. The major feature of this graph is that the rate of change of solution pH is inversely related to the mole % Al_2O_3 in the glass.

The Si^{+4} concentration in solution versus corrosion time shown in Figure 28 corresponds to the Li^+ concentration in solution shown in Figure 26 (i.e., same glass compositions and corrosion times). The rate of change of Si^{+4} in solution increases as the Li^+ in the glass increases (maintaining a constant 5 mole % Al_2O_3, Figure 27a), and as the mole % Al_2O_3 in the glass decreases (maintaining a constant 33 mole % Li_2O, Figure 27b).

Si^{+4} concentration versus mole % Al_2O_3 (constant 33 mole % Li_2O) for various corrosion times is shown in

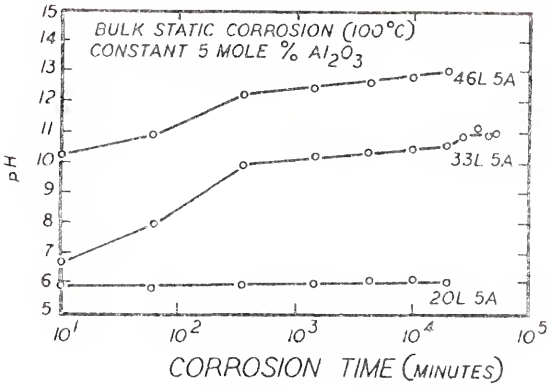

(a)

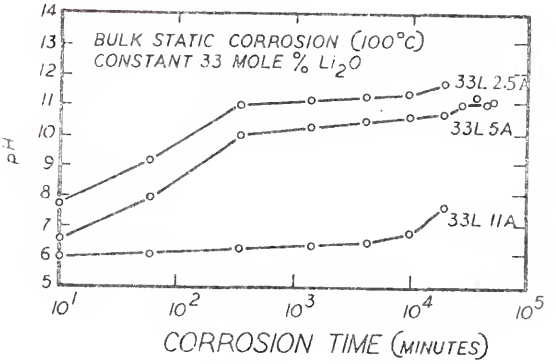

(b)

Figure 27. pH solution data for bulk corrosion in the following glass series:
(a) $(X)Li_2O\cdot(0.05)Al_2O_3\cdot(1-X)SiO_2$ glasses and
(b) $(0.33)Li_2O\cdot(X)Al_2O_3\cdot(1-X)SiO_2$ glasses.

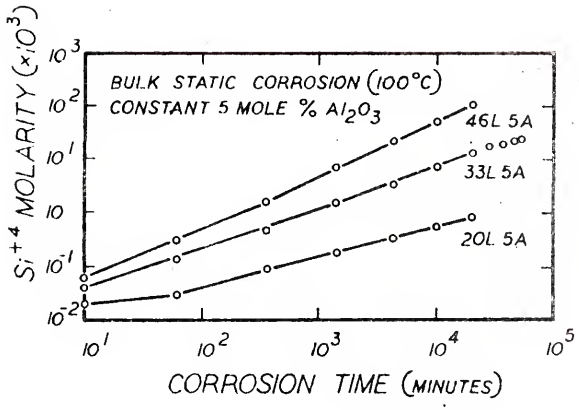

(a)

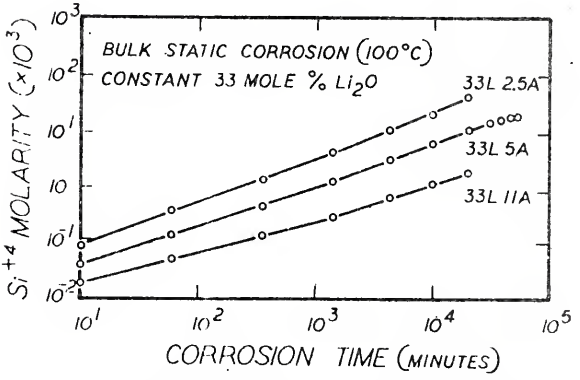

(b)

Figure 28. Si^{+4} solution data for bulk corrosion in the following glass series:
(a) $(X)Li_2O\cdot(0.05)Al_2O_3\cdot(1\text{-}X)SiO_2$ glasses and
(b) $(0.33)Li_2O\cdot(X)Al_2O_3\cdot(1\text{-}X)SiO_2$ glasses.

Figure 28. Although increasing the mole % of Al_2O_3 up to 11% continually decreases the rate of Si^{+4} dissolution, the most significant improvements in glass durability are observed for the first 2.5 mole % addition.

Li^+ concentration versus mole % Al_2O_3 (constant 33 mole % Li_2O) for various corrosion times is shown in Figure 29. Li^+ results from Figure 30 follow the same trends established by Si^{+4} results of Figure 29; however, in this case, there is more nearly a linear behavior for Li^+ dissolution and the effect for the first 2.5% is less than that for larger percentages.

Figures 31-35 represent a series of projected isochronal corrosion plots of the Si^{+4} solution concentrations for a set of specific corrosion times and for a 100°C solution temperature. The lines representing constant Si^{+4} dissolution were constructed from curves similar to those represented in Figure 29. All glass compositions shown on the ternary phase diagram falling on a given isochronal line yield the same Si^{+4} concentration for the indicated corrosion time. Although not shown, similar isochronal corrosion plots can be constructed for Li^+ solution concentrations (using the type of plots shown in Figure 30) and for the Al^{+3} solution concentrations.

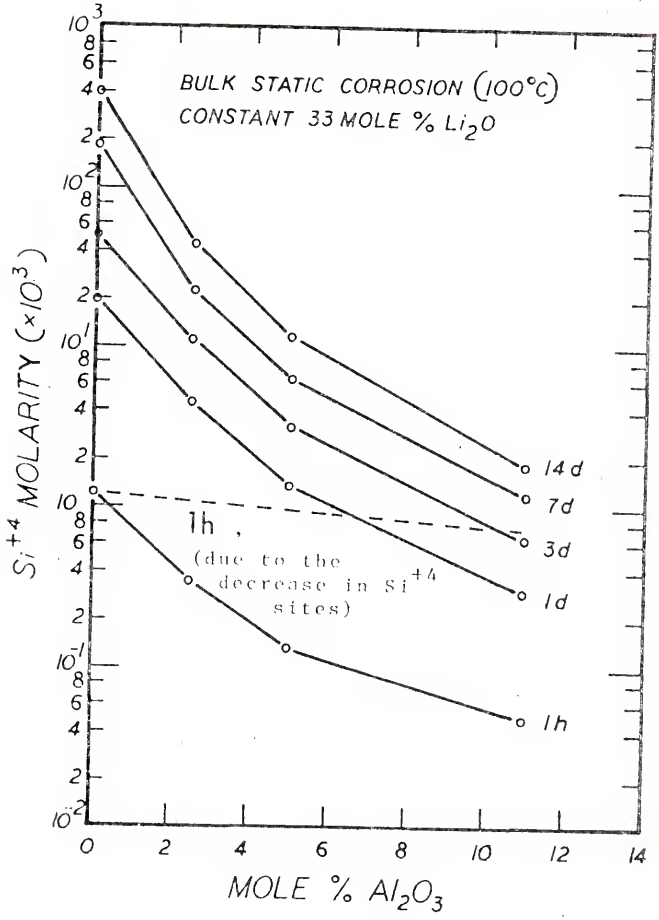

Figure 29. Si^{+4} solution data for bulk corrosion in the $(0.33)Li_2O\cdot(X)Al_2O_3\cdot(1-X)SiO_2$ glass system.

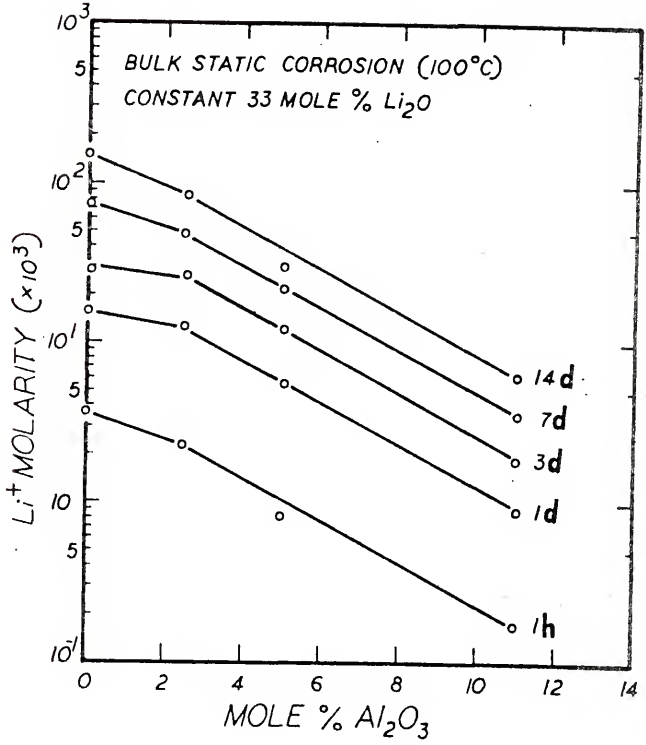

Figure 30. Li^+ solution data for bulk corrosion in the $(0.33)Li_2O\cdot(X)Al_2O_3\cdot(1-X)SiO_2$ glass system.

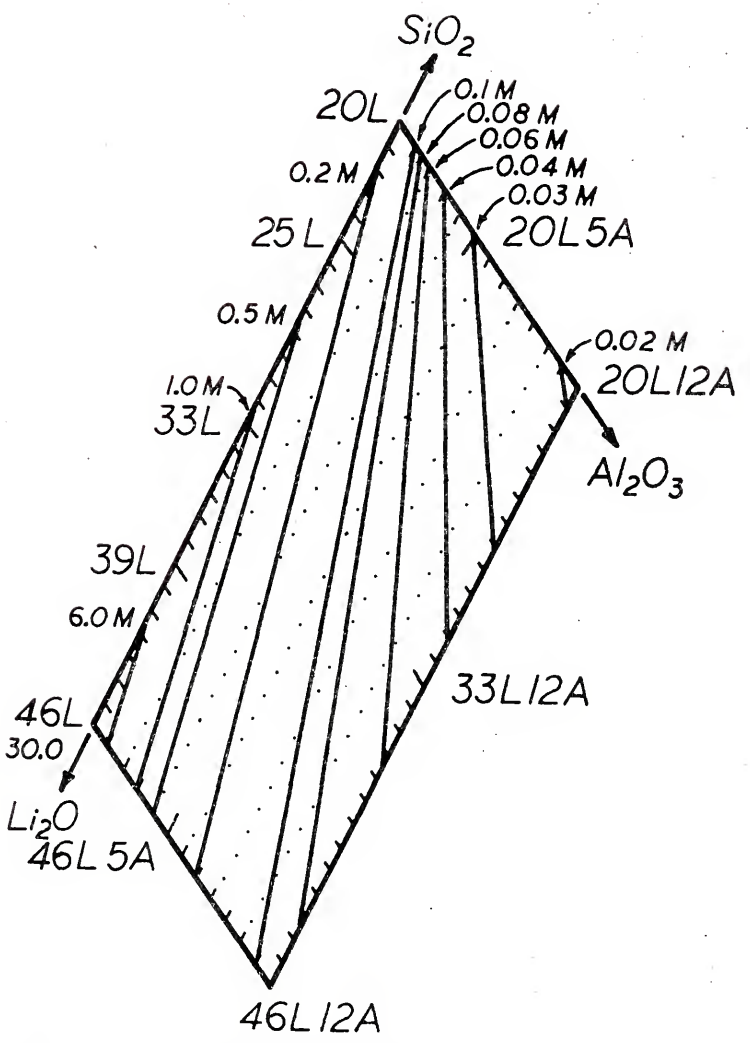

Figure 31. Projected isochronal Si^{+4} molarity ($X10^3$) ternary diagram for bulk static corrosion of Li_2O-Al_2O_3-SiO_2 glasses at 100°C for 1 hour.

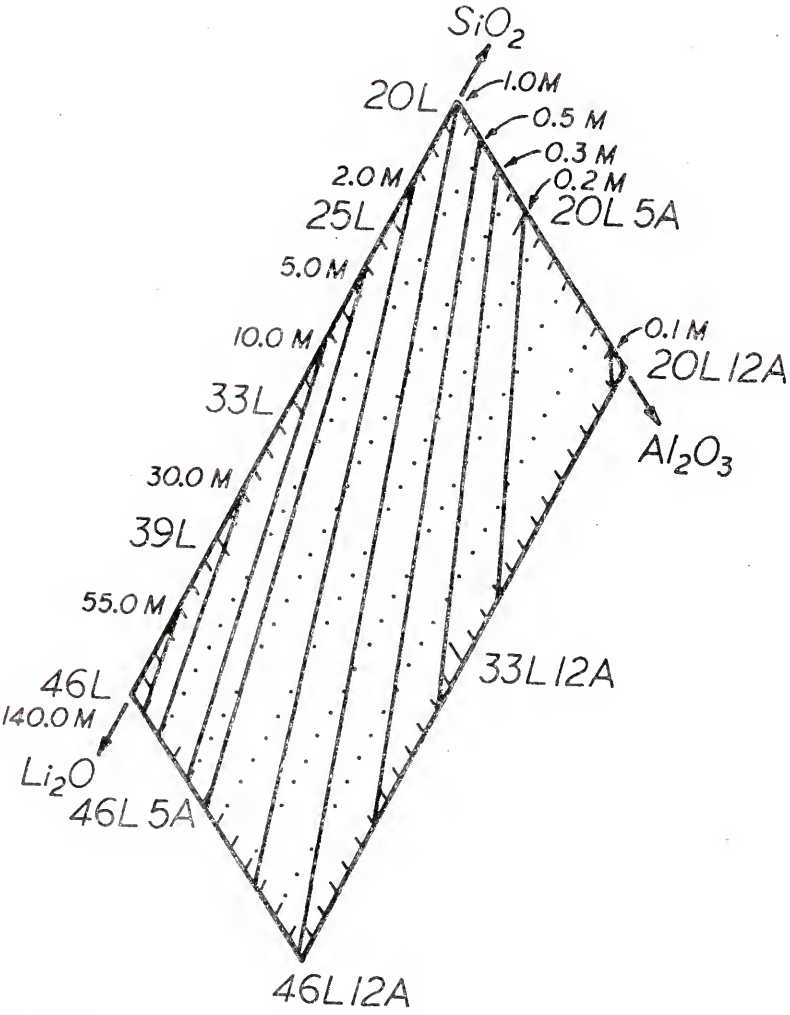

Figure 32. Projected isochronal Si^{+4} molarity ($X10^3$) ternary diagram for bulk static corrosion of Li_2O-Al_2O_3-SiO_2 glasses at 100°C for 1 day.

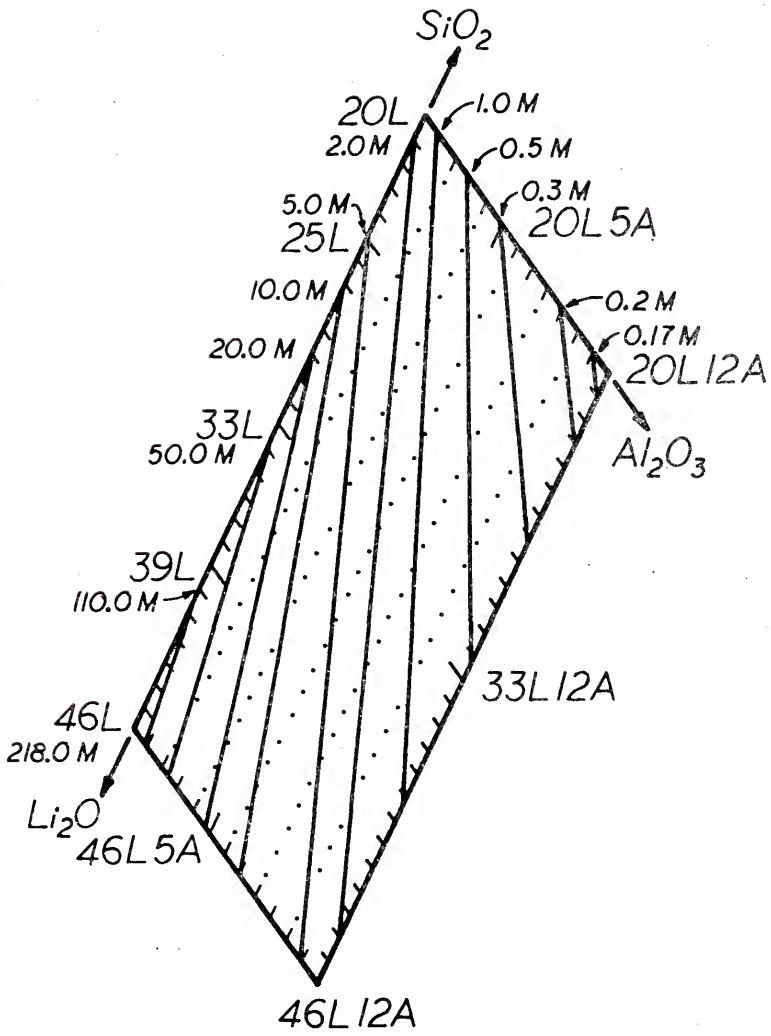

Figure 33. Projected isochronal Si^{+4} molarity ($X10^3$) ternary diagram for bulk static corrosion of Li_2O-Al_2O_3-SiO_2 glasses at 100°C for 3 days.

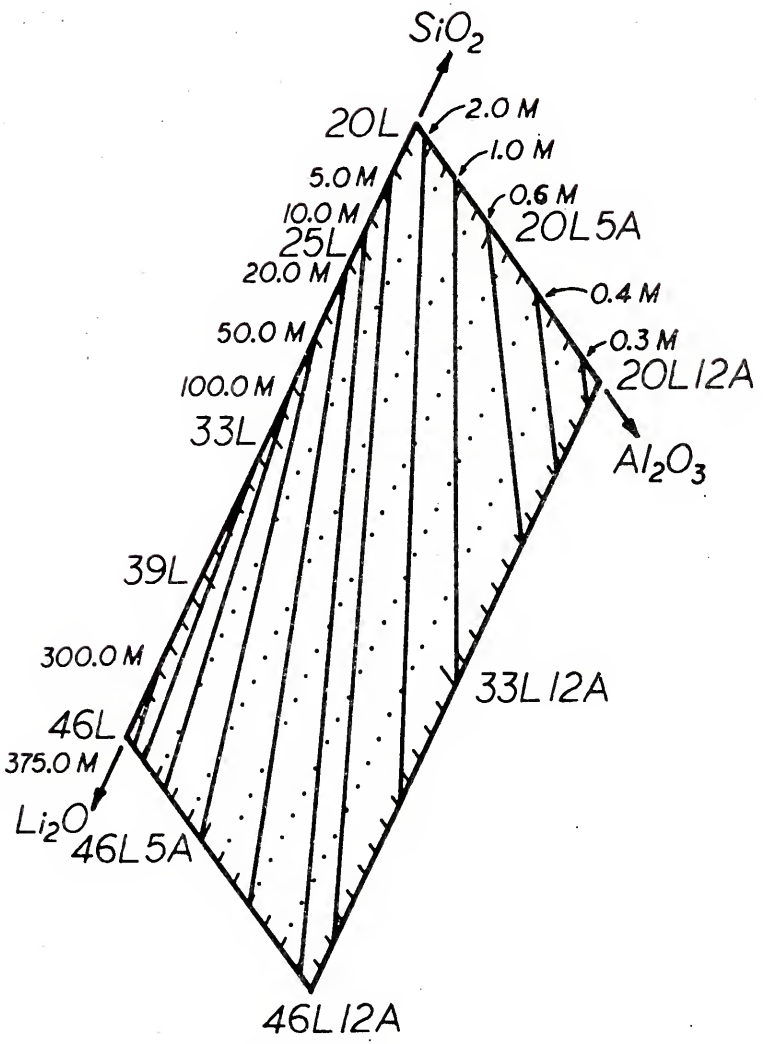

Figure 34. Projected isochronal Si^{+4} molarity ($X10^3$) ternary diagram for bulk static corrosion of Li_2O-Al_2O_3-SiO_2 glasses at 100°C for 7 days.

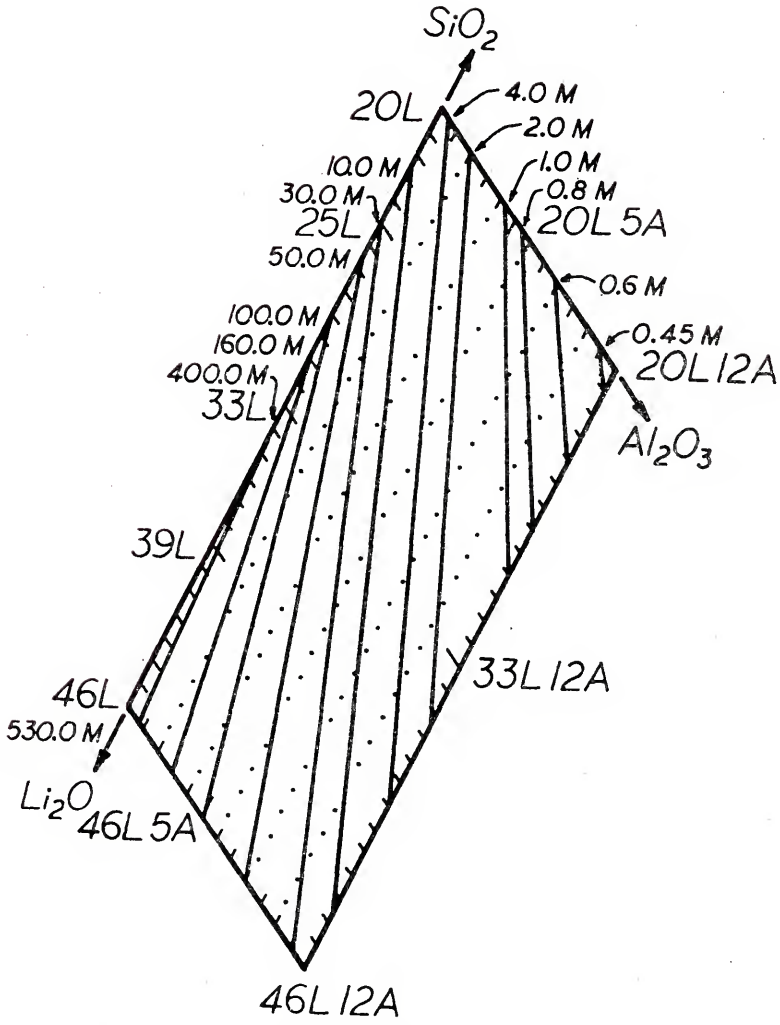

Figure 35. Projected isochronal Si^{+4} molarity ($X10^3$) ternary diagram for bulk static corrosion of Li_2O-Al_2O_3-SiO_2 glasses at 100°C for 14 days.

The Al^{+3} solution concentrations for the same conditions as the solution concentrations of Figure 26 are shown in Figure 36. In general, for short corrosion durations, i.e., $\leq$ 7 days, the solution concentrations of Al^{+3} increases as the Li_2O concentration in the glass increases (constant 5 mole % Al_2O_3) and as the Al_2O_3 in the glass decreases (constant 33 mole % Li_2O). No significant change in Al^{+3} solution concentration occurs for the 20L5A glass composition for the times investigated. The remainder of the glass compositions in Figure 36 reached a maximum in Al^{+3} solution concentration and gradually decreased for longer corrosion times (i.e., > 7 days).

Figures 37 and 38 show the results obtained from Auger electron spectroscopy (AES) for the 33L5A glass composition. In Figure 37, the AES signal for oxygen (560 eV), silica (200 eV), and aluminum (460 eV) are plotted versus ion-milling time (1 minute $\cong$ 30 Å milling depth[16]) for the freshly abraded (fa) glass. In Figure 38, the AES Al/Si signal ratios are plotted versus ion-milling time for several corrosion times. The Al/Si ratio is low at the near surface (<300 Å) but increases with ion-milling time for the freshly abraded glass (fa), 1 hour, and 7 day corroded specimens. At > 300 Å into the surface, the fa and 1h Al/Si ratios were almost identical while the

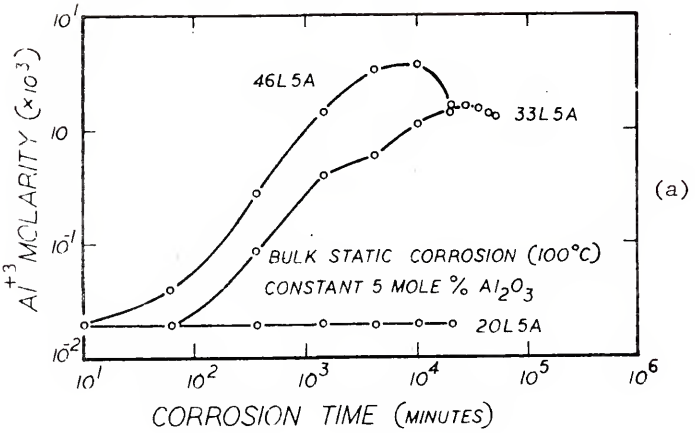

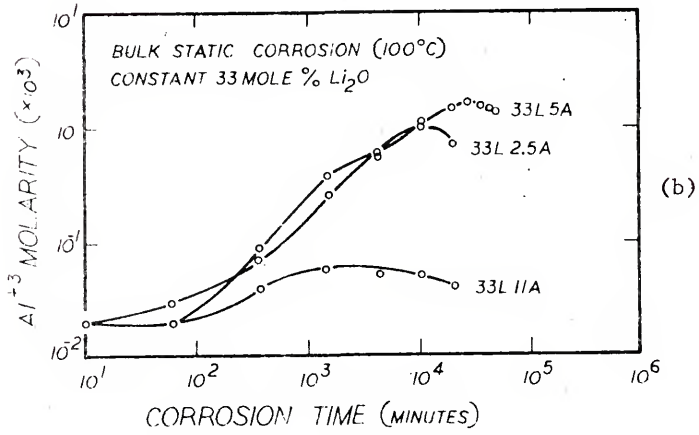

Figure 36. Al^{+3} solution data for bulk corrosion in the following glass series:
(a) $(X)Li_2O\cdot(0.05)Al_2O_3\cdot(1-X)SiO_2$ glasses and,
(b) $(0.33)Li_2O\cdot(X)Al_2O_3\cdot(1-X)SiO_2$ glasses.

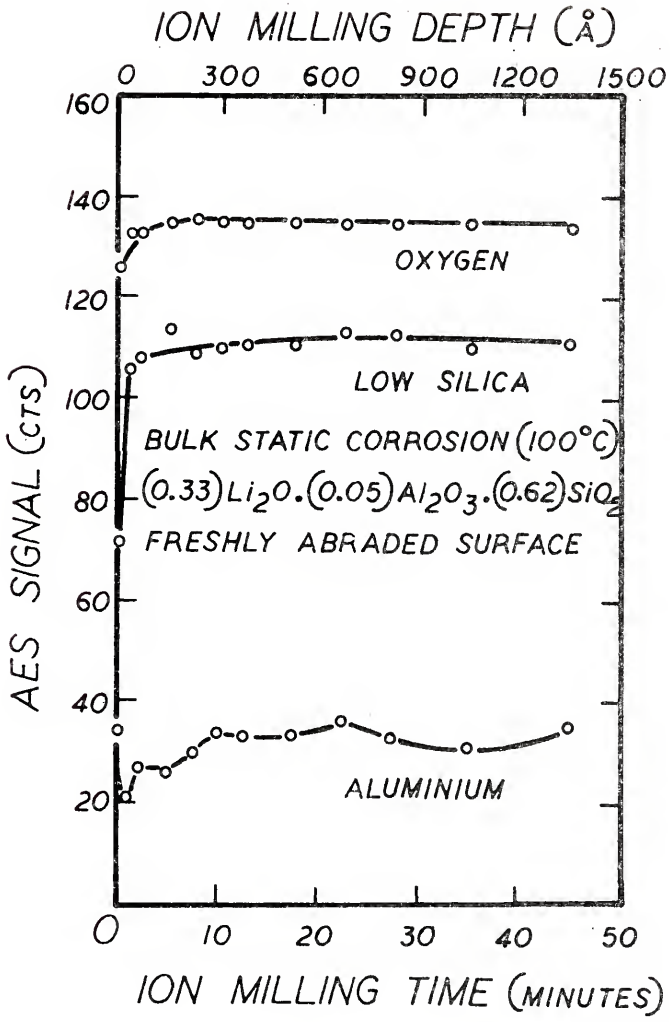

Figure 37. Auger electron spectroscopy (AES) signal at various depths for a freshly abraded bulk 33L5A glass.

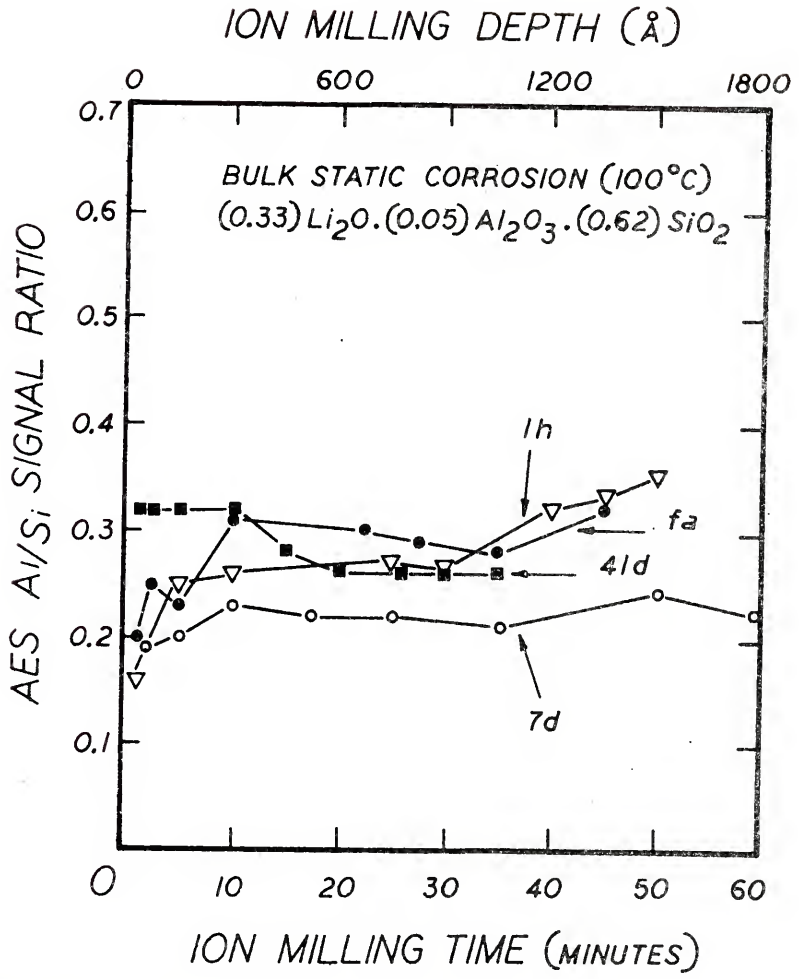

Figure 38. Auger electron spectroscopy (AES) Al/Si signal ratio at various depths for a bulk 33L5A glass after corrosion (1h - 41d).

Al/Si ratio for the 7d specimen was much less. In contrast, the Al/Si ratio for the 41d (41 day) specimen, although significantly higher at the near surface than the fa specimen, remained constant for a depth of ∿400 Å into the surface before decreasing to the value obtained for the fa and 1h specimens.

A parameter useful for evaluating the relative leaching tendency and total dissolution of glasses is α (equation 5).

Figure 39 illustrates the α (degree of selective alkali/aluminum leaching or total glass dissolution) dependence upon corrosion time for both glass series. The α values are low for short periods of time (< 1 hour) indicating the primary mode of corrosion to be selective leaching. As the corrosion time increases, α reaches maximum values and then decreases for longer corrosion times. All of the glass compositions attained maximum values of α except the 33L2.5A glass where α was still increasing after 10^4 minutes.

Another method of characterizing the selective leaching of alkali/aluminum and total glass dissolution mechanisms is to plot the molarity of the solution ions on a ternary plot. The comparison of the molarity-time compositional path with the actual ternary glass composition is

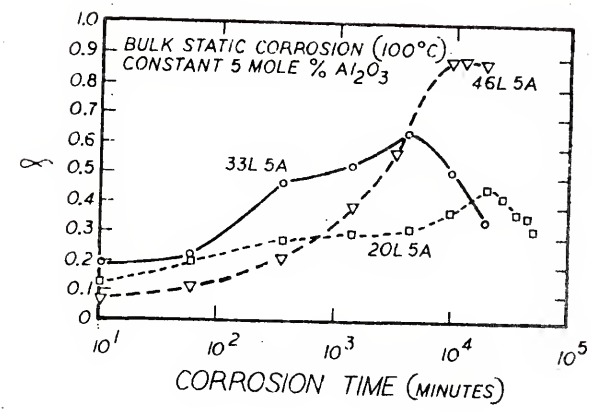

(a)

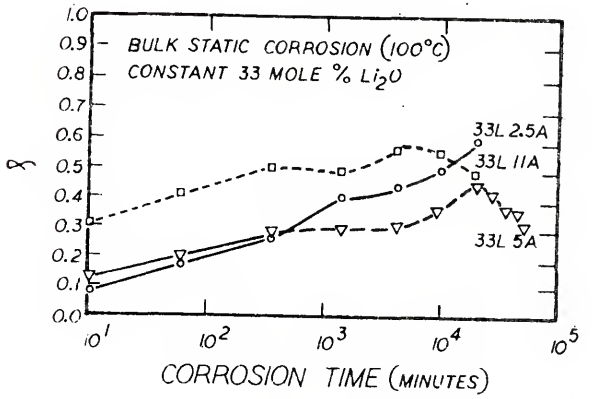

(b)

Figure 39. Alpha values for bulk corrosion in the following glass series:
(a) $(X)Li_2O\cdot(0.05)Al_2O_3\cdot(1\text{-}X)SiO_2$ glasses and
(b) $(0.33)Li_2O\cdot(X)Al_2O_3\cdot(1\text{-}S)SiO_2$ glasses.

an indication of the extent of selective leaching versus extent of total glass dissolution that occurred. When the solution ion ratio is equal to the glass ion ratio (i.e., solution molarity = glass molarity) total glass dissolution is occurring. The curves in Figures 40 and 41, shown on a ternary phase diagram, demonstrate the actual compositional corrosion path of the corroding glass. Consistent with Figure 39b, the 33L2.5A glass does not exhibit a reversal in its path toward total glass dissolution (Figure 41a).

Infrared reflection spectroscopy (IRRS) spectra of the compositions of Figures 40 and 41 are shown in Figures 42 and 43. Silica rich film formation (measured on IRRS spectra as an increase in the Si-O-Si stretch peak, $\sim$1080 μm^{-1}) occurs at a more rapid rate for the glasses high in lithia (low silica) than for glasses of low lithia (high silica) as shown in Figure 42. However, the films of the low lithia glasses are considerably more stable (spectral intensity remains relatively constant) over long periods of corrosion. In Figure 43, as the alumina content of the glass increases, the magnitude of the IRRS peak increases at a slower rate as compared to the spectra of Figure 42 and also shows less of a tendency to decrease with time (indicating only slight surface roughening).

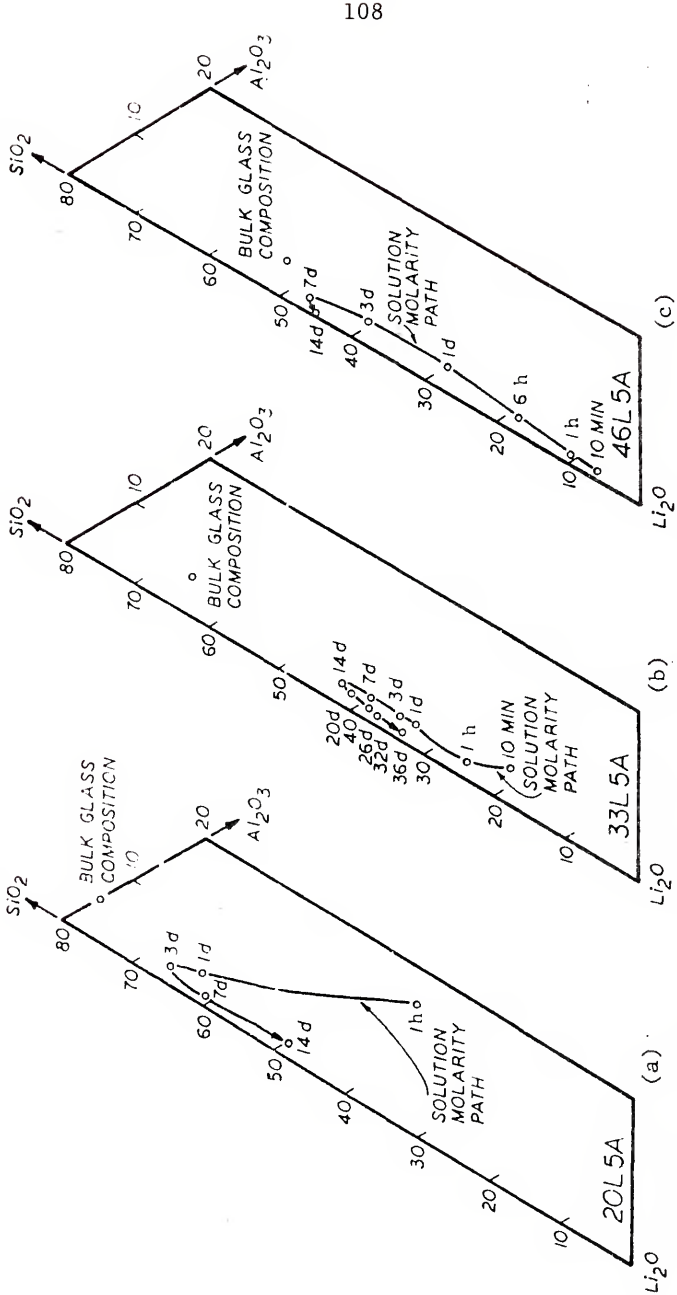

Figure 40. Alpha values plotted on a ternary diagram for bulk corrosion at 100°C of the following glasses: (a) 20L5A, (b) 33L5A and (c) 46L5A.

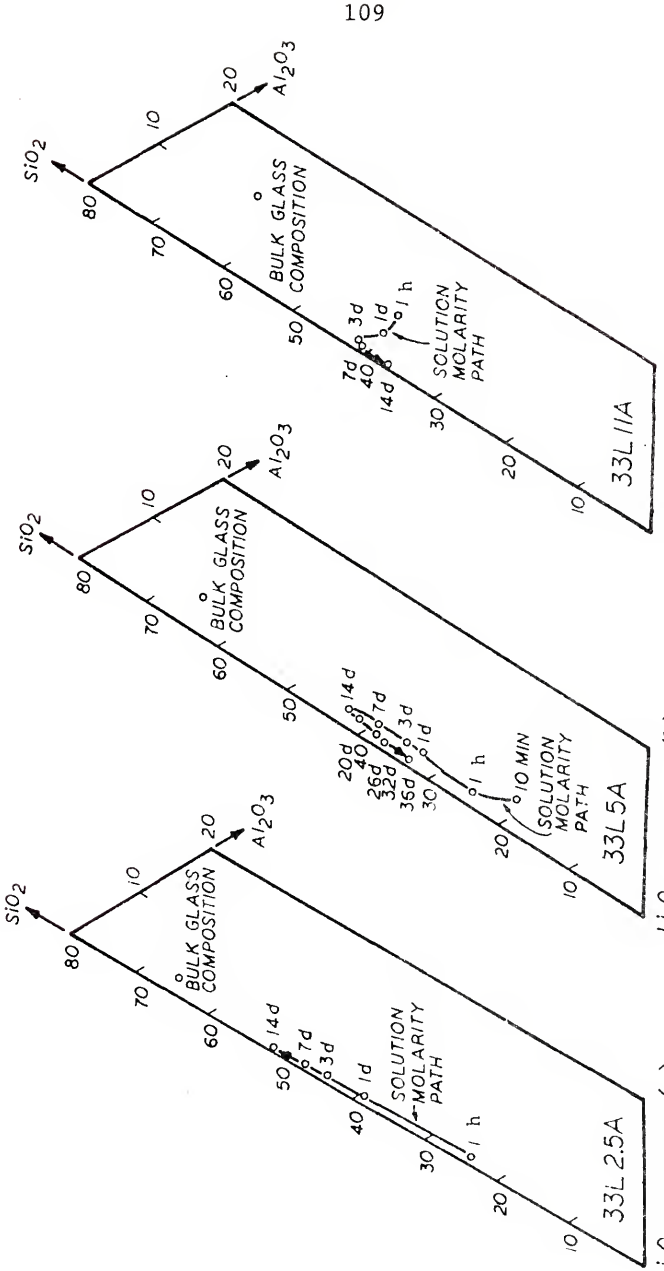

Figure 41. Alpha values plotted on a ternary diagram for bulk corrosion at 100°C of the following glasses: (a) 33125A, (b) 33L5A and (c) 33L11A.

Figure 42. Infrared reflection spectra for bulk corrosion at 100°C of the following glasses: (a) 20L5A, (b) 33L5A and (c) 46L5A.

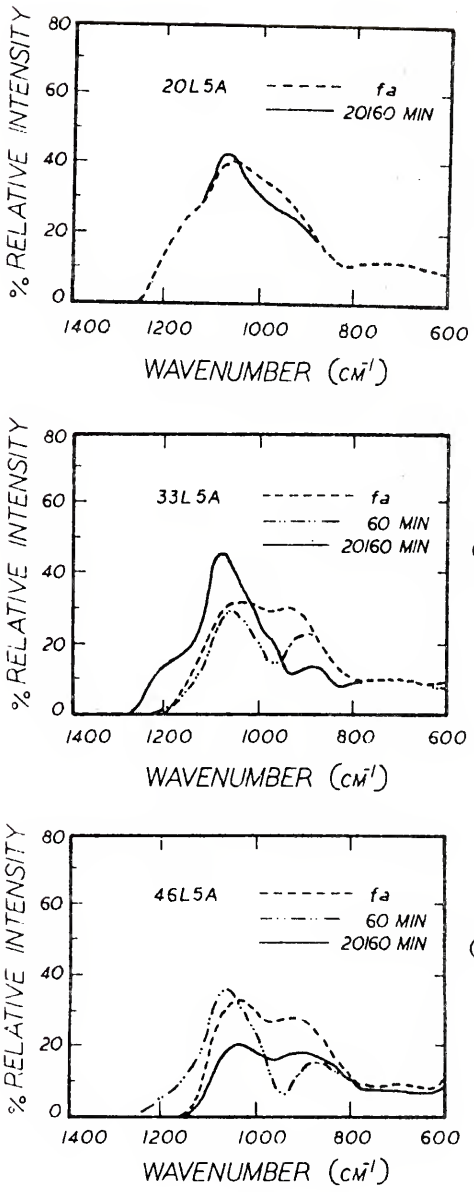
% RELATIVE INTENSITY
80
60
40
20
0
20L5A
fa
20160 MIN
1400
1200
1000
800
600
WAVENUMBER (cm⁻¹)
(a)
33L5A
fa
60 MIN
20160 MIN
(b)
46L5A
fa
60 MIN
20160 MIN
(c)

Figure 43. Infrared reflection spectra for bulk corrosion at 100°C of the following glasses: (a) 33L2.5A, (b) 33L5A and (c) 33L11A.

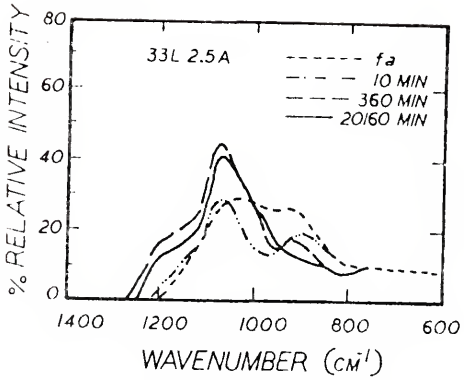
33L 2.5A
fa
10 MIN
360 MIN
20160 MIN
% RELATIVE INTENSITY
WAVENUMBER (cm⁻¹)

(a)

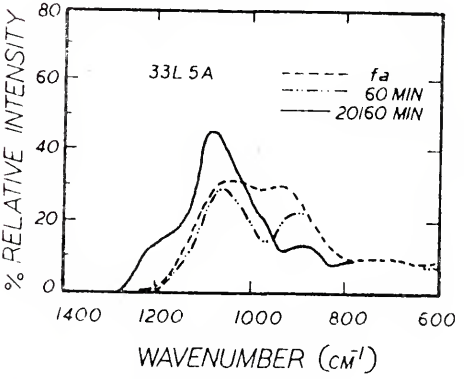
33L 5A
fa
60 MIN
20160 MIN
% RELATIVE INTENSITY
WAVENUMBER (cm⁻¹)

(b)

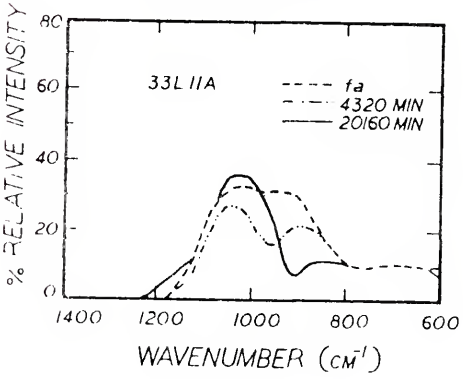
33L 11A
fa
4320 MIN
20160 MIN
% RELATIVE INTENSITY
WAVENUMBER (cm⁻¹)

(c)

Scanning electron micrographs (SEMs) are shown in Figure 44 for a freshly abraded (fa) glass surface and for various glass compositions of the $(X)Li_2O\cdot(0.05)Al_2O_3\cdot(0.95\text{-}X)SiO_2$ glass series exposed to a 3 day static 100°C corrosion test. The corroded glass surfaces in these micrographs are consistent with the results shown in Figure 28a, i.e., effect of increased lithia additions. Glasses low in alkali (high silica, constant 5 mole % Al_2O_3) are found to be very durable as shown in Figure 44b, while glasses of higher alkali (low silica, constant 5 mole % Al_2O_3) are found to be less durable as shown in Figures 44c, d, e.

From Figure 44b, the 20L5A composition (3 days, 100°C) exhibits excellent corrosion resistance. The surface in general suffered little attack, with the corrosion attack occurring mainly along the scratch lines produced during the sample polishing process. The 33L5A composition (3 days, 100°C), Figure 44c, exhibited a greater extent of corrosion attack of the general surface and the scratch lines as compared to the 20L5A composition. From Figures 44d and e, the 46L5A sample is shown to have experienced severe surface attack. In Figure 44d, this attack is manifested by the formation of a non-adherent

Figure 44. Scanning electron micrographs for bulk glasses under the following conditions:
(a) 33L5A freshly abraded surface (10,000X),
(b) 20L5A corroded 3 days at 100°C (5,000X),
(c) 33L5A corroded 3 days at 100°C (5,000X),
(d) 46L5A corroded 3 days at 100°C (50X),
(e) 46L5A corroded 3 days at 100°C (500X).

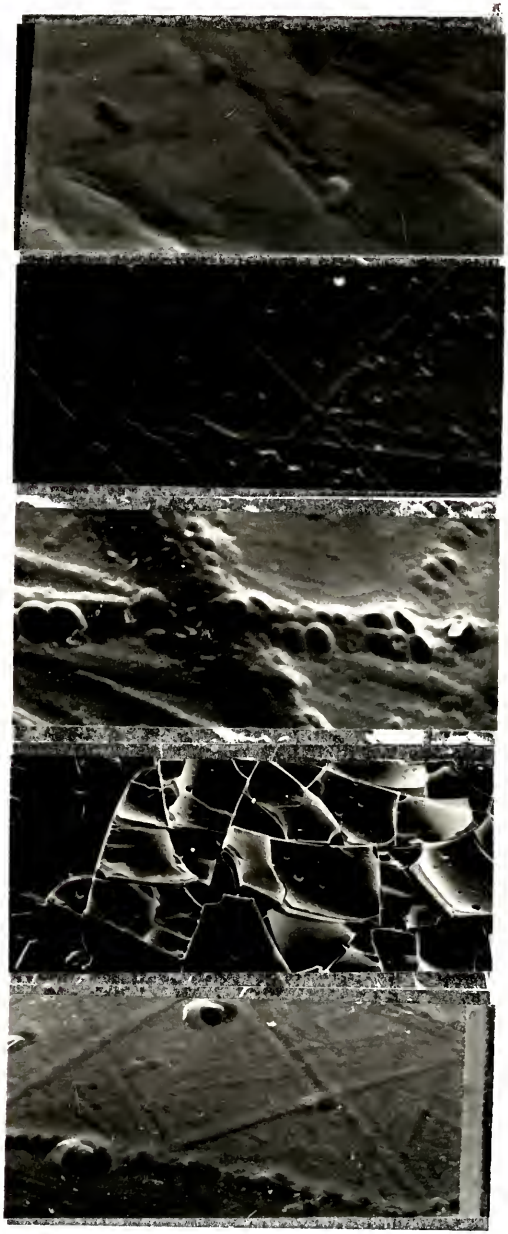

(a)

(b)

(c)

(d)

(e)

surface film. In Figure 44e, the severe attack is more apparent from the lack of definite scratch lines, compared to the 33L5A and 20L5A compositions.

Scanning electron micrographs (SEMs) are shown in Figure 45 for a freshly abraded (fa) glass surface and for various glass compositions of the $(0.33)Li_2O\cdot(X)Al_2O_3\cdot(0.67\text{-}X)SiO_2$ glass series exposed to a 3 day static 100°C corrosion test. The corroded glass surfaces in these micrographs are consistent with the results shown in Figure 28b. Glasses high in alumina (low silica, constant 33 mole % Li_2O) are found to be very durable as shown in Figure 45e, while glasses of lower alumina content (high silica, constant 33 mole % Li_2O), are found to be less durable as shown in Figures 45b, c, d.

From Figures 45b and c, 33L0A and 33L2.5A compositions, the effects of low percentages of alumina additions upon durability can be seen (3 days, 100°C). From these two figures, the absence of scratch lines, the presence of an "orange peel" surface character, and severe surface roughening are characteristic of glasses of low alumina ($0 \rightarrow 2.5$ mole % Al_2O_3). The lack of general surface attack and the presence of scratch lines for the 33L5A and 33L11A compositions, Figures 45d and e, are characteristic of glasses of high alumina ($5 \rightarrow 11$ mole % Al_2O_3).

Figure 45. Scanning electron micrographs for bulk glasses under the following conditions:
(a) 33L5A freshly abraded surface (10,000X),
(b) 33L0A corroded 3 days at 100°C (5,000X),
(c) 33L2.5A corroded 3 days at 100°C (5,000X),
(d) 33L5A corroded 3 days at 100°C (5,000X),
(e) 33L11A corroded 3 days at 100°C (5,000X).

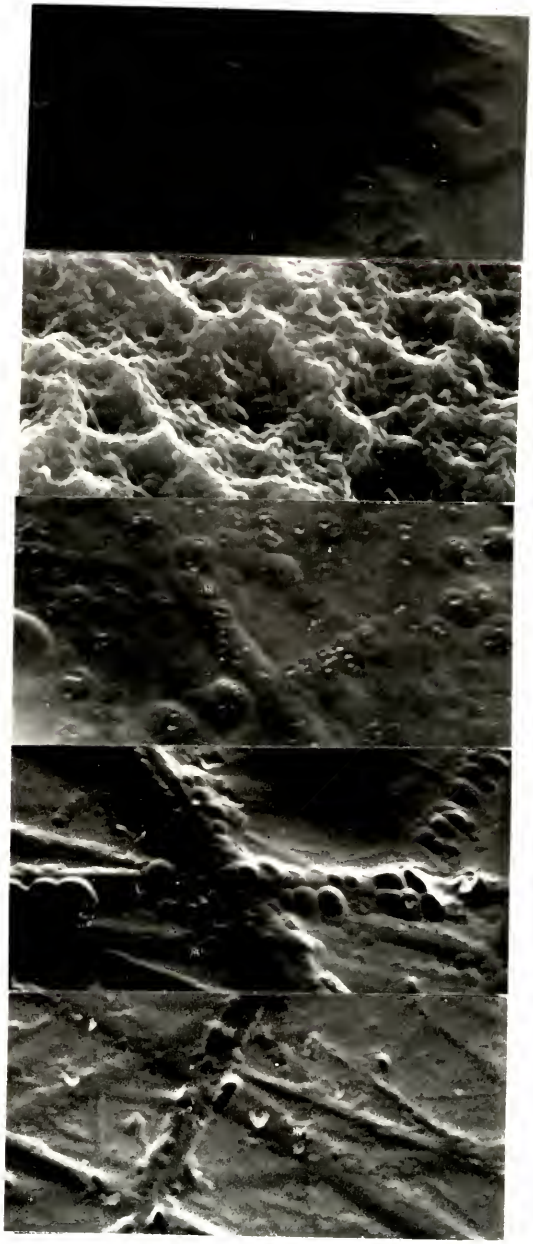

(a)

(b)

(c)

(d)

(e)

Discussion

The general increase in chemical durability caused by Al_2O_3 additions to glasses has already been established.[1,5,6,41-45] A sharp increase in chemical durability is observed for glasses when small percentages (2.5%) of alumina are added. Higher quantities of Al_2O_3 continue to increase the chemical durability but not as significantly as the first 2.5 mole %.[1,6,41,45] However, earlier papers show little detail about the relative effect of increased Al_2O_3 additions in glasses, the effect of constant Al/Li ratios, or mechanisms of the role of the Al_2O_3 upon glass durability.

The results in Figure 26 show that corrosion in the two glass series investigated is dominated by diffusion (slope = 1/2) rather by total dissolution (slope = 1). For pH values > 9, total breakdown of the silica network has been shown to be important, i.e., total dissolution.[11,13,58,59,24] Thus, above pH = 9, two reactions contribute to the presence of Li^+ in solution: a) selective leaching; and, b) total dissolution, when the total network breakdown becomes the most significant contribution of Li^+ in solution, the slopes of log Li^+ versus log time should approach a value of 1. When this slope is

between 1/2 and 1, both reactions contribute Li^+ ions to the solution.

In Figure 27, the pH of the corrosion solution is > 9 for the 46L5A ($\geq$ 10 minutes), 33L2.5A ($\geq$ 60 minutes), and 33L5A ($\geq$ 140 minutes) compositions. However, the 33L11A and 20L5A compositions do not attain pH = 9, for the corrosion times investigated. The slope of the Li^+ curves of Figure 26 for the 46L5A, 33L2.5A, and 33L5A compositions remains at $\sim$1/2 up to 7 days indicating selective leaching to be the dominant reaction even though the pH in most instances is > 9 (Figure 27). The α values shown in Figure 39 also support selective leaching of Li^+ ions as the rate controlling reaction during the same time period, i.e., up to 7 days. However, the importance of total dissolution increases slightly up to 7 days as indicated by the positive slope of the α curves shown in Figure 39.

The sequential order of the Si^{+4} concentration curves shown in Figure 28 confirms the relative tendency toward glass corrosion as was shown by Li^+ concentration curves in Figure 26, i.e., less Si^{+4} and Li^+ dissolution occurs for high alumina and high alkali glasses. The dissolution of Si^{+4} exhibits a root time dependence for the 20L5A and

33L11A compositions, while the other glasses exhibit approximately linear dissolution behavior (slope = 1). As previously, the extent of total dissolution is dependent upon pH. For pH > 9, the rate of Si^{+4} dissolution is sufficiently rapid so as to make the absolute value unimportant.

However, for pH $\leq$ 9, the pH is dependent upon the Li^{+} - H^{+} exchange and hence, Si^{+4} dissolution may be indirectly diffusion dependent[39] as is observed from the slope = 1/2 (from Si^{+4} curves of Figure 28) for the 20L5A and 33L11A glasses. For other glasses where the slope = 1, the pH has reached a value > 9 within 10^{1}-10^{2} minutes.

The importance of the first 2.5 mole % Al_2O_3 additions on Si^{+4} dissolution can be seen in Figure 29. Greater additions also improve the glass durability, but to a lesser extent than the first 2.5 %. Assuming no beneficial effects of alumina, replacing SiO_2 with Al_2O_3 will decrease the dissolution rate of Si^{+4} simply by decreasing the number of Si^{+4} sites per unit area of glass surface exposed to the corrosion solution. This should be a linear effect with the Si^{+4} dissolution decreasing proportionally to the decrease in the number of surface Si^{+4} sites. The difference between the actual Si^{+4}

dissolution and that expected from surface effects only (calculated from decrease in Si^{+4} surface sites) is shown in Figure 29 for a 1 hour corrosion period.

Similar beneficial effects from alumina additions on Li^{+} dissolution are shown in Figure 30 in which the Li_2O content is held constant for all the glasses. However, the first 2.5 mole % Al_2O_3 does not have as great an effect in decreasing the Li^{+} dissolution rate as it did for the Si^{+4} dissolution. Assuming no alterations in structure or potential for ion-exchange, a plot of Al_2O_3 additions versus Li^{+} solution concentration is expected to exhibit ideal behavior, i.e., curves similar to the ideal curves for the 14 day experiment. The ideal curve is expected since one mole Al_2O_3 structurally "ties up" one mole of Li_2O.[17,47,49] Since ideal behavior is not observed in Figure 30, and less Li^{+} dissolution is occurring than expected from ideality, changes in structural or ion-exchange potentials must be also affected by alumina additions to the glass. Ionic conductivity (alkali ion diffusion) increases as the % Al_2O_3 increases.[5,17,56] This alone would suggest that the extent of alkali leaching is directly related to the % alumina present in the glass. Since the reverse effect is observed (i.e., higher Al_2O_3

yields less alkali leaching), surface effects induced by the presence of alumina such as ion-exchange potential must be responsible for the reduced leaching rate.

The construction of the isochronal concentration curves for the "idealized" $Li_2O \cdot Al_2O_3 \cdot SiO_2$ glass system of Figure 46 represents theoretical cases for selective leaching and total glass dissolution. For total dissolution, glasses containing equivalent SiO_2 percentages (i.e., varying the Al_2O_3 and Li_2O mole %) yield equivalent solutions Si^{+4} concentrations. Likewise, glasses containing equivalent Li_2O and Al_2O_3 yield equivalent solution concentrations of these ions for total dissolution. Hence, for the "ideal" total dissolution case, the isochronal lines are parallel to the line containing the other two members of the ternary system.

A similar situation should be observed for selective leaching of Li^+. Assuming equal leaching rates for compositions containing equivalent quantities of Li_2O, the isochronal lines are parallel to the SiO_2-Al_2O_3 base line as shown in Figure 46a. However, these lines will be displaced (toward the Li_2O ternary point) from total dissolution lines since selective leaching usually precedes total dissolution during early stages of glass corrosion. Since Al^{+3} also selectively leaches, similar results are observed in Al^{+3}.

Figure 46. (a) Theoretical isochronal Si^{+4}, Al^{+3} and Li^{+} molarity curves for the $Li_2O \cdot Al_2O_3 \cdot SiO_2$ glass system.

(b) Alumina theory isochronal Si^{+4} molarity curves for the $Li_2O \cdot Al_2O_3 \cdot SiO_2$ glass system.

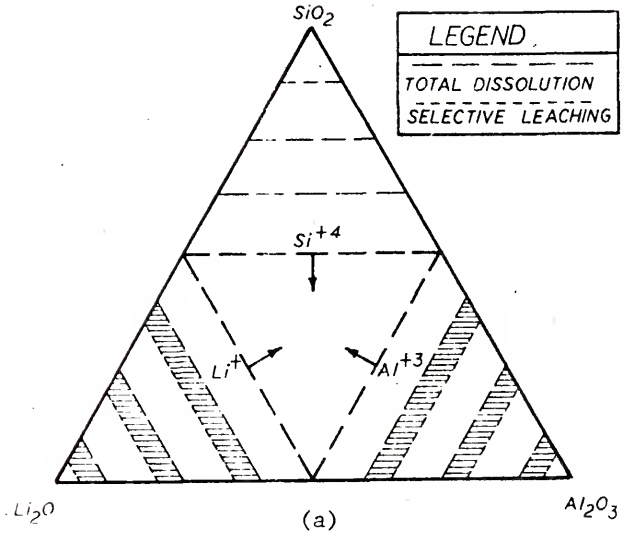
SiO_2
LEGEND
TOTAL DISSOLUTION
SELECTIVE LEACHING
Si^{+4}
Li^{+}
Al^{+3}
Li_2O
Al_2O_3

(a)

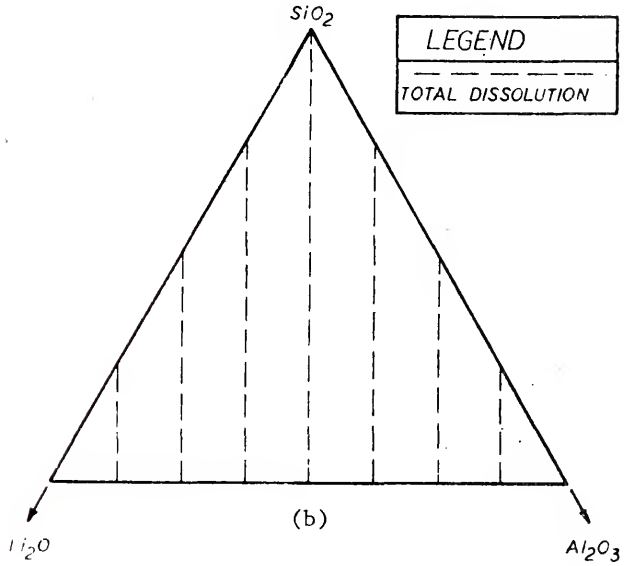
SiO_2
LEGEND
TOTAL DISSOLUTION
Li_2O
Al_2O_3

(b)

According to the classical theory of Al_2O_3 additions to glass compositions proposed by Weyl et al.,[17] the behavior of alkali-alumina-silicate glasses is governed by the principle that equivalent percentages of alkali-oxide and alumina added to a silicate glass do not produce any non-bridging oxygens, i.e., all alkali ions (for ratios $R^+/Al^{+3} \leq 1$) are associated with aluminum ions.[17,47-49] This effect is illustrated schematically in Figure 46b. The lines perpendicular to the Li_2O-Al_2O_3 base line represent "ideal" isochronal Si^{+4} dissolution lines. The dashed line drawn through the SiO_2 apex and equally dividing the Li_2O-Al_2O_3 line represents the series of glasses that exhibit equivalent dissolution behavior to that of pure SiO_2 (Si^{+4} dissolution). The other lines to the left and right of this line represent series of glasses with equivalent Si^{+4} dissolution behavior. In other words, the Si^{+4} dissolution behavior of all ternary glasses can be represented by the dissolution of binary glasses (lithia-silicates, and alumina-silicates).

From the theory of alumina effects in alkali-silicate glasses, if the Al^{+3} and Li^+ ions are in a molecular ratio of 1 (all Al^{+3} ions are in a 4-fold co-ordination[49-52]), the ternary glass should behave as pure SiO_2, as shown in

Figure 46b. For $Li^{+}/Al^{+3} < 1$ (all Al^{+3} ions associated with Li^{+} ions will be in a 4-fold co-ordination, and the excess Al^{+3} ions will be in a 6-fold co-ordination in the silicate network[49-52]), the ternary glass will behave as a binary lithia-silicate glass, represented by the left-hand side of Figure 46b. Since the 1:1 ratio (Li^{+}/Al^{+3}) theoretically acts as pure SiO_2, any change in this ratio yields information concerning the chemical durability of various alkali glasses containing alumina.

Projected isochronal Si^{+4} concentration curves are shown in Figures 31-35, for up to 14 days of corrosion time. The constant Si^{+4} lines in the top right side of the diagram, 20L to 20L12A range, confirm the theory of alumina in glasses since the dissolution lines are similar to those lines predicted by theory (right-hand side of Figure 46b, i.e., vertical lines). However, as the percent of Li_2O is increased, the Si^{+4} lines are slightly deflected to the left side of the diagram (no longer vertical and strictly adhering to alumina theory). Since the Si^{+4} concentration lines are deflected to the left, the glasses are corroding to a lesser extent than predicted by the classical alumina theory. This deflection is suggestive of formation of an alumina-silicate surface rich layer. Figures 36-41 indicate that Al^{+3} does

precipitate from solution which could lead to the formation of an alumina-rich protective surface film. This same general trend is present through all the corrosion time sequences shown in Figures 31-35. The importance of this type of curve may be realized if there is a need to tailor-make an alumina glass with certain chemical durability properties where melting temperature is a limiting factor. By choosing a specific isochronal Si^{+4} dissolution line (all compositions on an isochronal line have the same Si^{+4} dissolution behavior), the desired corrosion (Si^{+4}) level is set. By traveling in the down direction (in the region investigated, the melting temperature decreases toward the Li_2O ternary component) on an isochronal line and knowing the melting points of the various glasses from the Li_2O-Al_2O_3-SiO_2 ternary equilibrium phase diagram, the necessary temperature-composition may be chosen with the desired Si^{+4} dissolution characteristic.

The maximum followed by a decrease in Al^{+3} concentration shown in Figure 36 is suggestive of precipitation of Al^{+3} onto the corroded glass surface, probably in the form of an alumina-silicate structure.[43,44,48]

From Auger electron spectroscopy (AES) and ion-beam milling (Figures 37 and 38) the change in Al^{+3} concentration in the glass surface can be seen for various corro-

sion times. In general, the amount of Al^{+3} ions present in the surface is decreased as the corrosion time is increased up to 7 days. However, the Al^{+3} concentration for the specimen corroded for 44 days is higher at the near surface than for the freshly abraded (fa) glass. Furthermore, the Al^{+3} concentration remains constant for the first 12.5 minutes of ion-milling suggesting that an aluminum-rich surface film of constant composition $\sim$450 Å thick has been formed. These results are in agreement with those found for the Al^{+3} concentration curves in Figure 36, (i.e., a decrease in the solution Al^{+3} concentration curves between 7 and 14 days of corrosion).

In Figure 39a, the α's for all three compositions attained maximum values near total dissolution before decreasing. A decrease in α may be indicative of an aluminum- or silicon-rich surface layer formed on the corroded glass. The 46L5A glass almost attained a value of $\alpha = 1$ before reaching an equilibrium value. In Figure 39b, both of the higher alumina content glasses (3315A, 33L11A) have reached maximum α values and eventually decrease with time. However, the 33L2.5A glass does not acquire an equilibrium value over the corrosion times investigated. The continuous increase means that the glass is still approaching total dissolution after 7

days. Apparently, as the Al_2O_3 content decreases, the tendency towards total dissolution decreases. The 46L5A composition represents the least chemically durable glass in the compositional range investigated. The α's presented in Figure 39 are more appropriate for binary glass systems (for binaries, a relative composition profile can be established, i.e., when $\alpha = 0$, only alkali ions are coming out, when $\alpha = 1$, alkali ions and silica are coming out in the same ratio as they are in the glass).

In a ternary glass, if the ions in the corrosion solution are plotted on a mole % basis, a compositional corrosion profile can be empirically established. Figures 40 and 41 demonstrate this sequential compositional change from selective leaching → total dissolution → selective leaching. From these graphs, the actual compositional corrosion path can be observed. The ternary plots in Figures 40 and 41 are in agreement with curves shown in Figure 39. From the compositional paths, it is obvious that compositions which tend towards the Li_2O apex are experiencing a decrease in silica and aluminum ions in the corrosion solutions. This behavior is again suggestive of formation of an alumina-silicate rich surface film.[43,44,48]

Figure 42a (20L5A) illustrates a very durable high silica glass. Since this composition is high in silica (from alumina theory, the corrosion behavior of the 20L5A glass should be similar to that for the 15L0A glass), the increase in the Si-O-Si stretch peak occurs very slowly and is present for long periods of time (up to 14 days, 20,160 minutes). This can be contrasted to the case in Figure 41c, where the glass is not as durable (46L5A, low silica), but the increase in the Si-O-Si stretch peak is more rapid than the 20L5A glass. However, in the latter case, the Si-O-Si peak decreases very rapidly after several days indicating severe surface attack and roughening.[36]

If the alumina content is increased (2.5 - 11 mole % Al_2O_3) at a constant 33 mole % Li_2O, the corrosion resistance increases significantly over the corrosion behavior observed for a binary $Li_2O{\cdot}2SiO_2$ glass. The IRRS spectra for freshly abraded surfaces of the 33L2.5A, 33L5A, and 33L11A glasses are approximately equal as shown in Figure 43. From the spectra of the corroded surfaces of the three compositions, it is seen how the increased alumina additions decrease the corrosion reaction rates occurring for the various glasses, i.e., the 10 minute spectra of the 33L2.5A ≃ the 60 minute spectra of the 33L5A ≃ the

4320 minute (3 day) spectra of the 33L11A. Upon further spectral analysis, it may be generally concluded that the corrosion time required to attain a certain spectral intensity increases as the percent of Al_2O_3 in the glass increases. This reduction in corrosion reaction kinetics results from the Al^{+3} ion "tieing up" Li^{+} ions in the glass structure thereby decreasing the selective leaching process, and the formation of a protective alumina-silicate surface film, as was shown from Auger analysis (Figure 38), and Al^{+3} solution analysis (Figure 36).

Scanning electron micrographs (SEMs) shown in Figure 44 demonstrate the relative importance of Li_2O additions on the chemical durability of glasses with constant 5 mole % Al_2O_3. Figures 44b (20% Li_2O), 44c (33% Li_2O) and 44d and e (46% Li_2O) represent increased Li_2O additions to the alumina-silicate glasses after 3 days corrosion time. Figure 44a is the SEM of the uncorroded, freshly abraded glass surface for any composition. From these micrographs, the decrease in chemical durability can be seen as the Li_2O additions increase. In Figure 44b, 20L5A, very little general surface attack occurred; however, there was a small extent of attack along scratch lines formed during sample preparation. The 33L5A composition, Figure 44c, has

experienced slight general surface attack and moderate attack along the scratch lines indicating higher corrosion rates as compared to the 20L5A composition. In Figures 44d and e, the 46L5A is shown to have experienced a severe surface attack (surface roughening and total dissolution). The corroded surface film shown in Figure 44d for the 46L5A was not very adherent, and cracked upon drying. From this micrograph, the surface character appears to have been totally destroyed. However, upon close inspection, Figure 44e, light original scratch lines are still evident, indicating that total dissolution has not become the dominant corrosion mechanism even after 3 days of corrosion (compare with Figure 45b, where total dissolution is definitely the dominant corrosion mode). The IRRS Si-O-Si stretch peak (Figure 42c) increased during the first 60 minutes of corrosion indicating extensive selective leaching and high silica surface film formation. After 14 days, the IRRS spectra was almost identical to the freshly abraded surface with the overall reflected intensity being less. This means that the glass is corroding almost entirely in the total dissolution mode after 14 days accompanied by surface roughening and only minor selective leaching of Li^+ occurs.

These data are in agreement with the α values shown in Figure 39a, which show that the 46L5A glass is the least durable of the compositions investigated. The 46L5A is a good example of all the processes that occur during the glass corrosion. For short periods of time and pH $\leq$ 9, selective leaching is the dominant corrosion mechanism; this results in the formation of a high silica surface film (confirmed from IRRS results). For longer periods of time and pH > 9, total dissolution is the dominant corrosion mechanism. Also shown is the fact that when the Li_2O content in the glass is increased to high concentrations, the possible improvements in the chemical durability due to Al_2O_3 additions are overridden, and therefore cannot improve the chemical durability over long ranges of corrosion time.

Scanning electron micrographs shown in Figure 45 demonstrate the relative effect of alumina additions on glass durability. Figure 45a represents a freshly abraded glass surface which appears the same regardless of composition. Figures 45b (0% Al_2O_3), 45c (2.5% Al_2O_3), 45d (5% Al_2O_3) and 45e (11% Al_2O_3) represent increased Al_2O_3 additions while maintaining a constant 33 mole % Li_2O in the glass composition. From Figure 45b (0% Al_2O_3), the

apparent corrosion mechanism is total dissolution, manifested from the severe surface attack and hence surface roughening. Although total dissolution is not as severe in Figure 45c (2.5% Al_2O_3), it is still the dominant corrosion mechanism as demonstrated by the "orange peel" surface character and the absence of scratch lines. From Figures 45d and e, it can be seen that total dissolution is no longer the dominant corrosion mechanism, evidenced by the small extent of general surface attack, and the presence of scratch lines. For these two compositions, corrosion attack has been directed mainly to these scratches with little attack occurring on the general surface.

From these micrographs, the importance of the first 2.5% Al_2O_3 (Figure 45c) on reducing glass deterioration can be seen (as was shown by the Si^{+4} concentration curves in Figure 29). From Figures 45d (5% Al_2O_3) and 45e (11% Al_2O_3), it can be seen that higher Al_2O_3 additions increase the overall chemical durability, but not to the same extent as the first 2.5% addition.

Conclusions

I. The first 2.5 mole % Al_2O_3 addition has the greatest effect on decreasing Si^{+4} dissolution from Li_2O-

Al_2O_3-SiO_2 glasses. Larger Al_2O_3 additions also decrease the Si^{+4} dissolution rate, but to a lesser extent than the first 2.5%.

II. The reduction in Si^{+4} dissolution may be attributed to two factors: (i) a small decrease in Si^{+4} dissolution due to a reduction in the number of Si^{+4} surface sites caused by the Al_2O_3 additions; and, (ii) large reductions in Si^{+4} dissolution occurring because of Al_2O_3-glass interactions.

III. The rate of Li^+ dissolution from the glasses decreases in inverse proportion to the % Al_2O_3 present (0-11%).

IV. Adding alumina in glasses appears to decrease the importance of pH in glass dissolution. For example, for binary lithia-silicate glasses at pH > 9, total dissolution is the dominant mode of corrosion. However, for glasses containing Al_2O_3, selective leaching is very important in the regime of pH > 9.

V. In the early stages of corrosion, selective leaching of both Li^+ and Al^{+3} ions occurred with the corrosion path headed in the direction of total dissolution (SiO_2 apex). For alumina additions > 2.5%, there was a reversal in the compositional corrosion path during the later stages of corrosion. This is

indicative of precipitation of an alumina-silicate complex from the corrosion solution and reversal of the compositional path from the SiO_2 direction to the Li_2O direction.

VI. The isochronal curves obtained may be placed into two categories: (i) isochronal lines that are in direct accord with the alumina theory of glasses (top right section of the isochronal plots); (ii) isochronal lines that deviate from those expected from alumina theory. The curves deviating from theory indicate that less Si^{+4} dissolution occurs than expected from "ideal" behavior, and hence, are suggestive of a protective alumina-silicate surface film.

VII. Glasses with constant Li^{+}/Al^{+3} ratios have similar Si^{+4} dissolution properties. High silica glasses show little departure from the ideality of alumina glass theory. However, for low silica glasses, the departure from ideality increases, and the glasses corrode to a lesser extent than predicted by theory.

VIII. The isochronal lines may be used in selecting a glass composition with a particular corrosion behavior. If the melting point of a particular

glass is a problem, the isochronal lines may be used in selecting a glass series with an equivalent corrosion behavior and decreasing melting point. Thus, optimization of glass processing-corrosion behavior may be obtained.

IX. Al^{+3} solution results, IRRS and AES results all confirm the formation of an alumina-silicate surface film on the lithia-alumina-silicate glasses investigated.

CHAPTER IV
GLASS DURABILITY IN AQUEOUS SOLUTIONS OF ALUMINUM

Introduction

The importance of aluminum, as Al_2O_3 additions to glass compositions on improving glass durability has been known for many years. However, the beneficial effects of adding soluble aluminum salts, such as $AlCl_3$, $Al_2(SO_4)_3$, etc., to the corrosion solution of glasses has not been explored to any great extent. Previous investigations[60,63-66] have been limited to pure SiO_2 glasses or multicomponent commercial glass compositions and only a few concentrations of Al^{+3} ions in solution have been studied. Total dissolution is the only mode of corrosion for pure SiO_2 and hence the effects of solution Al^{+3} on selective leaching cannot be investigated with this material. Furthermore, most commercial glass compositions contain alumina which makes it difficult to separate the effects of Al^{+3} in the glass from the Al^{+3} ions present in the corrosion solution. To date, no effort has been made to separate the effects of soluble Al^{+3} concentrations on total dissolution as opposed to the selective leaching/ ion-exchange reaction. Ideally, the glass system utilized

should be as simple as possible and still have potential commercial importance.

Several investigators have proposed that for corrosion inhibition it is essential that Al^{+3} ions have a high tendency for adsorbing onto the glass surface. It has also been proposed that Al^{+3} ions should form only relatively insoluble alumino-silicate compounds based on silicon-oxygen groups in order to be effective as inhibitors.[61,66]

One group of investigators, Molchanov and Prikhid'ko,[61] suggest that the important characteristic of inhibitors, namely that the rate of glass corrosion (dissolution) is reduced considerably from the unhibited state, is due to preferential adsorbtion of ion inhibitors on active centers of the glass surface. Such active centers are proposed to be those characterized by the lowest activation energy for attack of the glass by OH^- ions. Thus the corrosion reaction can continue only at the less active centers associated with a higher activation energy, resulting in a general reduction of the corrosion process. Therefore, according to these investigators, the inhibition of corrosion occurs mainly from the action of the aluminum ions on the elementary corrosion processes rather than due to the formation of "thick" surface layers

that render interaction between the glass and corrosion solution physically difficult.

According to Iler,[64] soluble aluminum ion inhibitors are presumably coordinated with four oxygen ions on the glass surface, forming a negatively charged alumino-silicate surface site. If the glass surface contains negatively charged alumino-silicate sites, negatively charged hydroxyl ions (OH^-) will be repelled thereby resulting in a decrease in the total dissolution of silica. This theory corresponds to the rate of total dissolution of silica being proportional to the concentration of OH^- ions and their accessibility to the reaction glass surface.

From recent zeta potential measurements made by Onoda et al.,[67] a positive surface charge was observed for soluble aluminum ions attached to silica particles. This is in direct conflict with the theory proposed by Iler. Therefore the decrease in Si^{+4} dissolution must be due to some mechanism other than surface charge.

As stated earlier by Molchanov and Prikhid'ko,[61] the inhibition of corrosion occurs mainly from the action of the cations (i.e., aluminum ions) on the elementary corrosion processes. Although the idea is correct in this author's opinion, the explanation is so general that it does not help describe the actual process of inhibition.

Glass dissolution inhibition apparently occurs because of the effect of the cations on increasing the bonding strengths of the Si-O-Si bonds at the glass surface. An idealized glass surface is shown in Figure 47 both without (a) and with (b) Al^{+3} surface species. Because of the excess charge on the surface bound Al^{+2} ion, the oxygen from the glass structure will be more attracted to the Al^{+2} ion than it will be to the Si ion. If this occurs, the Si ion therefore will have a higher bonding strength with the three remaining oxygen ions, thereby strengthening the Si-O-Si bonds from the possibility of attack by the OH^- ions from the corrosion solution. This explanation is more plausible than that proposed by Iler, because his experiments cannot be used to explain the effects of adding divalent cations to the corrosion solution as inhibitors, whereas in the above theory divalent inhibitor cations still have a plus charge even when attached to the glass surface. From this type of theory, quadrivalent ions should be the most effective at strengthening the surface bonds with monovalent ions having the least effect. However, the effectiveness of trivalent and quadrivalent ions in solution will depend very greatly upon their affinity to other ionic species in the corrosion solution.

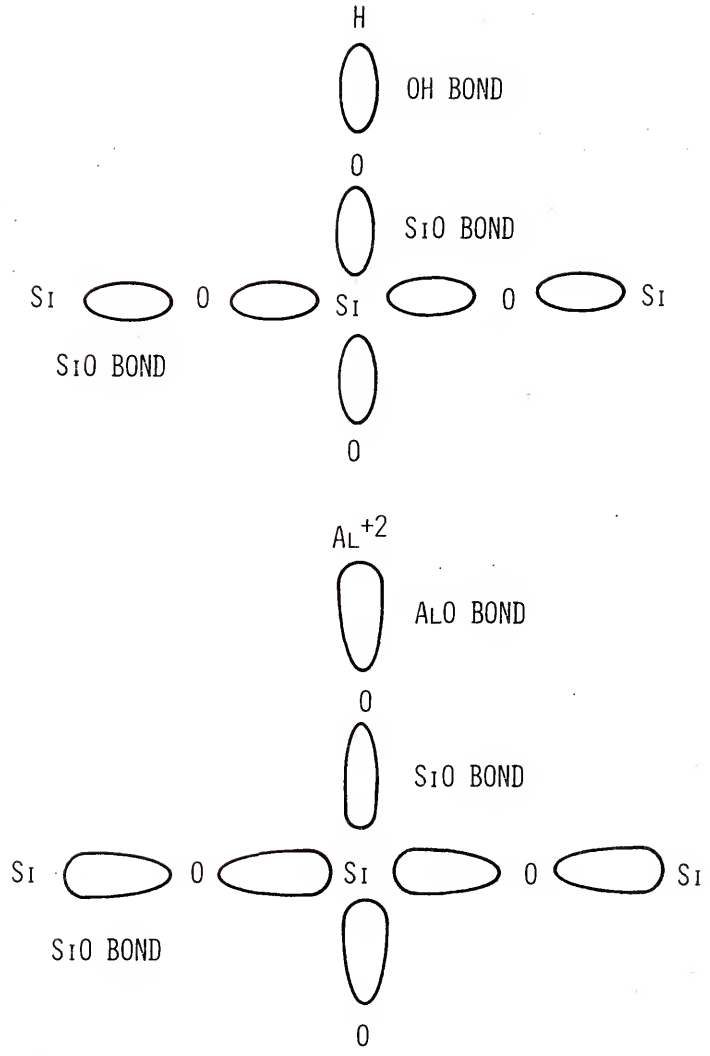

Figure 47. Schematic of the surface Si-O-Si bond changes due to the presence of Al^{+3} ions.

The objectives of this investigation are: (a) determine the effects of various Al^{+3} concentration levels upon glass corrosion and surface film formation; (b) determine the role of soluble Al^{+3} on total dissolution and selective leaching/ion-exchange reactions; (c) investigate the effects of various types of aluminum salt compounds ($AlCl_3$, $Al(NO_3)_3$, and $Al_2(SO_4)_3$) on surface film formation; and, (d) determine through the use of Auger Electron Spectroscopy (AES) if the Al^{+3} ions are only on the glass surface (adsorbed from solution) or if they are diffusing into the bulk of the glass.

If the role of aluminum is similar when added as Al_2O_3 to a glass or as soluble Al^{+3} ions in solution additions (i.e., promoting alumino-silicate film formation), it may be possible to treat a simple binary or ternary glass surface with a specific Al^{+3} solution concentration and impart the same degree of corrosion protection as a multicomponent glass with a specific Al_2O_3 content. This phenomenon could be very useful if additional durability is required of an item already in service or if improved durability of low melting temperature silicate glasses is desirable.

Experimental Procedure

The glass used in this investigation, 33L (33 mole % Li_2O, 67 mole % SiO_2), was prepared from reagent grade Li_2CO_3 and 5 μm SiO_2 powder.* The glass batches were melted in a closed Pt crucible for 24 hours in an electric muffle furnace at 1325°C. The molten glass was cast between graphite blocks and given a 4 hour annealing period at 450°C.

Specimens ∿3/4" x 3/4" x 1/4" were sectioned from glass plates, polished through 600 grit SiC paper, and stored in a dessicator. Prior to the testing procedure, the specimens were given a final abrasion with 600 grit dry SiC paper to eliminate any previous environmental effects.

Static bulk corrosion tests were performed using methods and procedures described in previous papers.[25,26] Various concentrations of soluble aluminum salt compounds in the corrosion solution were used (0-250 ppm Al^{+3}) and for various corrosion times (10 minutes-14 days). The ratio of glass surface area to corrosion solution volume was 0.77 cm^2/cm^3 (cm^{-1}).

*Min-U-Sil from Pennsylvania Glass Sand Corp., Pittsburg, Pa.

The Si^{+4}, Al^{+3}, and Li^{+} solution ion concentrations were determined by atomic absorption* and atomic emission**spectroscopy. The pH of the corrosion solution was determined with pH indicator paper.*** The resolution of the various solution analysis techniques described above are shown in Table II.

Bulk samples were vacuum coated with ∿150A of Au-Pd and analyzed with the Scanning Electron Microscope.**** Bulk samples not coated were analyzed using Auger Electron Spectroscopy (AES)***** and by Infrared Reflection Spectroscopy (IRRS)****** by the methods and procedures developed by Pantano[16] and Sanders,[15] respectively. IRRS scans were run at a medium rate from 1400 cm^{-1} to 600 cm^{-1}. The spectra of the corroded samples were compared with the spectra of the freshly abraded glass surface.

*Perkin-Elmer Model 303 Spectrometer, Perkin-Elmer Corp., Norwalk, Conn.
**Beckman B Spectrometer, Beckman Instruments, Inc., Fullerton, Calif.
***Gallard-Schlesinger Chemical Mfg. Corp., Carle Place, N.Y.
****Cambridge Stereoscan, Kent Cambridge Scientific, Inc., Morton Grove, Ill.
*****Physical Electronics Inc., Model 10-150 spectrometer
******Perkin-Elmer Model 467 IRRS, Perkin-Elmer, Norwalk, Conn.

Results

The concentration of Si^{+4} in the corrosion solution after 3 days of reaction at 100°C versus the concentration of Al^{+3} ($AlCl_3$) added to the solution is shown in Figure 48. The concentration curve of Si^{+4} increases for small Al^{+3} additions ($\leq$25 ppm) until a maximum is attained and then decreases rapidly for larger additions (>25 ppm).

In Figure 49, the Li^{+} concentration in the corrosion solution after 3 days at 100°C versus the concentration of Al^{+3} ($AlCl_3$) added to the solution is shown. As was observed for Si^{+4}, the Li^{+} concentration curve also exhibits a maximum at the same Al^{+3} concentration before leveling off to approximately the same value observed for the zero Al^{+3} addition, i.e., 3D-H_2O.

Solution pH before and after corrosion versus the concentration of solution Al^{+3} ($AlCl_3$) addition is shown in Figure 50. Al^{+3} solution additions decrease the solution pH prior to the glass corrosion reaction. After the corrosion process has occurred, 3 days at 100°C, the pH of the corrosion solutions attained an equilibrium value of 12 over the entire Al^{+3} ($AlCl_3$) concentration range.

Corrosion solution pH values are shown in Table VI as a function of time and concentration of Al^{+3} ($AlCl_3$) solution additions. The solution pH increases to a value of

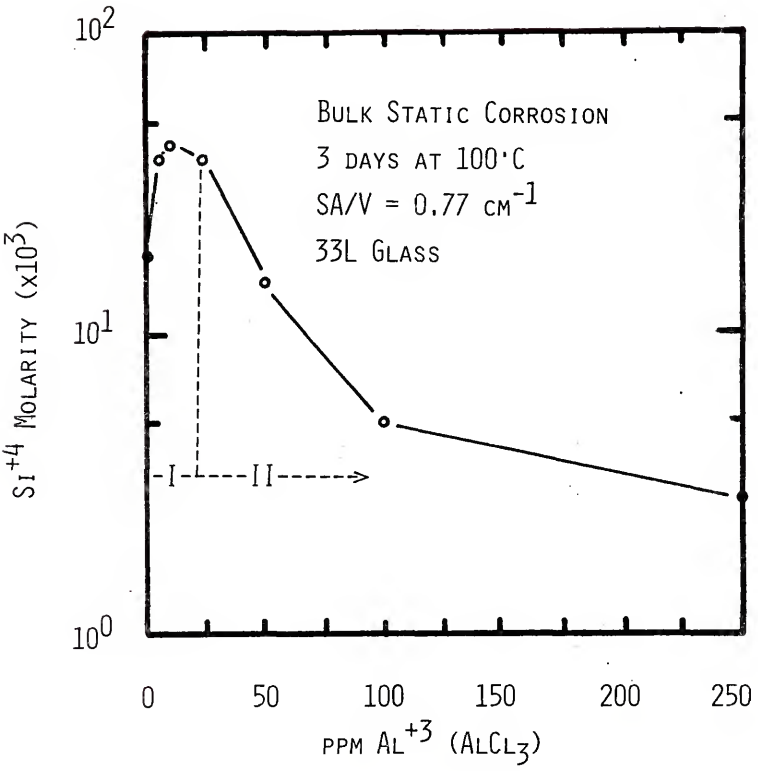

Figure 48. Si^{+4} solution data for bulk 33L glasses corroded in triple-distilled water and solutions containing various Al^{+3} ($AlCl_3$) concentrations for 3 days.

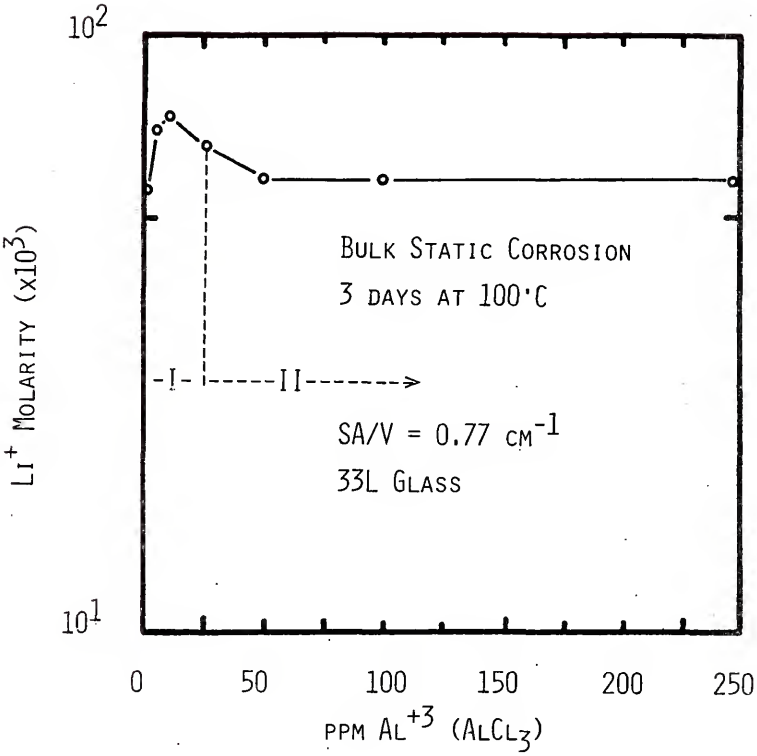

Figure 49. Li^+ solution data for bulk 33L glasses corroded in triple-distilled water and solutions containing various Al^{+3} ($AlCl_3$) concentrations for 3 days.

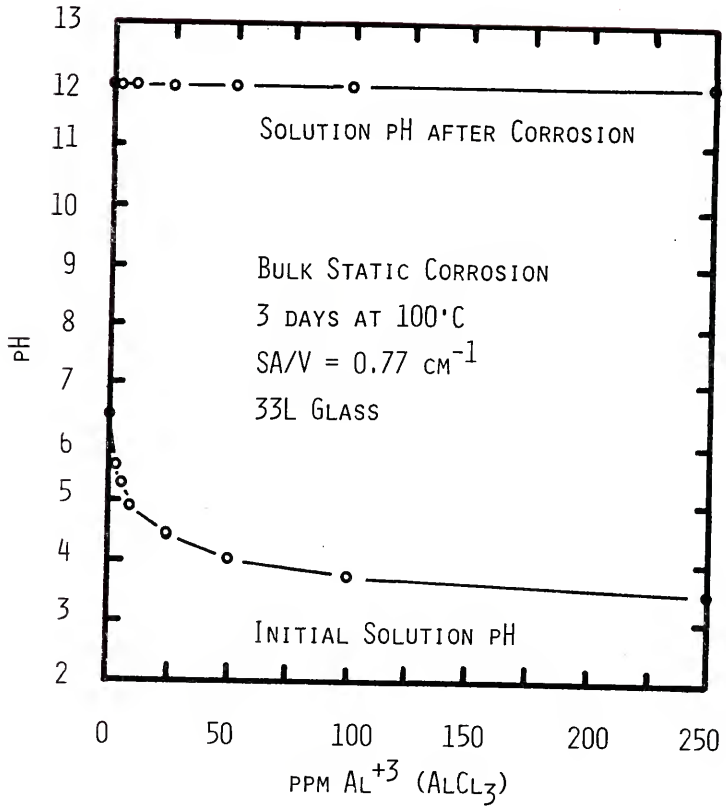

Figure 50. pH solution data before and after the corrosion process for bulk 33L glasses.

Table VI

pH Values for a Bulk 33L Glass Corroded in Solutions Containing Various Concentrations of $AlCl_3$ for 3 Days at 100°C

	$AlCl_3$ Concentrations							
Time	0 ppm pH	$(\Delta pH)_{0t}$	25 ppm pH	$(\Delta pH)_{0t}$	50 ppm pH	$(\Delta pH)_{0t}$	250 ppm pH	$(\Delta pH)_{0t}$
0 min	6.5	--	4.5	--	4.0	--	3.5	3.5
45 min.	9.8	3.3	8.8	4.3	4.7	0.7	3.7	0.2
90 min.	10.1	3.6	10.1	5.6	8.7	4.7	3.8	0.3
4 hrs.	10.4	3.9	10.7	6.2	10.5	6.5	4.0	0.5
16 hrs.	11.7	5.2	12.0	7.5	11.7	7.7	11.0	7.5
20 hrs.	11.8	5.3	12.0	7.5	11.9	7.9	11.5	8.0
24 hrs.	12.0	5.5	12.0	7.5	12.0	8.0	11.7	8.2
72 hrs.	12.0	5.5	12.0	7.5	12.0	8.0	12.0	8.5

10 within 90 minutes for solutions containing 25 ppm or less of Al^{+3}. For short periods of time, the corrosion solutions with large Al^{+3} additions show only small changes in solution pH with glass corrosion. However, within 16 hours even the solution containing 250 ppm Al^{+3} has reached the pH = 12 value. Thus, Table VI shows that the major difference is rate of change of pH. The rate is initially very high with 0 to low Al^{+3} additions and very low with large Al^{+3} additions.

A dissolution parameter, α, is very useful for investigating the relative leaching due to ion-exchange and total dissolution of binary glass (equation 5).

Since there were no aluminum ions in the initial glass, α does not yield any direct information concerning their presence, but does show the influence of the Al^{+3} ions on the process of selective leaching and/or total dissolution.

Figure 51 illustrates the dependence of α upon the Al^{+3} ($AlCl_3$) concentration in the corrosion solution. The α values are intermediate for low levels of Al^{+3} ($<$10 ppm) indicating a simultaneous occurrance of selective leaching and total dissolution. Additions in the range of 10-225 ppm Al^{+3} cause the α values to increase, indicating that total dissolution is becoming more important.

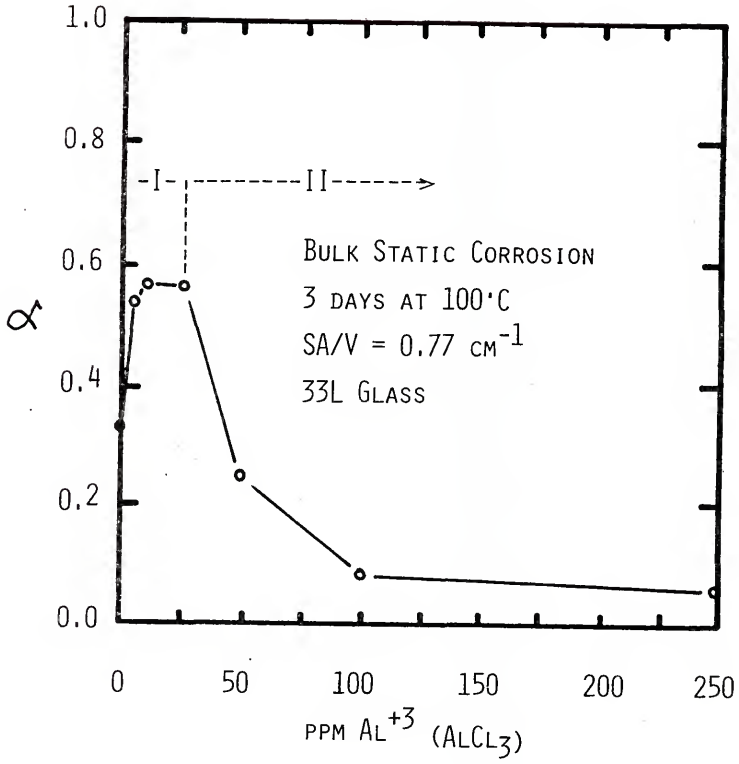

Figure 51. Alpha values for bulk 33L glasses corroded in solutions containing various Al^{+3} ($AlCl_3$) concentrations for 3 days.

For additions >25 ppm, the α curve decreases dramatically indicating that selective leaching is the primary mode of corrosion at higher concentrations of Al^{+3} additions.

In Figure 52, the concentration of Al^{+3} in solution after 3 days of corrosion for a 33L glass at 100°C is shown versus the concentration of Al^{+3} ($AlCl_3$) added to the solution before corrosion. Since both axes represent Al^{+3} concentration, a straight diagonal line results for the "before corrosion" situation. After the corrosion process occurs, the amount of Al^{+3} in solution is approximately one-half of that for the "before corrosion" concentrations for additions $\leq$ 50 ppm. For additions > 50 ppm and up to 250 ppm, the amount of Al^{+3} present in solution after corrosion decreases significantly in comparison to the "before corrosion" condition.

The ratios of Al/Si signals determined by Auger electron spectroscopy (AES) versus ion-beam milling time for the 33L glass exposed to 25 and 250 ppm Al^{+3} solutions are shown in Figure 53. Since the 33L glass initially contains no aluminum, the Al AES signal found must be due to the Al^{+3} ions diffusing into the glass from the corrosion solution. The Al^{+3} concentration is high at the near surface but decreases rapidly into the bulk of the glasses ($\sim$300Å). Because of the higher concentration of aluminum

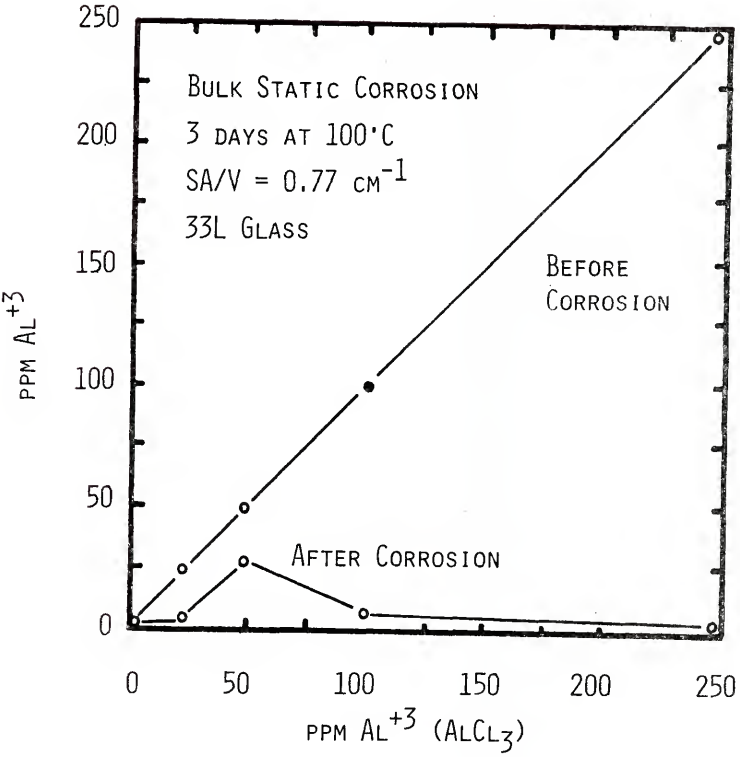

Figure 52. Al^{+3} solution data before and after the corrosion process (3 days) for bulk 33L glasses.

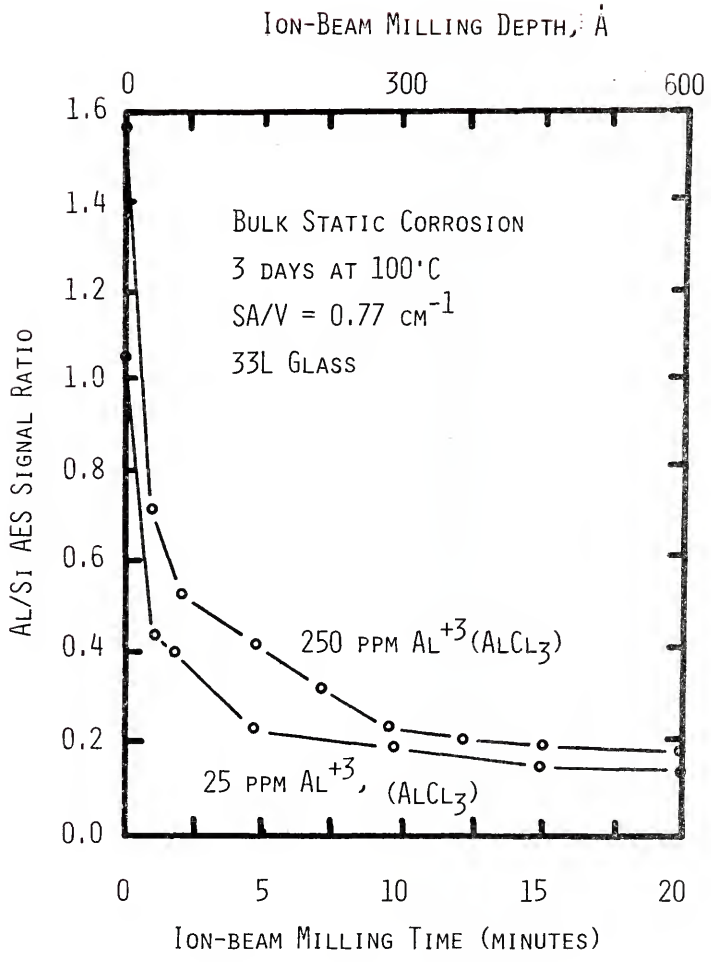

Figure 53. Al/Si Auger electron spectroscopy (AES) signal ratio at various depths for the bulk 33L glass after a 3 day corrosion period.

in solution for the 250 ppm Al^{+3} additions, the surface corroded in the 250 ppm Al^{+3} solution is higher in aluminum than the surface corroded in the 25 ppm Al^{+3} solution; this is evidenced in the Al/Si signal ratio.

Infrared reflection spectroscopy (IRRS) results are shown in Figure 54 for various Al^{+3} ($AlCl_3$) concentration levels after 3 days corrosion time at 100°C. The amplitude of the Si-O-Si stretch peak ($\sim$1080 cm^{-1}) is used as an indicator of the relative durability of silicate glasses, i.e., low amplitude, low durability and high amplitude, high durability.[40] The amplitude of the stretch peak for the 0 ppm Al^{+3} sample is approximately 25 intensity units after 3 days of corrosion. After corrosion in the 25 ppm Al^{+3} solution, the amplitude of the peak is 5, and for glasses corroded in solutions containing >50 ppm Al^{+3}, the amplitude is $\geq$45, which is similar to that observed for fused silica.[25] These data show that the durability of the binary glass is decreased by the additions of $\leq$25 ppm Al^{+3}, but increased by the additions of $\geq$50 ppm Al^{+3}.

In Figure 55, IRRS results for glasses corroded in $Al(NO_3)_3$, $AlCl_3$, and $Al_2(SO_4)_3$ solutions at a 50 ppm Al^{+3} level are shown. All three solutions cause similar and approximately equal spectra in the range of the Si-O-Si stretch peak ($\sim$1080 cm^{-1}).

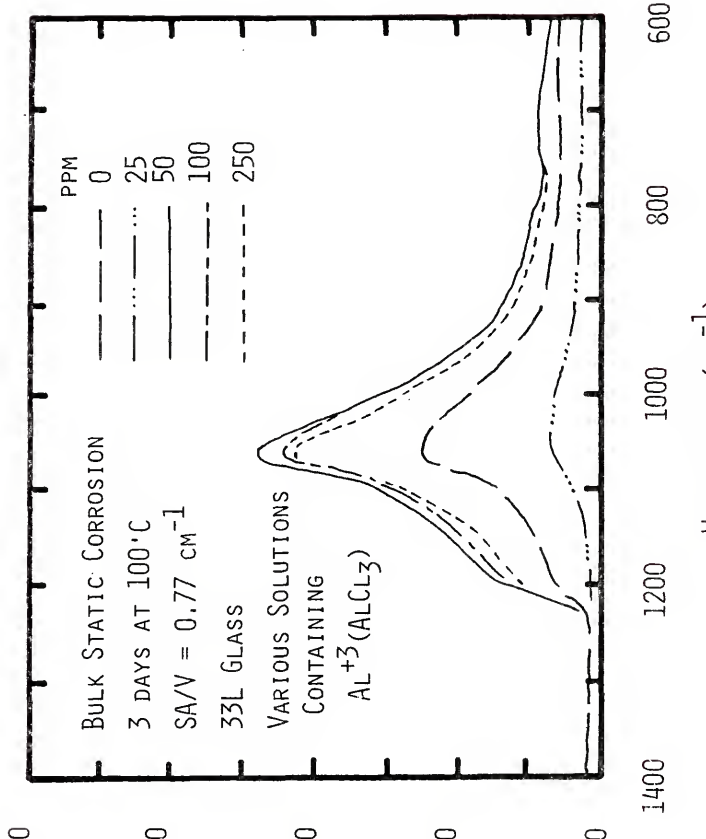

Figure 54. Infrared reflection spectra for bulk 33L glasses corroded in triple-distilled water and solutions containing various Al^{+3} ($AlCl_3$) concentrations for 3 days.

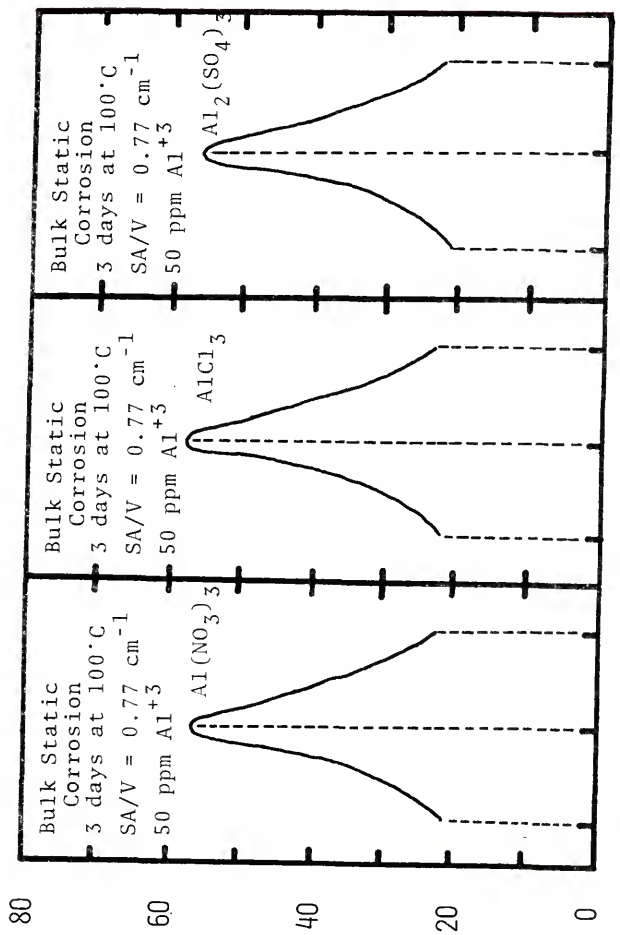

Figure 55. Infrared reflection spectra for bulk 33L glasses corroded in solutions containing $Al(NO_3)_3$, $AlCl_3$ and $Al_2(SO_4)_3$, at a constant 50 ppm Al^{+3} level.

Li^+ and Si^{+4} ion concentrations after 3 days corrosion at 100°C are shown in Table VII as a function of the type of aluminum salt compounds added to the solution. From this table, it is seen that the particular anion has little if any effect on either Li^+ or Si^{+4} dissolution rates of the 33L glass for 3 days at 100°C.

Si^{+4} concentration versus corrosion time for the 33L glass is shown in Figure 56 for 0 ppm Al^{+3} (3D-H_2O) and 100 ppm Al^{+3} ($AlCl_3$) corrosion solutions. These solution results are consistent with IRRS results presented in Figure 54 for the 3 day corrosion period, i.e., corrosion is greater for glasses in 0 ppm Al^{+3} (3D-H_2O) solutions than in 100 ppm Al^{+3} solutions.

Li^+ concentrations versus corrosion time for the 33L glass is shown in Figure 57 for 0 ppm Al^{+3} and 100 ppm Al^{+3} ($AlCl_3$) corrosion solutions. These Li^+ results are consistent with the Li^+ results of Figure 49, i.e., approximately equal selective leaching rates.

Figure 58 illustrates the dependence of α with corrosion time for 0 ppm Al^{+3} and 100 ppm Al^{+3} ($AlCl_3$) corrosion solutions. These α values are consistent with the α values of Figure 51, i.e., 0 ppm α values are higher than the 100 ppm α values. The data of Figure 58 also show that there is a large difference in the rate of change of α dependent upon the $AlCl_3$ addition.

Table VII

Solution Data for a Bulk 33L Glass Corroded in Solutions Containing Various Aluminum Salt Compounds for 3 Days at 100°C

Compound	Li^{+} Molarity ($x10^{3}$)	Si^{+4} Molarity ($x10^{3}$)
50 ppm $Al(NO_3)_3$	58.0	14.0
50 ppm $AlCl_3$	58.0	14.0
50 ppm $Al_2(SO_4)_3$	56.0	14.0

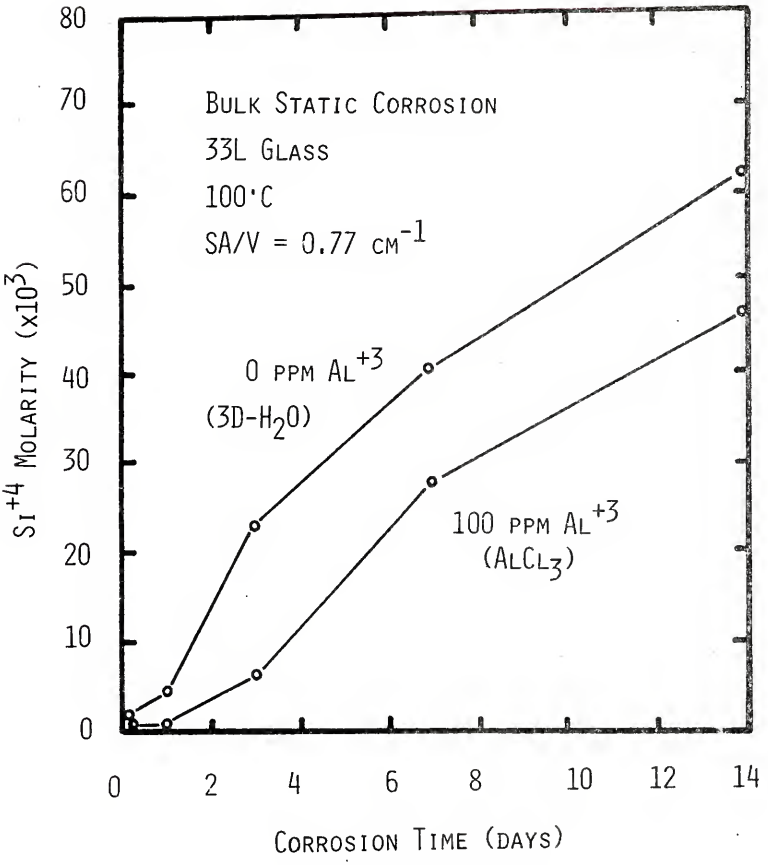

Figure 56. Si^{+4} solution data for bulk 33L glasses corroded in solutions of 0 ppm Al^{+3} triple-distilled water and 100 ppm Al^{+3} ($AlCl_3$).

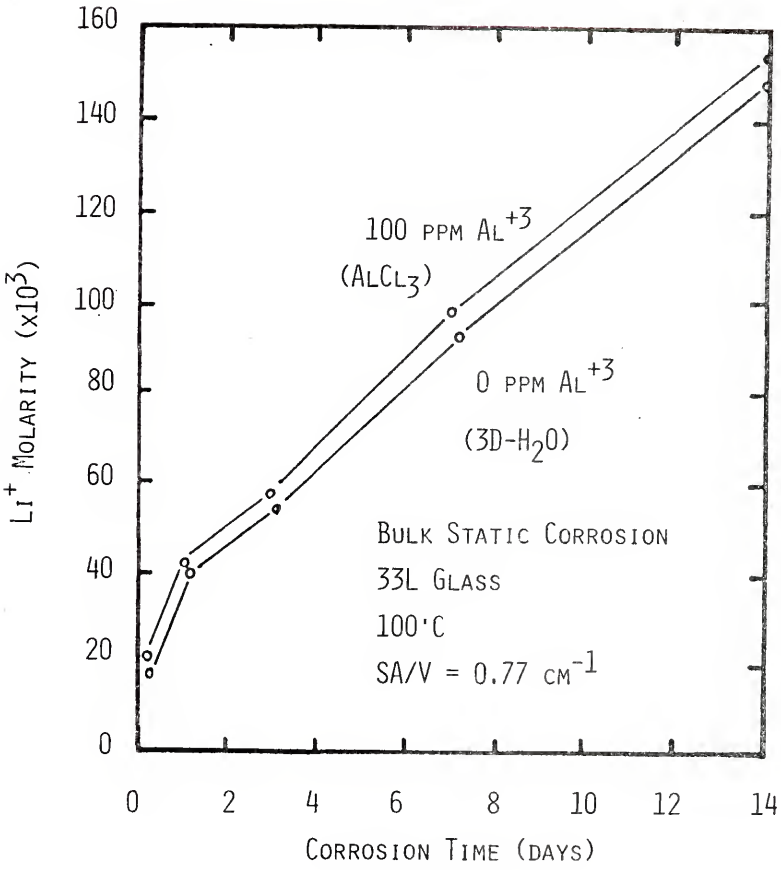

Figure 57. Li^+ solution data for bulk 33L glasses corroded in solutions of 0 ppm Al^{+3} triple-distilled water and 100 ppm Al^{+3} ($AlCl_3$).

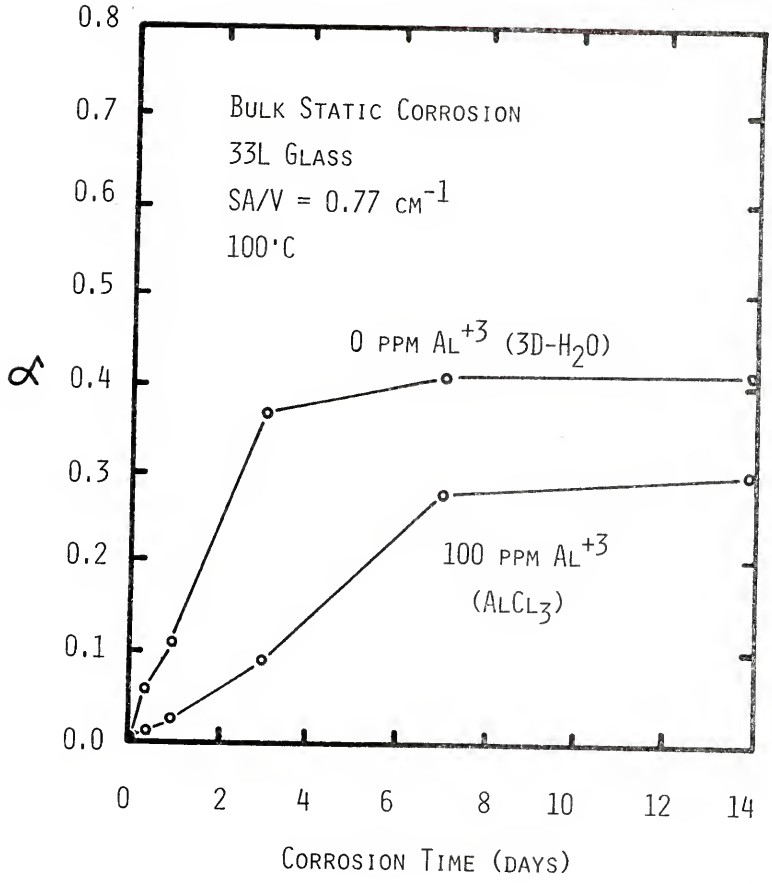

Figure 58. Alpha solution values for bulk 33L glasses corroded in solutions of 0 ppm Al^{+3} triple-distilled water and 100 ppm Al^{+3} ($AlCl_3$).

IRRS spectra for the glasses corroded in 100 ppm Al^{+3} ($AlCl_3$) solution for various corrosion times are shown in Figure 59. The Si-O-Si stretch peak attains a maximum value after 3 days of corrosion and decreases thereafter indicating either total dissolution and surface roughening or the formation of a precipitate on the glass surface.

Scanning electron micrographs (SEMs) are shown for glasses corroded for 3 days at 100°C in 0 ppm Al^{+3} (3D-H_2O), 25 ppm Al^{+3}, and 100 ppm Al^{+3} solutions in Figures 60a, 60b and 61a. Figure 61 shows SEM results for the 100 ppm Al^{+3} solution after 14 days of corrosion. All of the results shown in Figures 60 and 61 are consistent with the data of Figures 48, 49, 51, 54 and 56-59. The glass corroded in the 25 ppm Al^{+3} solution was the least durable of the various Al^{+3} concentration series as indicated by severe surface roughening (Figure 60b). The 100 ppm Al^{+3} solution resulted in one of the most durable surfaces (Figure 61). The glass corroded in triple distilled H_2O with no Al^{+3} addition is in between the extremes in behavior. The surface of the 14 day 100 ppm Al^{+3} specimen has started to deteriorate (Figure 61), but has not proceeded to the extent of that found for the 3 day 0 ppm Al^{+3} or 25 ppm Al^{+3} glass surfaces, Figures 60a and 60b.

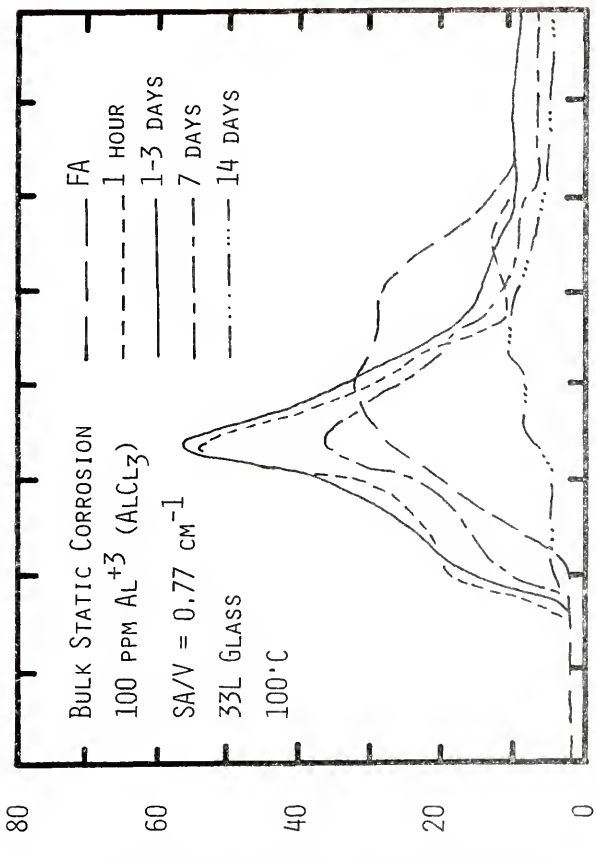

Figure 59. Infrared reflection spectra for bulk 33L glasses corroded in a solution containing 100 ppm Al^{+3} ($AlCl_3$).

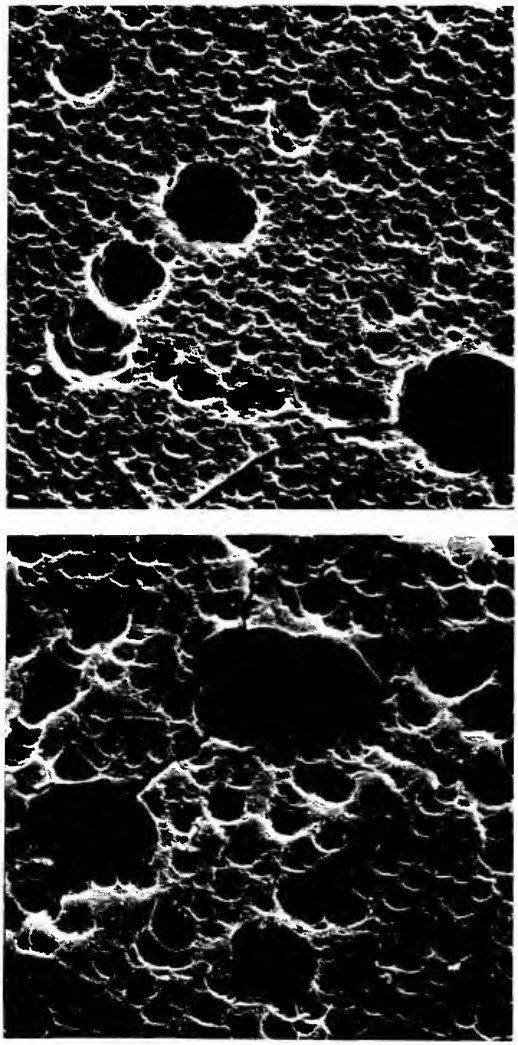

(a)

(b)

Figure 60. Scanning electron micrographs for bulk 33L glasses corroded for 3 days at 100°C in (a) 0 ppm Al^{+3} triple-distilled water solution, (1000X) and (b) 100 ppm Al^{+3} ($AlCl_3$) solution, (1000X).

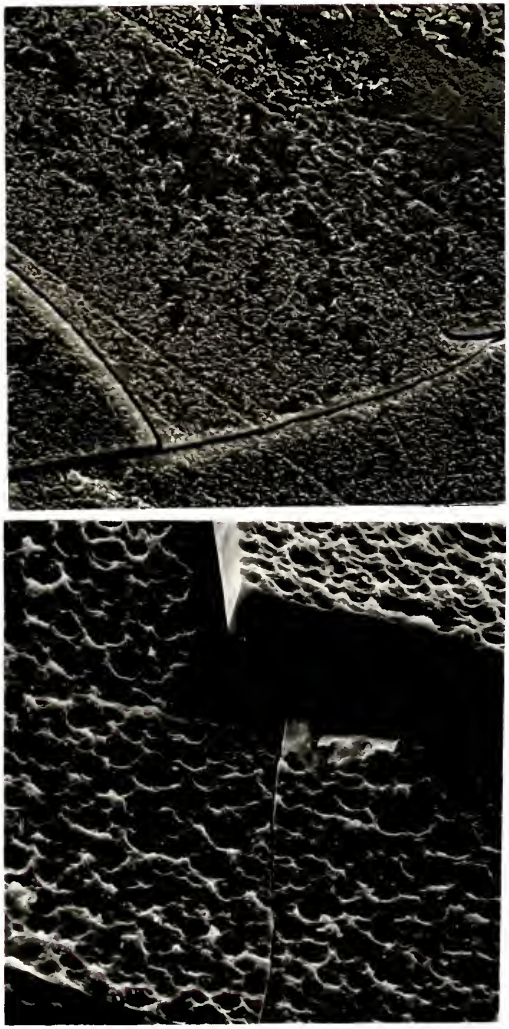

(a)

(b)

Figure 61. Scanning electron micrographs for bulk 33L glasses corroded in a 100 ppm Al^{+3} ($AlCl_3$) solution at 100°C for (a) 3 days, (1000X) and (b) 14 days, (1000X).

Discussion

Aqueous solutions of certain metal cations, especially aluminum, have been found to exhibit a strong inhibiting effect upon glass dissolution.[60,63-66] It has been concluded that this reduction in glass solubility occurs mainly because of a disruption in the basic corrosion processes rather than the formation of thick films that physically shield the reactive glass surface from the corrosion solution.[61,66] Although there is general consensus on the results, there are several factors that have not been considered that may also influence the inhibiting process.

Previous studies have not evaluated the following factors in detail: (a) various Al^{+3} concentration levels; (b) ion-exchange effects upon inhibition; and, (c) corrosion time. Problems also resulted in previous investigations from the specific glass composition chosen (i.e., SiO_2 glasses and commercial glasses in contrast to a simple binary alkali-silicate glass system) and the methods for expressing the degree of corrosion (i.e., depth of attack rather than specific ionic concentrations) that occurred.

It has been suggested by several investigators that since the breakdown of quartz glass with no ion-

exchangeable cations can be inhibited, inhibitors act not so much on the process of cation extraction as on the breakdown of the silicon-oxygen network of the glass structure.[61,62]

From Iler's experiments,[64] a continuous decrease in total dissolution of silica (SiO_2) is observed as the Al^{+3} concentration of the corrosion solution increases from 0 ppm - 112 ppm. However, the first 18 ppm Al^{+3} addition yields the largest reduction in total dissolution with higher additions decreasing dissolution at a decreased rate to that observed initially. It was found in Iler's experiments that at the 10 ppm Al^{+3} level (largest decrease in dissolution), there was a surface Si^{+4} site occupation by Al^{+3} of 10%. Therefore, total surface coverage by alumino-silicates is not necessary for a large decrease in the silica dissolution rate.

The Si^{+4} concentration curve of Figure 48, Li^{+} concentration curve of Figure 49, and the α curve of Figure 51 may be divided into two regions: (a) region I ($\leq$25 ppm Al^{+3}), with an increase in Si^{+4} and Li^{+} dissolution, hence an increase in the value of α; and, (b) region II (>25 ppm Al^{+3}), where a decrease in Si^{+4} and Li^{+} dissolution occurs and hence, a decrease in the value of α.

In region I, the increase in both Si^{+4} and Li^{+} and hence α, indicates that the total dissolution rates are increased over those observed for the binary 33L glass in 0 ppm Al^{+3} (3D-H_2O) corrosion solution. The results of these experiments on 33L glasses are not in agreement with the results obtained by Iler on quartz glasses.[64] Iler did not observe an increase in silica dissolution at low Al^{+3} additions, but rather observed a continuous decrease in silica dissolution for all Al^{+3} additions. This discrepancy in silica dissolution behavior must be explained in terms of the components (i.e., SiO_2 and Li_2O) present in the glass structure and their influence on the corrosion solution pH. In general, the total dissolution of quartz glass has a relatively minor effect on the solution pH. This can be seen in the following equations for total dissolution of quartz glass.

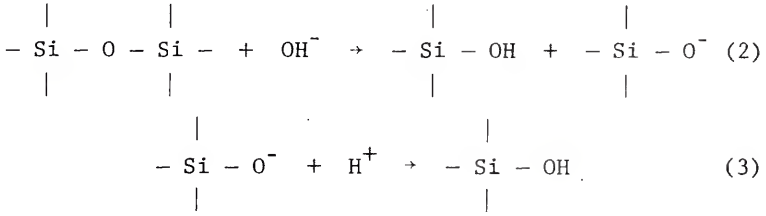

(2)

(3)

Assuming equal quantities of H^{+} and OH^{-} ions are reacting with the glass structure, there will be no build-up of either of these ions, and hence, no major change in pH occurs.

The reaction process is more complicated for the 33L glass. In this case, selective leaching of Li^+ ions can occur in addition to the total dissolution reaction as shown in the following equation.

$$\begin{array}{c} | \\ -Si-O-Li \\ | \end{array} + H_2O \rightarrow \begin{array}{c} | \\ -Si-OH \\ | \end{array} + Li^+ + OH^- \quad (6)$$

Since the H^+ ions are entering the glass structure, there is an excess of OH^- ions in solution and hence, the pH of the corrosion solution increases. This increase in solution pH ultimately results in a change of the reaction from only ion-exchange to both total dissolution and ion-exchange. According to Iler,[64] and Molchanov and Prikhid'ko,[61] the reduction of silica dissolution occurs because of surface passivation by inhibitors, i.e., the formation of alumino-silicate surface sites. If for some reason the inhibitor addition is too low to passivate the surface effectively, the rate of total dissolution may increase because of rapid pH changes that might occur in the solution containing the additive ions (refer to Figure 50 and Table VI). From Figure 50, the solution pH before and after corrosion is shown. Before corrosion, the pH decreases for increased Al^{+3} ($AlCl_3$) additions. After the corrosion process has occurred (3 days at 100°C), the pH

of all solution additions is 12. From Table VI, the pH is shown as a function of corrosion time and Al^{+3} ($AlCl_3$) concentration in solution. A comparison of the 0 ppm and 25 ppm solution pH values show that for times $\leq$ 90 minutes, the pH of the 25 ppm solution is less than or equal to the pH of the 0 ppm solution. For times > 90 minutes, the pH of the solution containing 25 ppm additive is greater than that observed for the pH of the 0 ppm solution. It is this increased pH for the 25 ppm solution that is responsible for the increased dissolution rates observed in Figures 48, 49, and 51. Since the Li^+ extraction is constant for the 0, 50, 100 and 250 ppm Al^{+3} additions, the increased Li^+ dissolution values observed for the 5, 10 and 25 ppm Al^{+3} addition over the constant value is most likely due to increased total dissolution. Persson[63] observed similar results in alkali extraction of commercial glasses but was not able to give a detailed explanation of this phenomenon.

In region II, the continuous decrease in Si^{+4} concentration and the approximate constant level observed for the Li^+ concentration suggest that the ion-exchange process is not appreciably affected by the Al^{+3} ($AlCl_3$) concentration while the total dissolution is greatly reduced. In other words, the presence of > 25 ppm Al^{+3} increases

the total dissolution resistance of the glass, as seen from α values, but does not significantly affect the selective leaching of Li^+ ions from the glass. This is an important result since the pH values of the corrosion solutions are in the regime (pH = 12) where total dissolution is normally the dominant mode of corrosion (Figure 50 and Table VI). Thus surface passivation by alumino-silicate site formation must be responsible for the observed decrease in Si^{+4} dissolution (Figure 47) and α values (Figure 51). The α values shown in Figure 51, region II, suggest that selective leaching is the primary corrosion mechanism. This data supports the theory that the major function of Al^{+3} ions in solution is to protect the Si-O-Si surface bonds and not to form a protective physical barrier to ion-exchange.[61,62]

In Figure 52, a large reduction of Al^{+3} ions in solution can be seen by comparing the data before and after corrosion. Since the Al^{+3} ions are no longer in solution, they must be on the glass surface or diffused into the near surface of the glass.

Proof of this surface Al^{+3} buildup and diffused Al^{+3} layer can be seen in the AES results shown in Figure 53. The relative Al/Si concentration profiles are shown in Figure 53 for glasses corroded in 25 and 250 ppm Al^{+3}

($AlCl_3$) solution additions. The surface concentration of Al^{+3} ions resulting from the reaction in the 250 ppm solution is greater than that for the 25 ppm level and remains greater to a depth of ~300Å. For depths >300Å, the relative concentrations of Al^{+3} from the 25 and 250 ppm solutions are approximately the same. As discussed previously, the formation of alumino-silicate surface sites is responsible for the general increase in chemical durability, and AES and solution analysis confirm this Al^{+3} buildup on the glass surface and in the near surface region.

The IRRS results of Figure 54 illustrate the relative tendency of the 33L glass to corrode in the various Al^{+3} solution concentrations as shown in Figures 48 and 49. The 25 ppm Al^{+3} ($AlCl_3$) spectra in Figure 54 suggests that this solution concentration is the most corrosive as demonstrated by the large decrease in total spectral intensity. However, Iler found that an 18 ppm Al^{+3} addition resulted in a high degree of surface passivation of quartz glass. From solution analysis of > 25 ppm Al^{+3} solution additions (Figures 48 and 49), apparently there are enough Al^{+3} ions to passivate the glass surface from OH^- attack, and hence increase glass durability. This is confirmed by IRRS spectra shown in Figure 54 for Al^{+3} additions >

25 ppm. For solutions containing < 25 ppm Al^{+3}, the surface has not been sufficiently passivated as evidenced by the shift in Si-O-Si peak position and amplitude and therefore remains susceptible to attack from the OH^- ions in the corrosion solution. Since the OH^- concentration is increased by the Al^{+3} ($AlCl_3$) addition to the solution (see Figure 50 and equation 6), the low $AlCl_3$ solutions increase the glass corrosion rate.

As shown in Figure 55, IRRS Si-O-Si peak spectral amplitudes for corrosion in the $Al_2(SO_4)$ and $Al(NO_3)_3$ solution additions (50 ppm Al^{+3}) are approximately the same as that observed for corrosion in the solution containing $AlCl_3$ (50 ppm Al^{+3}). From the amplitude and location of the Si-O-Si stretch peak and the silicon non-bridging oxygen (NSL) peak for all three soluble aluminum salt compounds, it is apparent that all three salts yield similar surface films. Li^+ and Si^{+4} dissolution results shown in Table VIII confirm that all three aluminum salt compounds produce approximately equal dissolution and are in agreement with the IRRS results of Figure 55, i.e., the anion portion of an aluminum salt compound has minimal effects upon chemical durability. These data suggest that the important surface active species is Al^{+3}, and that the associated anions have a relatively minor role, if any, on improving glass durability.

From Figure 56, the importance of soluble aluminum additions in the surface passivation range (> 25 ppm Al^{+3}), is compared to the non-additive solution for various corrosion times. The greatest difference in Si^{+4} dissolution was observed for corrosion times $\geq$ 3 days. If this figure is compared with Figures 31-35 (from Chapter III, "Aqueous Corrosion of Lithia-Alumina-Silicate Glasses"), the potential of soluble aluminum additions may be seen. The 33L glass behaves as follows in the 100 ppm $AlCl_3$ solution:

1 day ---- 33L6A (33% Li_2O-6% Al_2O_3-61% SiO_2)
3 day ---- 33L4A (33% Li_2O-4% Al_2O_3-63% SiO_2)
7 day ---- 33L3A (33% Li_2O-3% Al_2O_3-64% SiO_2)
14 day ---- 33L3A (33% Li_2O-3% Al_2O_3-64% SiO_2)

From these data, it is seen that the 33L glass in a solution of soluble aluminum ions behaves as a ternary Li_2O-Al_2O_3-SiO_2 glass. However, care must be taken to ensure that the concentration of Al^{+3} in solution is not too low so as to cause an increase in total dissolution (i.e., $\leq$25 ppm Al^{+3}) as was observed in Figures 48 and 49.

In Figure 57, little difference in Li^{+} extraction is observed over the entire corrosion regime for both 0 ppm and 100 ppm Al^{+3} ($AlCl_3$) additions to the corrosion solution. This appears to be in agreement with the results

shown in Figure 49 on Li^+ extraction, i.e., 0 ppm extraction = 100 ppm extraction.

Results shown in Figure 58 illustrate the α dependence with corrosion time for both 0 ppm and 100 ppm Al^{+3} ($AlCl_3$) solution additions. These results again suggest that Al^{+3} ions in solution have the greatest effect on the total dissolution mode as opposed to the selective leaching mode (Figure 57). If the Al^{+3} ions affected the ion-exchange mode to a greater extent than the total dissolution mode, an increasing difference in Si^{+4} dissolution and constant Li^+ dissolution (as observed in Figure 56) with corrosion time would not be present. Furthermore, for corrosion times $\geq$ 3 days, the pH of the resulting corrosion solution (i.e., pH = 12) favors total dissolution. As shown from Figure 58, significantly more total dissolution occurs for glasses corroded in 0 ppm Al^{+3} solutions than occurs in the 100 ppm Al^{+3} solution. This implies that the glass surface has been partially protected (passivated) from OH^- attack in the 100 ppm Al^{+3} solution, while the glass surface exposed to the 0 ppm Al^{+3} solution has been moderately attacked by the OH^- ions in solution.

The IRRS results in Figure 59 show that for times $\leq$ 3 days a high silica surface film forms (as noted from

the high magnitude of the Si-O-Si stretch peak ($\sim$1080 cm^{-1}) due to the selective leaching of Li^{+} (as noted from a sharp decrease in the silica non-bridging oxygen bonds ($\sim$900 cm^{-1}) with the 100 ppm Al^{+3} ($AlCl_3$) solution. However, for times > 3 days, there is a decrease in the intensity of the Si-O-Si stretch peak. This is indicative of surface roughening confirmed by the SEM micrographs in Figure 61. Thus for the 100 ppm Al^{+3} addition, the glass surface is not completely passivated, but the resistance to corrosion is certainly enhanced as can be seen by comparing these spectra to similar spectra for the 10 ppm Al^{+3} addition (Figure 54).

Scanning electron micrographs (SEMs) of glasses shown in Figures 60 and 61 confirm the results in Figures 48, 49, and 51, i.e., rates of glass dissolution occur in the order of 25 ppm Al^{+3} ($AlCl_3$) > 0 ppm Al^{+3} ($AlCl_3$) > 100 ppm Al^{+3} ($AlCl_3$) solutions. In Figure 60, the surface has been moderately attacked in the 0 ppm $AlCl_3$ solution. For the 25 ppm Al^{+3} solution, Figure 60b, the surface has been severely attacked thereby confirming the results of Figures 48, 49, and 51. In Figure 61a, the glass surface suffered very little attack in the 100 ppm Al^{+3} solution, because of apparent surface passivation. There appears to be a discrete precipitate growth on the

glass surface corroded in the 100 ppm solution in contrast to the surface deterioration observed for the 0 ppm and 25 ppm Al^{+3} solutions. The glass surface exposed to the 100 ppm Al^{+3} solution is relatively smooth as seen from SEM results of Figure 61a. This confirms the IRRS results of Figure 59, i.e., little surface attack, therefore a smooth surface high in silica. In Figure 61b, after 14 days of corrosion in the 100 ppm Al^{+3} solution, the surface is slightly roughened. Since the surface is now slightly roughened, a decrease in the Si-O-Si stretch peak amplitude occurs in the IRRS spectra of Figure 59.

Both the SEMs and the IRRS spectra (Figures 60 and 61, and 56, respectively) demonstrate that the glasses corroded for 3 days in the 100 ppm Al^{+3} solution are considerably more protected from attack (passivated) by OH^- ions than the glasses corroded for 3 days in 0 ppm Al^{+3} solution. These results suggest that the primary role of Al^{+3} ions in solution is to retard the total dissolution mode, and hence, prevent surface deterioration.

Conclusions

I. There are two distinct regions in glass dissolution dependent upon Al^{+3} solution concentration. In region I, the glass dissolution increased for

$\leq$ 25 ppm Al^{+3} ($AlCl_3$) corrosion solution additions. In region II, the glass dissolution decreased for > 25 ppm Al^{+3} ($AlCl_3$) corrosion solution additions to a minimum for solutions containing 250 ppm (Al^{+3} ($AlCl_3$). Studies of the pH time dependence of corrosion showed that the pH for the 25 ppm Al^{+3} solution increased more rapidly than that observed for the 0 ppm Al^{+3} (3D-H_2O) level, and the 100 ppm Al^{+3} level. It is these higher pH values that cause the increased dissolution rates (Li^+ and Si^{+4}) to occur at the 25 ppm Al^{+3} addition, thereby resulting in the appearance of regions I and II. Presumably, for $\leq$ 25 ppm Al^{+3}, there are not enough Al^{+3} ions in solution to passivate the glass surface, i.e., there is incomplete neutralization of the surface active sites by the formation of alumino-silicate surface complexes. Hence, total dissolution occurs. For > 25 ppm Al^{+3} additions, the increase in solution pH is compensated by Al^{+3} ions passivating the glass surface thereby reducing the total dissolution character.

II. In general, the presence of Al^{+3} ions in solu-

tion decreases the rate of total dissolution, while relatively unaffecting the rate of selective leaching.

III. All aluminum salt compounds investigated yielded similar glass corrosion behavior (solution analysis and IRRS spectra) indicating that Al^{+3} ions are the effective corrosion inhibiting species.

IV. AES analysis revealed that the Al^{+3} ions diffused into the near surface of the glass in addition to being adsorbed onto the surface. However, the diffused layer (near surface) does not appear to affect the rate of selective leaching.

V. Comparison of results from adding both soluble aluminum ions to the corrosion solution and adding alumina to glass compositions indicate that the net effect of the soluble Al^{+3} additions is to produce a glass surface that behaves as a ternary glass with a certain percent of alumina in its composition. The optimal percentage of alumina for surface passivation appears to be in the range of 3-6 mole %.

CHAPTER V
SUMMARY AND CONCLUSIONS

The purpose of this investigation was to use standardized experimental procedures, analysis techniques and data analyses in understanding the role of mixed alkali and aluminum ions in controlling glass corrosion phenomena. Strong emphasis was placed on the chemical and physical changes occurring at the corroded glass surface. These changes were investigated by solution analysis, infrared reflection spectroscopy (IRRS), Auger electron spectroscopy (AES), and scanning electron microscopy (SEM).

A number of parameters affecting glass corrosion and their interaction were investigated, as described in the Appendix, in order to standardize the experimental techniques. These parameters and their respective effects on glass corrosion are as follows: (a) effects of corrosion time and temperature--pH controls the corrosion process; (b) effects of glass composition--the radial size and percent of the alkali ions present in the glass controls the corrosion process; (c) effects of bulk "versus" powdered glass--glass surface area (SA) to corrosion solution

volume (V) ratio controls the corrosion process; (d) effects of surface roughness of bulk glass--SA/V ratio controls the corrosion process; (e) effects of soluble ions in the corrosion solution--certain soluble ions in the corrosion solution which prevent total dissolution of the glass control the corrosion process; (f) effects of buffered corrosion solutions--the pH of the buffered solutions and the time at which it is overridden controls the corrosion process. Therefore, parameters (a)-(f) were either held constant or varied systematically in the investigation of the mixed alkali and aluminum ion effects on glass corrosion.

The Mixed-Alkali Effect (MAE) has been evaluated for both powder and bulk glasses. The extent of the MAE was determined by plotting alkali solution concentration versus glass composition for chemically-mixed, mechanically-mixed and non-mixed glasses.

The MAE may be divided into 2 categories: (a) Mixed-Alkali Effect (MAE)--when the chemical-mixture dissolution curve falls below the "idealized" dissolution curve, i.e., mechanical-mixture dissolution curve; and, (b) Classical Mixed-Alkali Effect (CMAE)--when a minima in the chemical-mixture dissolution curve is observed with respect to the single alkali oxide end members.

Two contributions to the Mixed-Alkali Effect (both CMAE and MAE) have been established: (a) structural effects in which the mixed alkali ions present in the glass structure result in a decrease in the diffusion rates and hence reduce corrosion rates; and, (b) corrosion solution ion effects in which mixed-alkali ions present together in the same corrosion solution cause a lowering of the ion-exchange rate and a decrease in selective leaching at the glass-solution interface.

It has been established that the magnitude of the MAE and CMAE is dependent upon the pH of the corrosion solutions. For pH $\leq$ 9, the MAE or CMAE is present, but for pH > 9, the MAE or CMAE diminishes. Also, the magnitude of the CMAE or MAE is a function of corrosion time and temperature, glass composition and the ratio of the glass surface area to corrosion solution volume, SA/V. However, in this investigation, all of the effects of these parameters are directly or indirectly dependent on solution pH.

Physical evidence of the classical Mixed-Alkali Effect (CMAE) is bulk glasses is shown from scanning electron micrographs (SEMs) and from infrared reflection spectroscopy (IRRS). It was observed that the more durable CMAE glasses show a slower and less heterogeneous

surface attack as compared to the single alkali glass end members.

The effects of Al_2O_3 additions on the corrosion of binary lithia-silicate glasses has been investigated controlling the corrosion variables (a)-(f) summarized above. The projected isochronal Si^{+4} dissolution curves demonstrate that Al_2O_3 additions improve the chemical durability of binary lithia-silicate glasses in accordance with the role of alumina in glasses, i.e., equal amounts of Al^{+3} ions "tie up" equal amounts of Li^{+} ions, thereby increasing the chemical durability.

The effect of pH on glass durability does not appear to be as important with glasses containing alumina as it is in the binary lithia-silicate glasses. This is thought to occur because of the formation of an alumina-silica rich surface film that is resistant to the total dissolution processes, and hence high pH values.

Both solution analysis and Auger electron spectroscopy (AES) results show that an aluminum rich film forms on the surface of alumina glasses during the later stages of corrosion.

Ternary compositional corrosion paths and infrared reflection spectroscopy (IRRS) results show that total dissolution is the primary mode of corrosion only for

glasses containing high lithia (46%) and/or low alumina (2.5%). Glasses lower in lithia (<46%) or higher in alumina (>2.5%) all exhibit selective leaching limited by the alumina rich surface film.

The effects of soluble aluminum ions on the corrosion behavior of a binary lithia-disilicate glass have been also investigated. The presence of >25 ppm Al^{+3} ions in solution decreases the total glass dissolution but has relatively little effect on the selective leaching processes. For additions of <25 ppm Al^{+3}, the total dissolution behavior is significantly increased over the 0 ppm Al^{+3} solution, 3D-H_2O.

All aluminum salt compounds investigated yielded similar results indicating similar corrosion behavior and surface film formation, suggesting that Al^{+3} is the effective corrosion inhibiting species. The data also suggest that the mechanism of glass surface passivation is the formation of an alumina and silica-rich surface film on the glass surface that interferes with the basic total dissolution corrosion process and not the formation of a thick surface layer acting as a physical barrier to alkali diffusion.

Most commercial container and window glass compositions contain Al_2O_3 and mixtures of Na_2O and K_2O. Al-

though no commercial glass compositions were investigated in this study, the results obtained for the binary, ternary and quaternary glasses have provided a basic understanding of the glass corrosion processes that are operative in commercial glasses. The results obtained show that critical concentrations of Al_2O_3 and Na_2O/K_2O ratios are required to achieve maximum durability. Furthermore, the reasons for the critical ranges have been established using the simpler compositional systems of this investigation. By applying the basic principles developed in this study to more complex glass systems, optimal corrosion resistant glasses may be formulated.

Although the author has investigated some of the more important parameters and phenomena of glass corrosion, there are still parameters that are of great interest and importance that were not covered: (a) stresses present in the glass; (b) phase separation; (c) crystallization; (d) dynamic solution environment; (e) replenishing solution; and, (f) extensive relative humidity exposure and cycling.

Also, additional studies of soluble ions in corrosion solutions are warranted. The mechanisms of how various soluble ions affect the glass surface, surface charges and surface ion bonding strengths are yet to be determined. The procedures and principles established in this work should provide useful guidelines in defining such studies.

APPENDIX
PARAMETERS AFFECTING GLASS CORROSION

Introduction

Reviews by Bacon,[1] Holland,[2] Weyl,[3] Das,[4] Doremus,[5] Volf,[6] and Morey[7] discuss the various experimental techniques that have been utilized to investigate corrosion parameters over the past 75 years. These reviews show that, in general, each individual investigation was approached from a different standpoint and yielded results applicable only to a specific problem. Each investigative team generally used different experimental techniques and studied different corrosion parameters. The interaction of various corrosion parameters was usually not considered.

The objective of the research described in this Appendix was to measure what the author considers to be the more important corrosion parameters in a systematic way in some standard systems and to verify the experimental techniques. This investigation focused on the effect of the following parameters on glass durability: (a) corrosion time and temperature; (b) glass composition; (c) effect of glass sample state on corrosion; (d) effect

of surface roughness on bulk glass corrosion; (e) effects of particle size and the ratio of glass surface area to corrosion solution volume (SA/V) on corrosion of glass powders; (f) effects of soluble ions and pH of the corrosion solution on corrosion rates; and, (g) effects of SO_2 treatments upon 100% relative humidity weathering and aqueous glass corrosion.

The relative importance of each of the above parameters on glass durability was determined using several common glass compositions. The principles established were used to design experiments to study systematically some of the more controversial interpretations of corrosion phenomena present in the glass industry as discussed in Chapters 2-4. The experimental tools described in this Appendix, chemical analysis of corrosion solutions and infrared reflection spectroscopy (IRRS), provide a strong qualitative interpretation of the importance of the various corrosion parameters. However, the more difficult questions raised in this dissertation require the use of several of the more sophisticated analytical tools such as Auger Electron Spectroscopy (AES), and Scanning Electron Microscopy (SEM analysis).

Corrosion Parameters

I. Corrosion Time and Temperature

The effect of both corrosion time and temperature on a binary Na_2O-SiO_2 glass (NS-31, Table VIII) is shown in Figure 62. Bulk planar surfaces polished with 600 grit dry SiC paper were corroded in triple distilled (3D) H_2O while maintaining a constant ratio of glass surface area (SA) to volume of corrosion solution (V), i.e., SA/V = 0.77 cm^{-1}. No attempt was made to control the pH of the solution during the corrosion process. The Na^+ concentration in the corrosion solution was monitored as a function of time and temperature and the results plotted in Figure 62. Two regions of corrosion for each temperature were observed as a function of time, with both regions exhibiting linear behavior. The slopes of the Na^+ molarity curves as a function of corrosion time were approximately equal for the temperatures investigated in region I, and again were approximately equal in region II. The changeover from region I to region II occurs at approximately the same concentration of Na^+ loss regardless of the temperature. Although the slopes for each temperature are equal in region I (i.e., slope $\simeq$ 1/2), the extent of Na^+ dissolution at equivalent times becomes greater as the temperature increases. The same phenomenon is observed

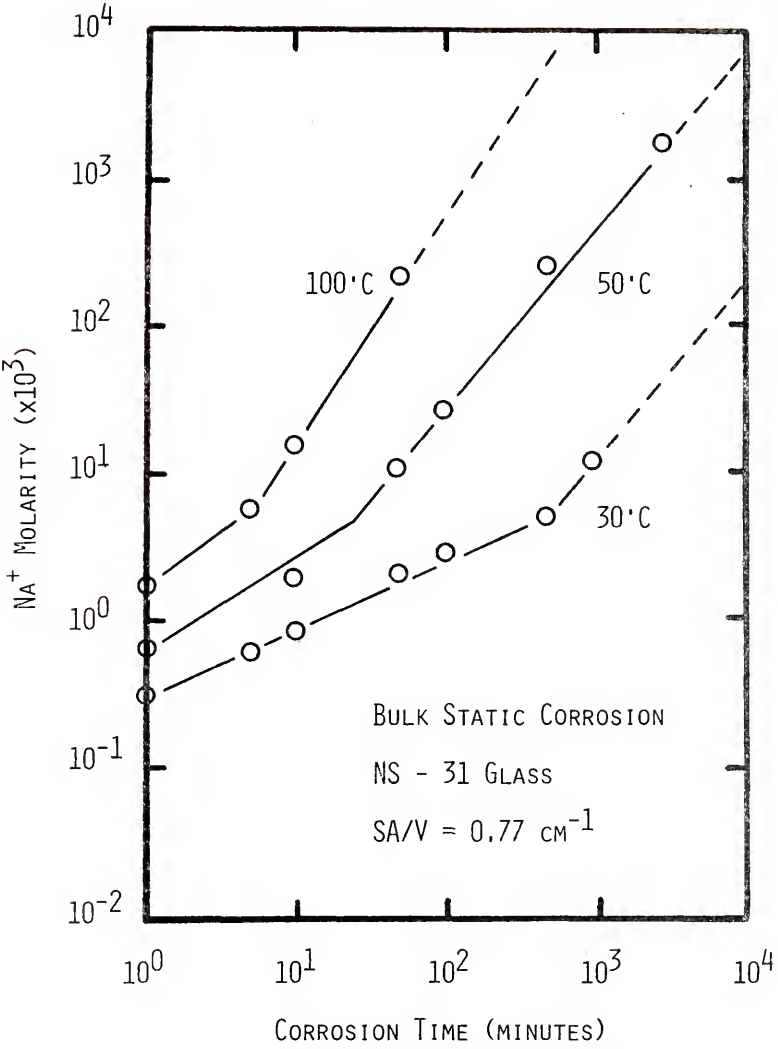

Figure 62. Na^+ solution data for bulk NS-31 glasses corroded in triple-distilled water.

for region II where the slope ≈ 1.0. The time at which the transition between region I and II occurs increases as the temperature of the corrosion solution decreases.

The data in Figure 62 is in accord with the results in the literature,[1-11,24,37,38,46,53,58,59,68,69] which verifies that the experimental techniques utilized in this research are valid means of studying the corrosion process of glasses. In region I, the most important reaction is the ion-exchange between the Na^+ ions (alkali ions) in the glass with the H^+ ions in the corrosion solution[11,68] (equation 1). As H^+ ions are removed from the corrosion solution, more H_2O molecules must dissociate in order to maintain the equilibrium, $[H_2O] \rightleftarrows [OH^-] + [H^+]$. As a result of H^+ ion removal ($[OH^-] > [H^+]$), an increase in pH occurs. Douglas and El-Shamy[11] have shown that when pH > 9, the OH^- ion attack of the Si-O-Si bonds becomes significant (equations 2 and 3). Therefore, at pH > 9, region II kinetics become dominant and total dissolution is the prevailing corrosion mechanism.

The quantity of Na^+ ions found in the corrosion solution in region I is dependent upon the diffusion of Na-ions (alkali ions) through the glass and/or through the surface corrosion layers.[14,28,39] Therefore, the extent of the Na^+ dissolution is a function of the square root of

time (equation 4). In region II, total glass breakdown occurs, and the rate of Na^+ dissolution is directly proportional to the corrosion time (equation 4).

Thus, the two general corrosion regimes reported by other investigators using a variety of techniques have been confirmed using the procedures adopted throughout the series of studies in this Appendix and Chapters 2-4.

II. Glass Composition

The effect of the type and percentage of various alkali ions in binary alkali-silicate glasses, $(X)Li_2O\cdot(1-X)SiO_2$ and $(0.20)R_2O\cdot(0.80)SiO_2$ (Table VIII), on glass corrosion are shown in Figures 63, 64 and 65, 66. Bulk planar surfaces polished with 600 grit dry SiC paper were corroded in triple distilled H_2O at 50°C while maintaining constant SA/V = 0.77 cm^{-1}. No attempt was made to control the pH of the solution during the corrosion process.

According to Weyl,[17] chemical durability is related to the degree of oxygen ion polarization (proportional to the radius of the alkali ions) and to the presence of highly polarized oxygen ions present in the glass structure (equal to the percent of alkali ions). In the Weyl theory, the oxygen ions associated with silicon ions are ionic-covalently bonded and therefore are not very

Table VIII

Glass Composition Investigated, Mole %

Code	Li_2O	Na_2O	K_2O	CaO	SiO_2
LS-20	20				80
LS-33	33				67
LS-46	46				54
NS-20		20			80
NS-31		31			69
KS-20			20		80
KS-25			25		75
NCS-1510		15		10	75
NCS-2010		20		10	70
NKCS-120310		12	3	10	75

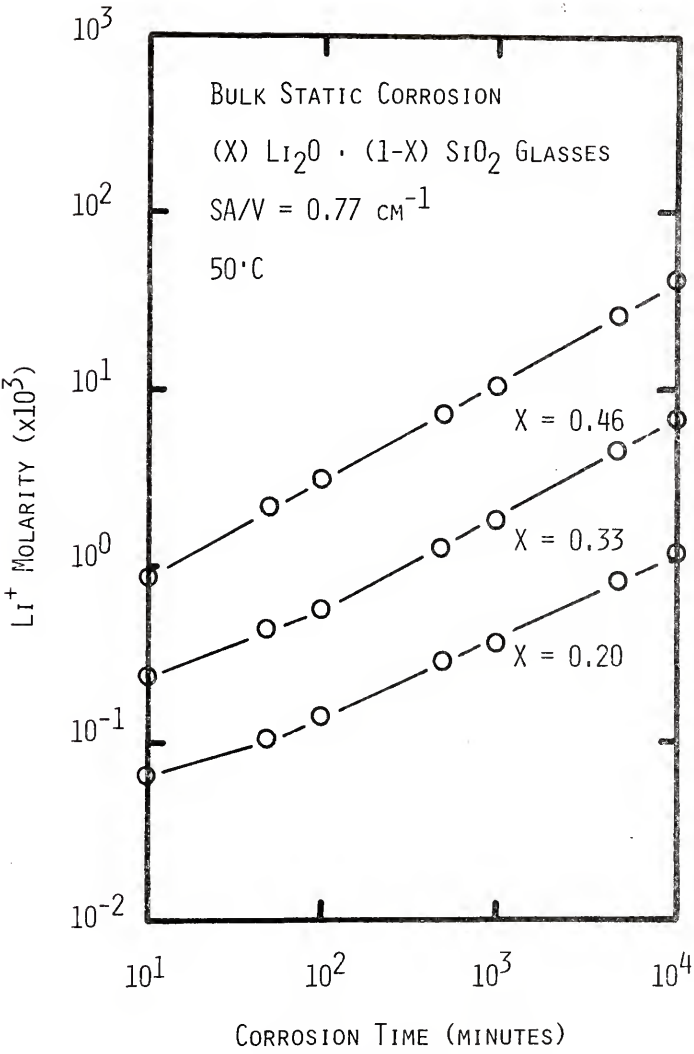

Figure 63. Li^+ solution data for bulk $(X)Li_2O\cdot(1-X)SiO_2$ glasses corroded in triple-distilled water.[2]

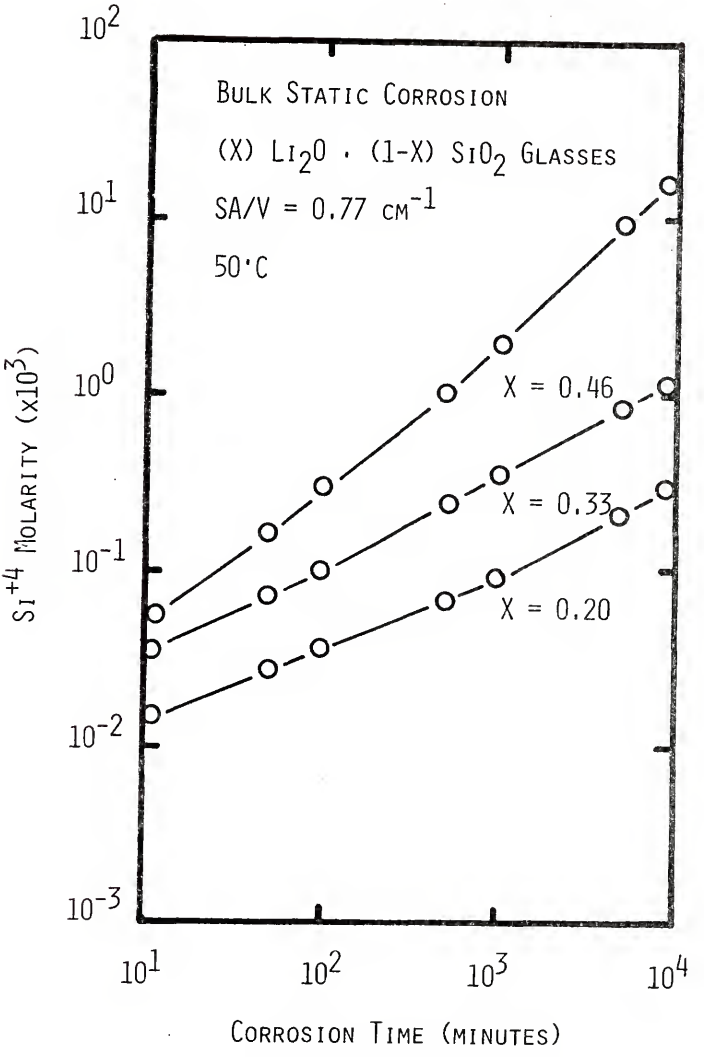

Figure 64. Si^{+4} solution data for bulk $(X)Li_2O\cdot(1-X)SiO_2$ glasses corroded in triple-distilled water.

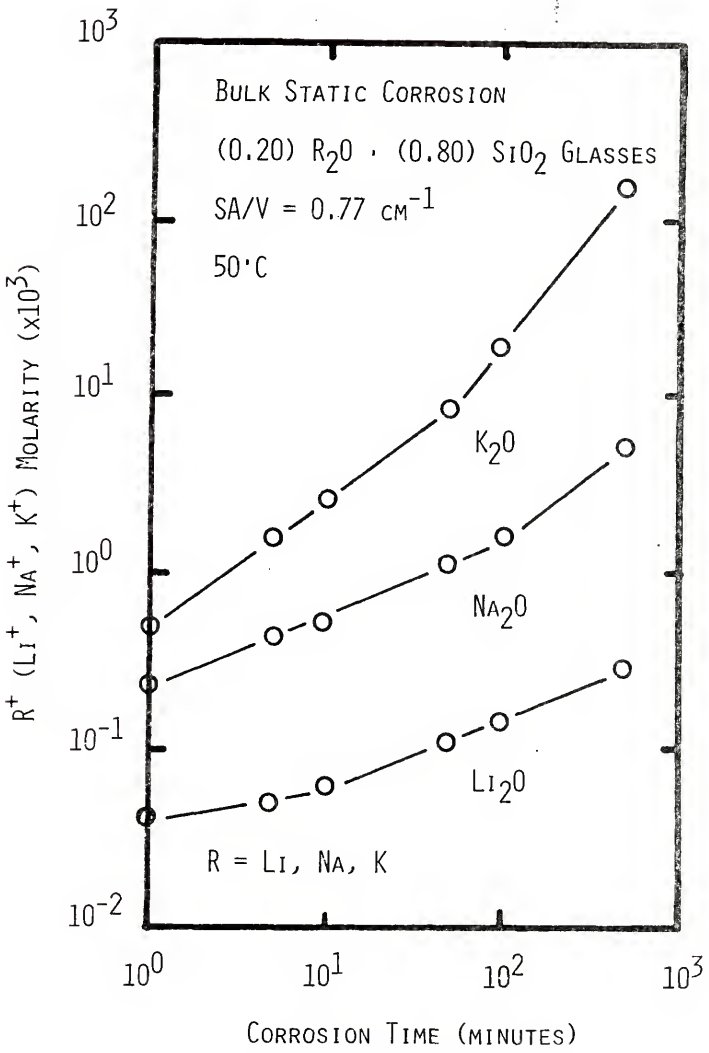

Figure 65. Li^+, Na^+ and K^+ solution data for bulk $(0.2)R_2O \cdot (0.8)SiO_2$ glasses corroded in triple-distilled water.

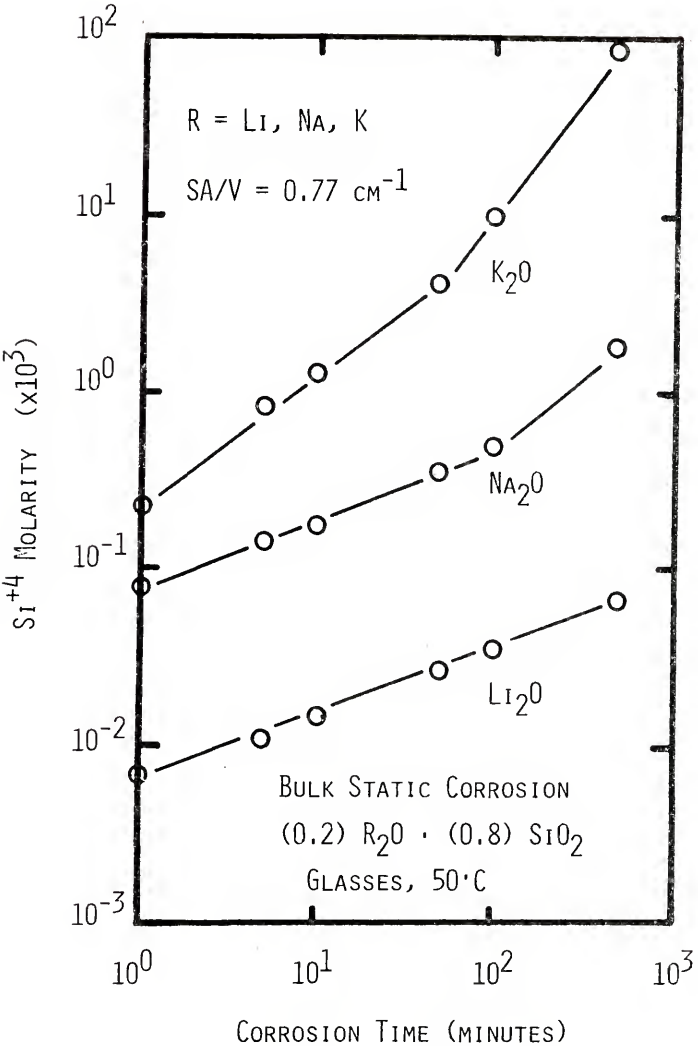

Figure 66. Si^{+4} solution data for bulk $(0.2)R_2O\cdot(0.8)SiO_2$ glasses corroded in triple-distilled water.

polarized. In contrast, when oxygen ions are ionic-bonded to the alkali ions, they are highly polarized. From this premise, a glass containing only oxygen ions of low polarization, a 100% SiO_2 glass, will corrode to a small extent. However, glasses containing oxygen ions of high polarization corrode at higher corrosion rates proportional to the polarization of the alkali ions and the percentage of alkali in the glass.

In accord with this theory, the Li^+ and Si^{+4} concentration of the corrosion solution was monitored as a function of time and plotted as a function of mole percent of lithium-oxide in the glass in Figures 63 and 64. It can be seen from these figures that increased glass dissolution (Li^+ and Si^{+4} concentration) occurs as the alkali content is increased. These results are consistent with the theory projected by Weyl[17] and the findings of numerous other investigators.[37,38,46,59]

As mentioned earlier, the degree of oxygen ion polarization has been assumed to be proportional to the ionic radius of the alkali ions present, i.e., oxygen ions associated with K_2O glasses have a higher degree of polarizability than that of Na_2O or Li_2O containing glasses. Therefore according to theory, the order of chemical durability should be in the following order, from

the highest durability to lowest: Li_2O > Na_2O > K_2O glasses.

The concentration of Li^+, Na^+ and K^+ and Si^{+4} of the corrosion solution was monitored as a function of corrosion time for several R_2O-SiO_2 glasses and plotted in Figures 65 and 66. At a constant 20 mole percent alkali-oxide, the relative order towards dissolution of either R^+ or Si^{+4} ions is as follows: Li_2O glasses > Na_2O > glasses > K_2O glasses. Again, these results are consistent with the theory proposed by Weyl[17] and the findings of numerous other investigators.[37,38,46,59]

Thus, the bulk glass methods used in this investigation confirm the behavior of simple binary alkali-silicate glasses and verify that the experimental techniques utilized in this research are valid means of studying the corrosion process.

III. Effect of Glass Sample State on Corrosion

Most previous investigations have used either glass powders with chemical solution analysis or planar glass corrosion with microscopic measurement of corrosion films to study the corrosion processes. There has been little effort in previous work to compare the behavior of bulk planar glasses with powders of the same composition, to change the glass powder particle sizes, or to vary their SA/V ratios.

The result of both bulk and powder corrosion of a ternary Na_2O-CaO-SiO_2 glass (NCS-1510, Table VIII) is shown in Figure 67. Bulk planar glasses were corroded in triple distilled (3D) H_2O at 100°C while maintaining a constant SA/V = 0.77 cm^{-1}. The experimental arrangement is shown in Figure 1. Powder glasses of the same composition were prepared by pulverizing with an alumina mortar and pestle. The particle size utilized was -60+100 mesh (149-250 μm). Corrosion was conducted at a SA/V ratio of 0.77 cm^{-1} and 0.077 cm^{-1} in 3D-H_2O at 100°C in the experimental setup shown in Figure 2. No attempt was made to control the pH of the solution during the corrosion process.

The Si^{+4} concentration in the corrosion solution was monitored as a function of corrosion time and is plotted in Figure 67. The Si^{+4} concentration curve for bulk corrosion exhibits linear behavior up to 14 days. Glass powder Si^{+4} dissolution, for corrosion times <3 hours, exhibits rapid increases up to 3 days of corrosion, with the 0.77 cm^{-1} SA/V ratio exhibiting a more rapid increase than the 0.077 cm^{-1} ratio. This rapid increase in Si^{+4} dissolution for both SA/V ratios in the first 3 days may be attributed to the following factors:[39] (i) dissolution of "fine" (<<100 mesh) particles attached to the -60+100

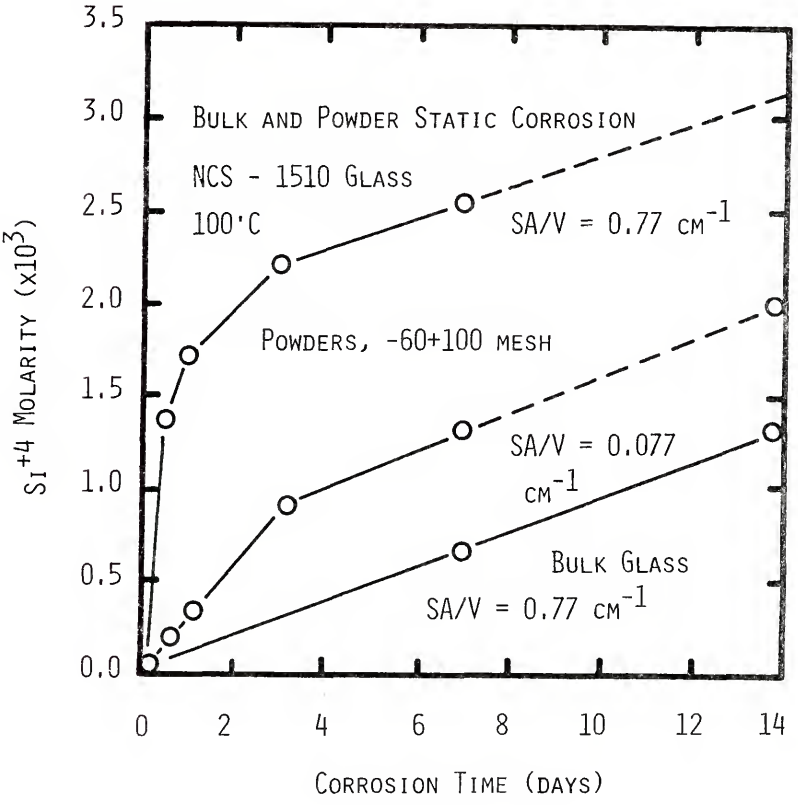

Figure 67. Si^{+4} solution data for bulk and powder NCS-1510 glasses corroded in triple-distilled water.

mesh particles (refer to Figure 68); and, (ii) concentration cell effects which cause a rapid increase in solution pH resulting in an increase in the corrosion kinetics of glass powders.

The approximately equal slopes observed for both bulk, 0.77 cm^{-1} SA/V ratio, and powders after 3 days regardless of SA/V ratios suggest equal rates of dissolution for the longer corrosion times. The equal dissolution rates observed for bulk surfaces and powder surfaces after 3 days is probably a result of the total dissolution of the "fine" particles associated with both powders and abraded surfaces of bulk glasses.

The effects of the ratio of glass surface area (SA) to corrosion solution volume (V) of a ternary Na_2O-CaO-SiO_2 glass (NCS-1510, Table VIII) is shown in Figure 69 for powder corrosion. Powdered glasses (-325+400 mesh, i.e., 37-46 μm) were prepared by pulverizing with an alumina mortar and pestle. The powders were corroded employing various SA/V ratios in 3D-H_2O for 12 hours at 100°C (see Figure 2). No attempt was made to control the pH of the solution during the corrosion process.

In Figure 69, linear behavior is observed for Si^{+4} dissolution versus SA/V ratio. This type of behavior is expected since an increase in glass surface area for a

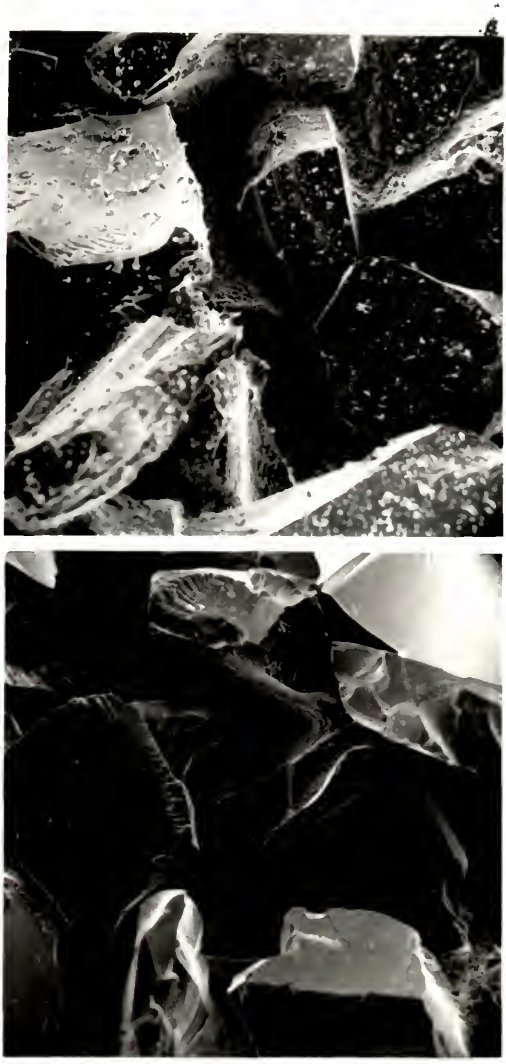

(a)

(b)

Figure 68. Scanning electron micrographs for -60+100 mesh NCS-1510 glass powders (a) corroded (1000X), and (b) corroded 3 days at 100°C (1000X).

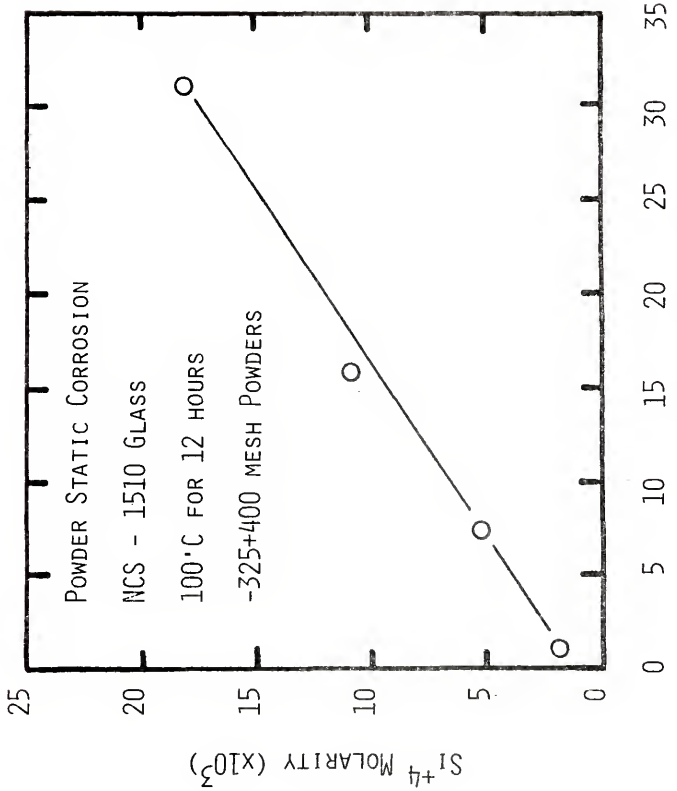

Figure 69. Si^{+4} solution data for powder NCS-1510 glasses corroded in triple-distilled water.

constant corrosion solution volume linearly increases the magnitude of Si^{+4} dissolution.[70,71]

It is expected that if a given glass surface area to corrosion solution volume is originally present before corrosion that varying the particle size would change the rate of glass dissolution only slightly due to a decrease in particle surface area during corrosion.

The effects of corrosion time and particle size on Na_2O-K_2O-CaO-SiO_2 glass powders (NKCS-120310, Table VIII) are shown in Figure 70. The Si^{+4} dissolution curves may be divided into three regions for this glass system. In region I, both particle sizes yield approximately equal dissolution rates with both exhibiting a rapid increase in Si^{+4} dissolution up to 12 hours (as evidenced by the slope of the curve). This rapid rate increase was explained earlier in this section as being due to the dissolution of the very fine glass particles. In region II (12 hours to 3 days), and region III (3 days to 7 days), although the magnitude of the curves are only approximately equal, the rates of Si^{+4} dissolution are equal. The small discrepancy observed in region I and the slightly larger discrepancy observed in regions II and III may be attributed to the fact that an average particle size for each powder distribution was used for preparing

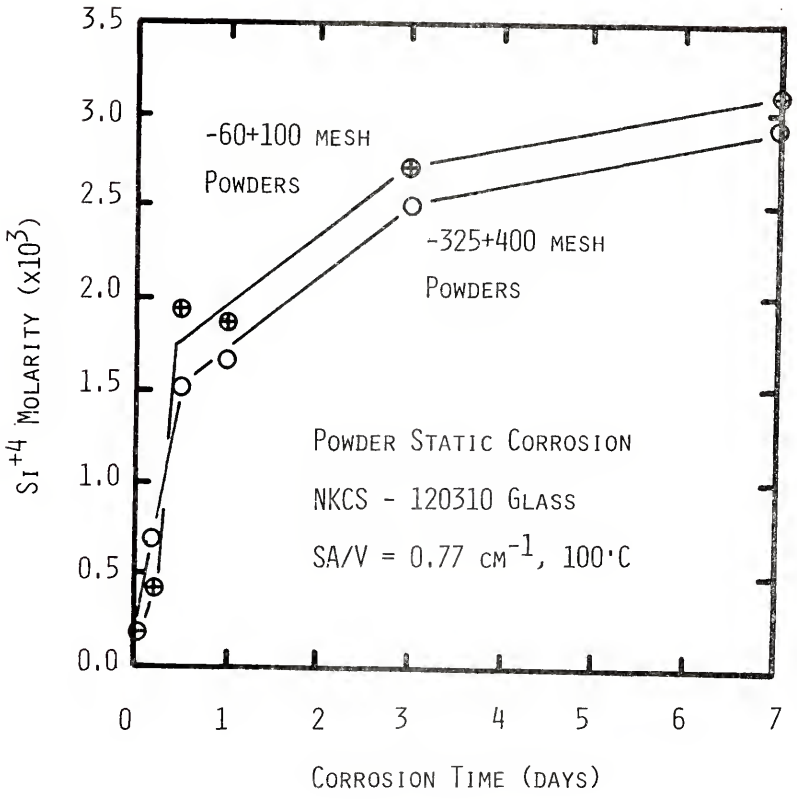

Figure 70. Si^{+4} solution data for powder NKCS-120310 glasses corroded in triple-distilled water.

the various SA/V ratios. This value was determined by averaging the mesh sizes associated with the two sieves used for collecting the powders. This technique does not always provide an accurate SA/V ratio since the average particle size of a powder distribution collected between two screens is not necessarily equal to the algebraic average.

The data illustrated in this section show that the SA/V ratio is an important parameter in glass corrosion. As the SA/V ratio increases, the corrosion rate also increases. The actual particle size used for evaluating glass corrosion does not appear to be important as long as the SA/V ratio is held constant. However, maintaining a constant SA/V is not trivial when a particle size distribution is utilized instead of a constant particle size. This is due primarily to the problem associated with calculating surface area from a non-uniformly distributed particle size and irregular particle geometry.

IV. Effects of Surface Roughness on Bulk Glass Corrosion

Mechanical strength and glass durability are both related to glass surface roughness.[72] The scratches present on bulk planar glass surfaces act as stress raisers[73] for crack propagation and loss of mechanical strength and as heterogeneous sites[46,74] for increasing the glass cor-

rosion process. Previous studies have shown that the size of the surface flaws is increased and their shape is altered by the corrosion process,[75] which influences the mechanical behavior and the development of corrosion films on the glass surface. However, previous investigations have not determined whether the role of surface scratches is simply one of increasing the SA/V ratio for corrosion or may in fact contribute one or more additional factors discussed above.

The effect of surface roughness on glass corrosion on a ternary Na_2O-CaO-SiO_2 glass (NCS-2010, Table VIII) is shown in Figure 71. Bulk planar glasses polished with 120, 320, and 600 grit SiC paper were corroded in triple distilled H_2O at 100°C. The apparent SA/V ratio was maintained at 0.77 cm^{-1}. The true glass surface area to corrosion solution volume (SA/V) was determined to be 0.77 cm^{-1} (600 grit), 1.24 cm^{-1} (320 grit), and 1.42 cm^{-1} (120 grit) from profilometry measurements. No attempt was made to control the pH of the solution during the corrosion process.

The Si^{+4} concentration in the corrosion solution was monitored as a function of corrosion time and surface roughness for the three SA/V ratios and plotted in Figure 71. The magnitude of the Si^{+4} concentration curve is

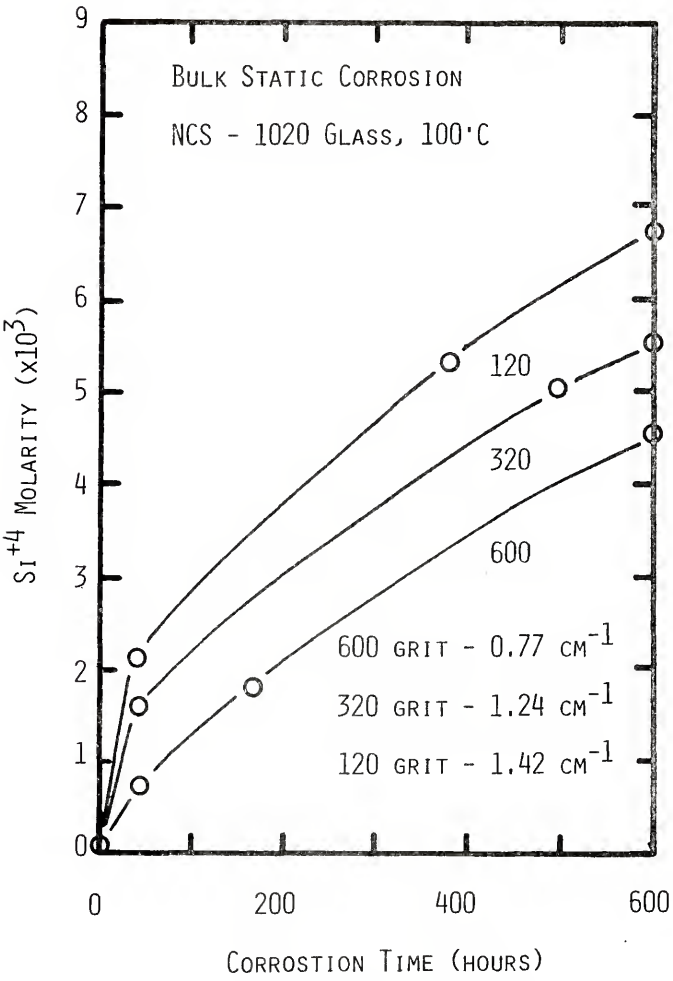

Figure 71. Si^{+4} solution data for bulk NCS-1020 glasses corroded in triple-distilled water.

proportional to the surface roughness and the corresponding SA/V ratio. The 120 grit surface is the roughest (1.42 cm^{-1}) and corrodes most rapidly. The 600 grit surface corrodes the slowest with the corrosion rate of the 320 grit (1.24 cm^{-1}) surface being in between that for the 120 and 600 grit surface.

Infrared Reflection Spectroscopy (IRRS) results for the above samples are shown in Figures 72-75. Freshly abraded (fa) glass spectra are shown in Figure 72 for the specimens with 120, 320, and 600 grit surfaces. The 600 grit surface exhibits the highest spectral peaks because it has the least surface roughness. Figure 73 illustrates the IRRS spectra for the 3 samples after 7 says of corrosion at 100°C. These spectra show that all three surface finishes exhibit a slight surface roughening since there is a general decrease in intensity at all wavenumbers. However, the shift of the Si-O-Si stretch peak ($\sim$1080 cm^{-1}) to slightly higher wavenumbers[36] is indicative of surface dealkalization and silica rich surface layer formation. The rate of dealkalization and silica film formation is dependent on the extent of surface roughness.[36] However, the surface reactions and corrosion mechanisms are unchanged. The importance of the surface scratches is to increase both the rate of attack

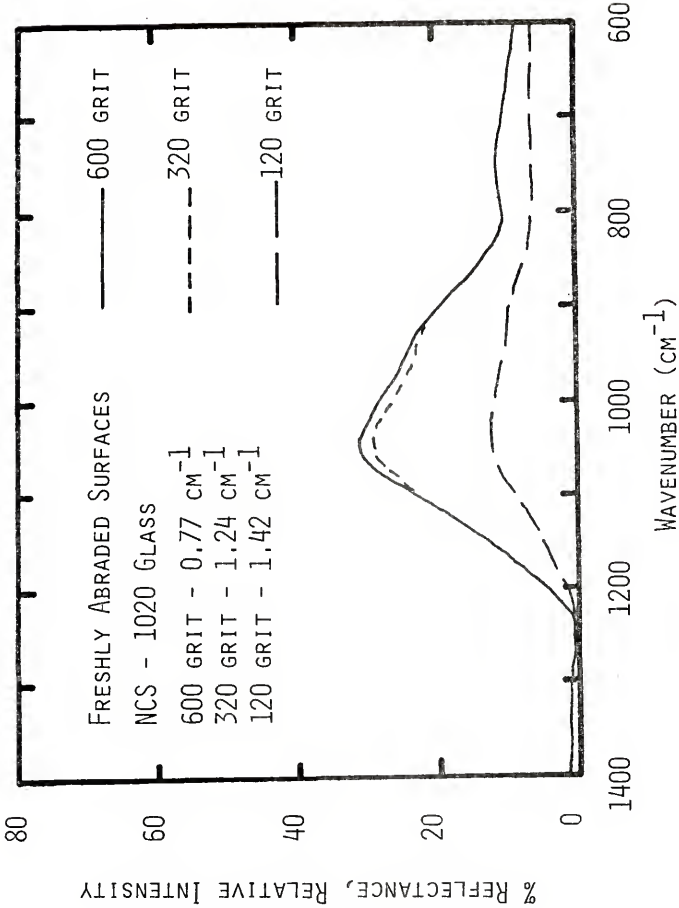

Figure 72. Infrared reflection spectra for freshly abraded bulk NCS-1020 glass surfaces.

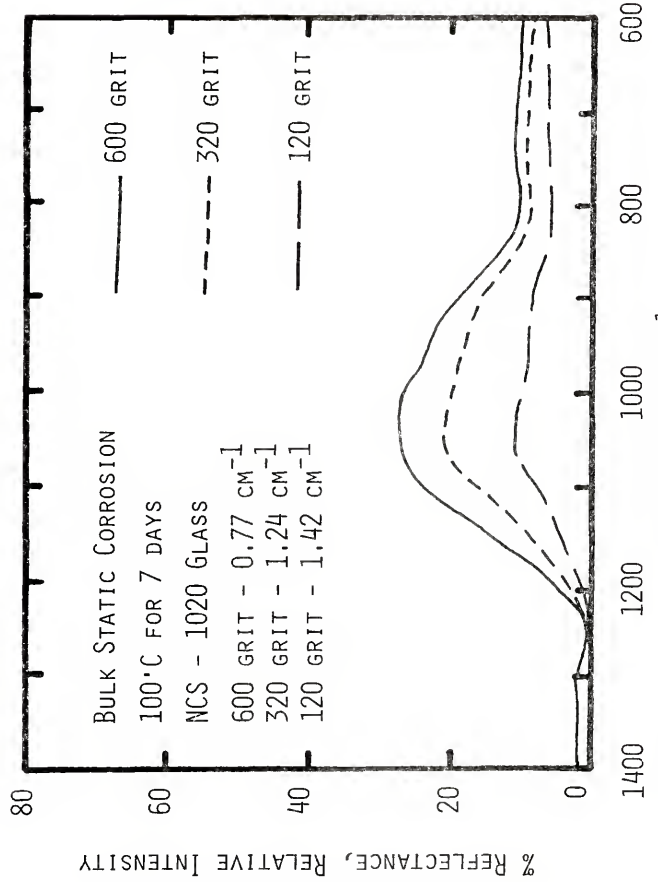

Figure 73, Infrared reflection spectra for bulk NCS-1020 glasses corroded in triple-distilled water for 7 days.

via an increase in SA/V ratio and an increase in the heterogeneity of the attack. However, the spectra shown in Figure 74 indicate that the surfaces for the 120 grit surface is becoming smoother after 21 days of corrosion. This is evident from the increase in the amplitude of the Si-O-Si stretch peak ($\sim$1080 cm^{-1}) for the spectra of the 120 grit glass surface. This increase in amplitude is not attributed to an increase in dealkalization, since the position of the Si-O-Si stretch peak is the same as for the 320 and 600 grit specimens which did not exhibit an increase in spectral amplitude.[36] IRRS spectra for the glasses subjected to 28 days of corrosion at 100°C are shown in Figure 75. Only a slight surface roughening is observed for the 600 and 320 grit surfaces as manifested by the small decrease in spectral intensity compared to the 21 day data. Severe surface roughening was observed for the 120 grit surface as shown by the large decrease in the Si-O-Si stretch peak intensity.

Thus, comparison of the Si^{+4} solution data for the various SA/V ratios reveals that the extent of glass dissolution is directly proportional to the surface area of the glass exposed to the corrosion solution volume. The presence of cracks, scratches and sharp edges which can act as stress raisers have very little influence on the

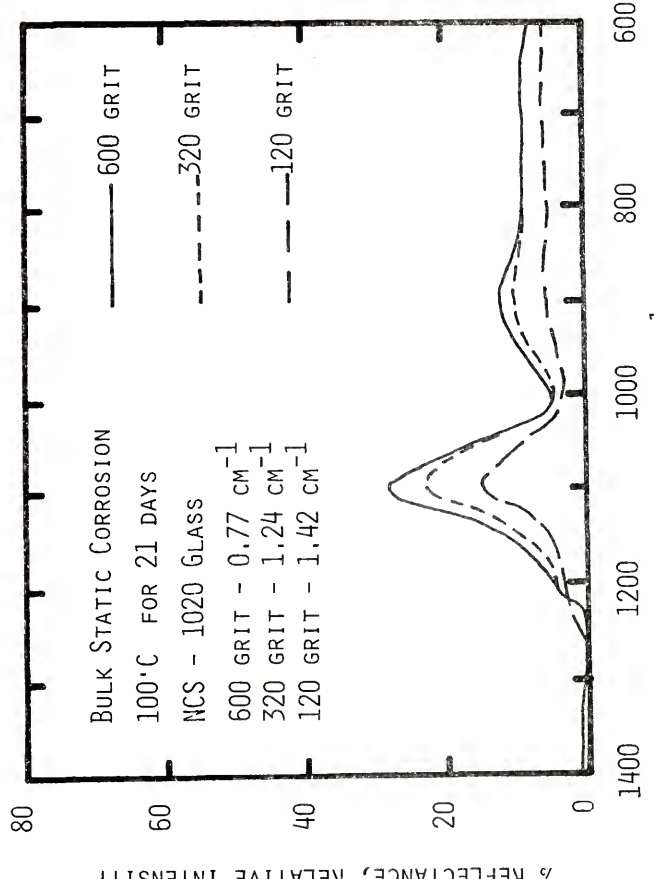

Figure 74. Infrared reflection spectra for bulk NCS-1020 glasses corroded in triple-distilled water for 21 days.

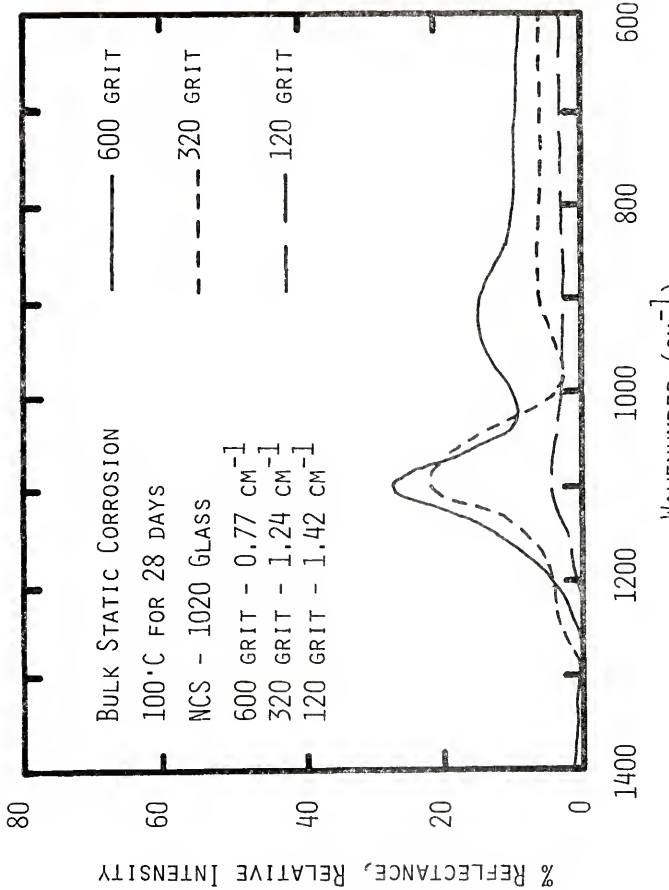

Figure 75. Infrared reflection spectra for bulk NCS-1020 glasses corroded in triple-distilled water for 28 days.

corrosion rate, other than increasing the SA/V ratio. However, the heterogeneity of the surface attack increases appreciably with roughness of the surface.

V. Effects of Solution Ions on Glass Durability

The effects on glass durability of adding soluble ions as glass corrosion inhibitors directly to the corrosion solution have not been evaluated extensively. Most investigations have focused attention on evaluating the effects of ions that were in most cases common to both the glass composition and the corrosion solution addition.[60-63] To date, no attempt has been made at separating the beneficial effects of the ions contributed to the solution via dissolution by the glass from those already present in the corrosion solution. In the present investigation, a binary glass was corroded in solutions containing various cations. The ions investigated, although commonly used in commercial glass compositions to improve durability, were not initially present in the $Li_2O{\cdot}2SiO_2$ glass used for this investigation. The effects of various divalent and trivalent cations as inhibitors on the corrosion process (Si^{+4}, Li^{+} dissolution) of a binary $Li_2O{\cdot}2SiO_2$ glass (LS-33, Table VIII) is shown in Table IX. Also presented in Table IX is a parameter, α, which is useful in discussing glass corrosion, and in particular, ion-exchange/total dissolution (equation 5).

Table IX

Solution Data for a Bulk LS-33 Glass Corroded in Solutions Containing Various Cations (100 ppm) and 3D-H_2O for 3 Days at 50°C

	3D-H_2O	$Al^{+3}(AlCl_3)$	$Ca^{+2}(CaCl_2)$	$Zn^{+2}(ZnCl_2)$	$Cu^{+2}(CuCl_2)$
Si^{+4} Molarity ($x10^3$)	0.42	0.23	0.03	0.13	0.53
Li^{+} Molarity ($x10^3$)	11.43	16.14	21.14	12.14	11.43
α	0.037	0.014	0.001	0.011	0.046

Bulk planar surfaces, polished with 600 grit dry SiC paper were corroded in triple distilled H_2O and in solutions containing 50 ppm of various cations while maintaining a constant SA/V = 0.77 cm^{-1}. No attempt was made to control the pH of the solution during the corrosion process. The Si^{+4} and Li^{+} molarity concentrations (x 10^3) and α values for various cations (50 ppm level, and 3D-H_2O) in solution are shown in Table IX for 3 days of corrosion at 50°C.

Since Si^{+4} ions can only enter the corrosion solution via total dissolution, the various salt compounds may be listed in the following decreasing order for their ability to prevent Si^{+4} dissolution (total dissolution): $CaCl_2$, $ZnCl_2$, $AlCl_3$, 3D-H_2O and $CuCl_2$. The addition of $CuCl_2$ to the corrosion solution results in an enhanced Si^{+4} dissolution value over that observed for 3D-H_2O, the uninhibited state.

From the α values of Table IX, the various compounds are listed in decreasing order of their ability to promote the ion-exchange reaction and thereby prevent total dissolution: $CaCl_2$, $ZnCl_2$, $AlCl_3$, 3D-H_2O and $CuCl_2$.

Infrared Reflection Spectroscopy (IRRS) spectra for 3D-H_2O and the various divalent and trivalent cations are shown in Figure 76 (3 days corrosion at 50°C) in compari-

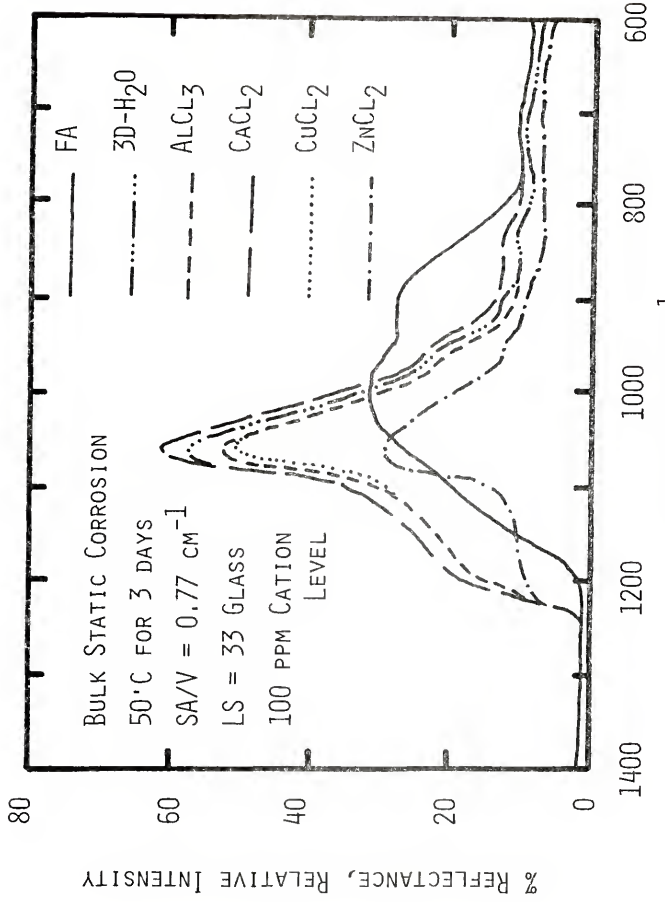

Figure 76. Infrared reflection spectra for bulk LS-33 glasses corroded in triple-distilled water and solutions containing various cations (100 ppm level).

son to the freshly abraded glass surface. The spectra demonstrate the ability of the various ionic solutions to improve glass durability. Since Si-O-Si stretch peak amplitude is affected by both film formation and surface roughness, the most accurate indication of glass corrosion are changes in the IRRS peak wavenumber position.[36] The more durable glasses exhibit the smallest changes in the wavenumbers of the Si-O-Si peak from the freshly abraded (fa) position during corrosion. As was shown from the solution data, the IRRS data also indicates that the $CaCl_2$ solution is the most effective solution ion for improving glass durability.

Thus, the importance of soluble ions as corrosion inhibitors in the corrosion solution has been demonstrated by comparing the corrosion resistance of a simple binary glass in 3D-H_2O with that for the same glass in solutions containing soluble ions. Ca^{+2} ions in solution improve the corrosion resistance of $Li_2O{\cdot}2SiO_2$ glass by a factor of 10 in comparison to 3D-H_2O. Cu^{+2} ions in solution were observed to greatly accelerate the corrosion reaction.

VI. Effects of Buffered Corrosion Solutions on Glass Durability

The pH of the corrosion solution is probably the single most important parameter affecting glass dur-

ability. The mechanism of corrosion is primarily dependent on the pH range of the corrosion solution, i.e., pH $\leq$ 9, ion-exchange is the dominant corrosion mechanism, pH > 9, total dissolution is the dominant mechanism. Thus, by controlling the solution pH via buffering agents, both the mechanism and the extent of corrosion can be controlled.

The effects of both corrosion time and corrosion solution (3D-H_2O, 5.4 pH buffer, and 9.4 pH buffer), on a K_2O-SiO_2 glass (KS-25, Table VIII) are shown in Figure 77 for bulk glass corrosion. Bulk planar surfaces, polished with 600 grit dry SiC paper were corroded in triple distilled (3D) H_2O, 5.4 pH succinate buffer,[76] and 9.4 pH glycine-NaOH buffer,[76] at 37°C. The glass surface area (SA) to corrosion solution volume (V) was maintained at a constant rate, i.e., SA/V = 0.77 cm^{-1}.

The Si^{+4} concentration was monitored as a function of corrosion time and corrosion solution as shown in Figure 77. Both 3D-H_2O and 5.4 buffer solution Si^{+4} concentrations start out significantly lower than the 9.4 buffer solution, and remain lower throughout the duration of the corrosion experiment. This is explained by the fact that the glass placed in the 9.4 solution experienced total dissolution during the entire corrosion period,

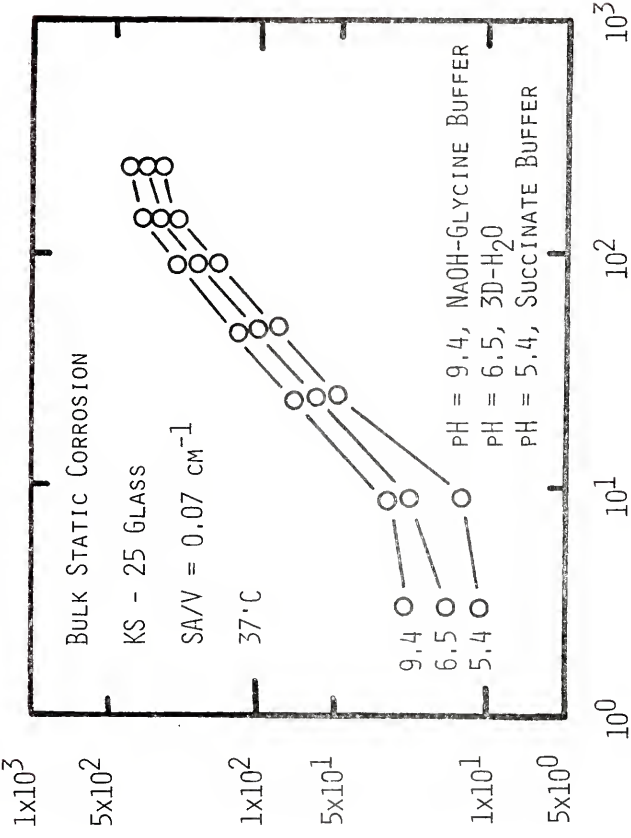

Figure 77. Si^{+4} solution data for KS-25 glasses corroded in triple-distilled water and pH = 5.4 and 9.4 buffered solutions.

whereas ion-exchange initially was the principal corrosion mechanism for the glasses corroded in the 5.4 and 3D-H_2O solutions.

From previous work,[77] the pH of buffered solutions (for a glass of similar chemical composition) is overridden between 10 and 25 hours at 37°C.

The breaks in the Si^{+4} dissolution curves occurring at ∿9 hours are thought to correspond to the point where the effects of the buffering agents in solution are overridden by the ion-exchange process. After >9 hours of corrosion, the rate of Si^{+4} dissolution in all three solutions are approximately equal and the difference in Si^{+4} concentration in each solution is the same after 400 hours as after 9 hours. The fact that the change in Si^{+4} dissolution rate occurred at approximately the same corrosion time for all three solutions suggests that the presence of Na^{+} ions in solution has little effect on either the ion-exchange process or the total dissolution process for glasses of high solubility.

From these experiments, it is seen that for short periods of corrosion time, buffered solutions can decrease glass dissolution. If the glass is relatively durable and the pH of the buffered solution is low, i.e., 5.4, the buffered solution can exert a high degree of corrosion

repression. However, as the solubility and SA/V ratio of the glass increases, the effects of the buffered solutions are overridden to a faster degree due to ion-exchange and as a result, do not offer much protection from total dissolution.

VII. SO_2 Surface Treatments

The potential use of SO_2 surface treatments in increasing glass durability has been known for many years.[1,2,78,79] According to Coward and Turner,[80] the "bloom" formed on SO_2 treated soda-lime glass was sodium sulphate (Na_2SO_4). From their experiments, the surface deposit formed was the same in 1% or 100% SO_2 atmospheres and repeated treatments of the surface gave successively thinner deposits.

It has been generally concluded by previous investigators[2,78-82] that during SO_2 heat treatment at 500°C, the alkali flows to the surface under a concentration gradient and is removed by the reaction with SO_2. This process therefore can be used to produce a glass with a low alkali content at the glass surface.

It has been proposed by several investigators[1,2,68] that water vapor in the SO_2 gas influences the dealkalizating process. The main conclusion is that if H^+ ions did not diffuse into the glass to replace the Na^+ ions

(alkali ions) removed from the glass, then the process would stop as the glass became electrically negative. An alternative model has been proposed in which the alkali must diffuse to the glass surface as Na_2O if the SO_2 gas is dry, but the dealkalizing process would then be much slower because of the lower diffusion constant of soda.[2,81,82]

Williams and Weyl[81,82] suggest that the formation of alkali sulphate (R_2SO_4) on a glass surface by the following two reactions:

(i) presence of H_2O in hot SO_2 treatment atmosphere

$$2R^+\text{-glass} + SO_2 + 1/2\ O_2 + H_2O = 2H^+\text{-glass} + R_2SO_4$$

(ii) absence of H_2O in hot SO_2 treatment atmosphere

$$R_2O + SO_2 + 1/2\ O_2 = R_2SO_4$$

According to Holland,[2] the second reaction only becomes important at temperatures above 600°C when diffusion of R^+ and O^{-2} ions to the surface dominates over the ion-exchange reaction.

The objective of the following investigation is to determine the effects of SO_2 treatments on the various processes of glass corrosion. In other words, an attempt was made to determine whether the SO_2 treatment improves glass durability by altering the ion-exchange process or

by retarding the total dissolution mechanism. The principal tool utilized for this investigation was infrared reflection spectroscopy (IRRS).

A. SO_2 Surface Treatments - Aqueous Corrosion

The effects of various SO_2 treatments on a $Li_2O{\cdot}2SiO_2$ glass (LS-33, Table VIII) are shown in Figures 78-81 for bulk aqueous corrosion. Bulk planar surfaces, polished with 600 grit dry SiC paper were given various SO_2 treatments at 500°C and then corroded in triple distilled (3D) H_2O while maintaining a constant SA/V = 0.77 cm^{-1}.

The infrared reflection spectra for glasses exposed to 5 and 30 minute SO_2 treatments before the corrosion process are shown in Figures 78 and 79. In general, a new peak appears at $\sim$1100 cm^{-1} which is at the wavenumber position normally assigned to Si-O-Si stretch peak vibrations in pure vitreous silica. The other two peaks at $\sim$1050 cm^{-1} and $\sim$950 cm^{-1} are assigned to Si-O-Si and silicon non-bridging oxygen (NSL) bonds in an alkali environment. The appearance of this spectrum suggests the presence of a thin high-silica surface film much less than 0.5 μm thick (0.5 μm ≈ depth of IRRS analysis), underneath an alkali sulphate surface layer, in this case, lithium sulphate, and bulk glass below the silica rich layer, i.e., unreacted glass. Since a spectrum can be seen for

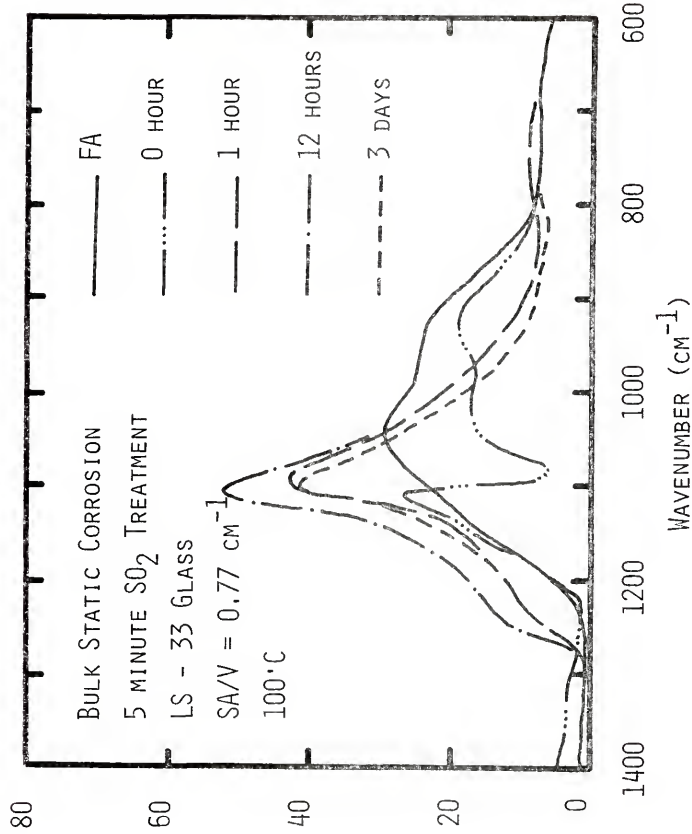

Figure 78. Infrared reflection spectra for bulk LS-33 glasses exposed to a 5 minute SO_2 treatment and corroded in triple-distilled water.

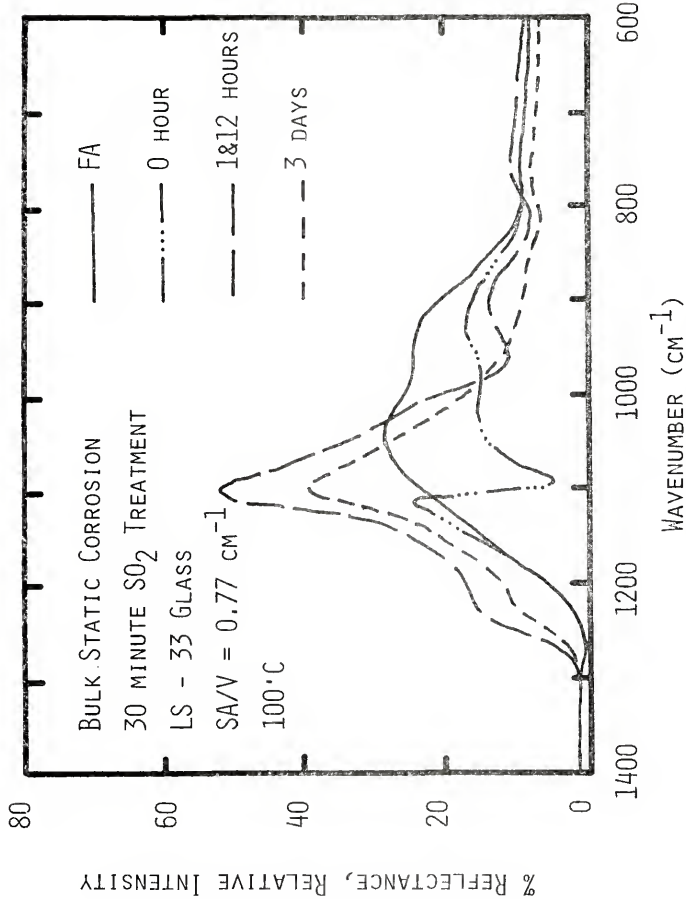

Figure 79. Infrared reflection spectra for bulk LS-33 glasses exposed to 0, 5, and 30 minute SO_2 treatments and corroded in triple-distilled water.

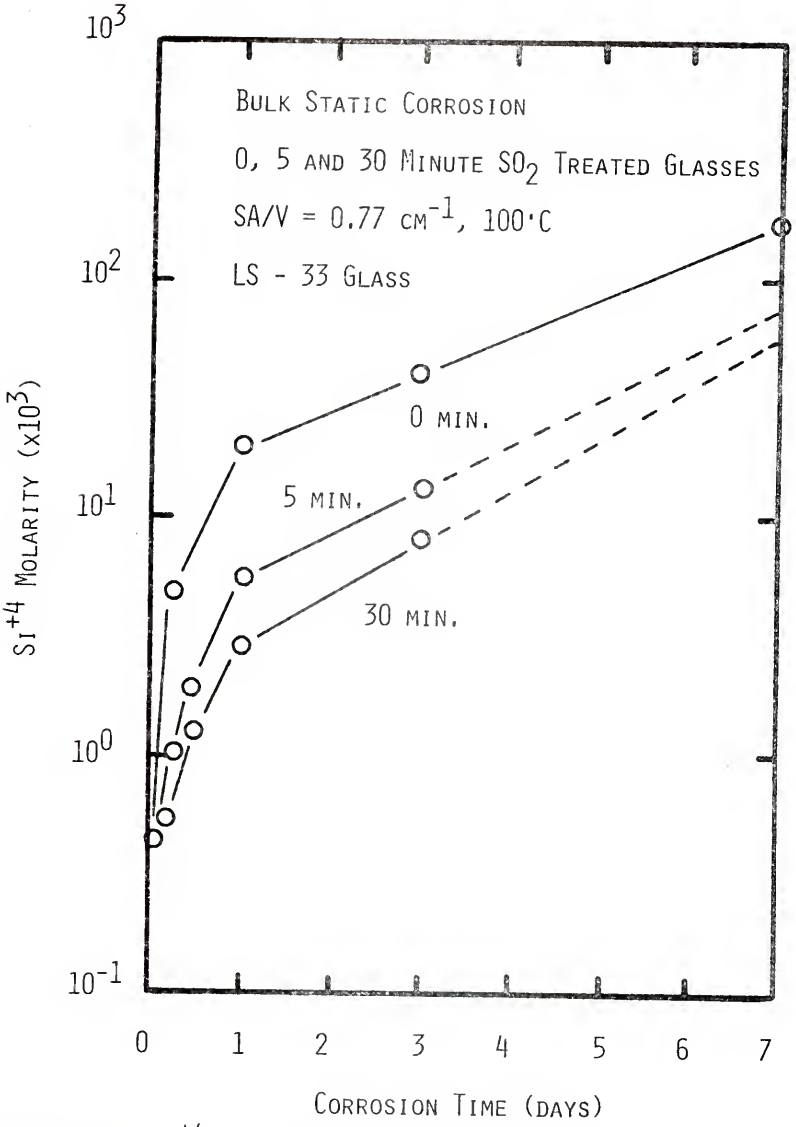

Figure 80. Si^{+4} solution data for bulk LS-33 glasses exposed to 0.5 and 30 minute SO_2 treatments and corroded in triple-distilled water.

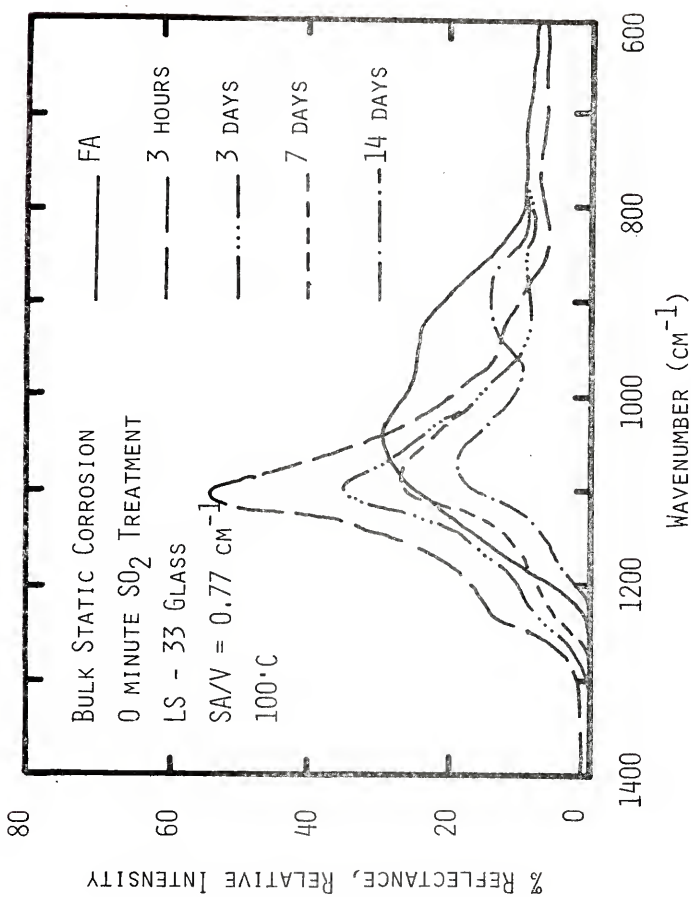

Figure 81. Infrared reflection spectra for bulk LS-33 glasses corroded in triple-distilled water.

the bulk underlying glass, apparently the two surface layers are sufficiently thin to allow IR beam penetration and reflection.

Corrosion of the SO_2 treated glasses was conducted in triple distilled H_2O at 100°C. No attempt was made to control the pH of the solution during the corrosion process. The Si^{+4} concentration was monitored as a function of corrosion time and various SO_2 treatments and plotted in Figure 80. There was a large reduction in Si^{+4} dissolution for the glasses with SO_2 treatments compared with that observed for non-SO_2 treated glass with a freshly abraded glass surface. From solution analysis, it is obvious that the 5 minute SO_2 treatment has the greatest effect on chemical durability with the 30 minute SO_2 treatment having less effect on improving durability. This reduction in Si^{+4} dissolution may be attributed to the silica rich layer formed on the glass surface during the SO_2 treatment process.

Infrared reflection spectroscopy (IRRS) spectra for the non-treated LS-33 glass is shown in Figure 81. There is a rapid increase in the Si-O-Si stretch peak ($\sim$1080 cm^{-1}) after 3 hours of corrosion, which decreases thereafter for 3 days, 7 days and finally reaches a minimum in spectral intensity after 14 days.

IRRS spectra for the glasses with the 5 minute SO_2 treatment are shown in Figure 78. From these spectra, the Si-O-Si stretch peak maximum is still present up to 12 hours of corrosion. Also the 5 minute SO_2 treatment results in the spectral intensity being considerably higher than that observed for the non-treated glass for the same 3 day time period.

IRRS spectra for the glasses with the 30 minute SO_2 treatment is shown in Figure 79. From these spectra, a maximum in the Si-O-Si stretch peak is attained after 1 hour of corrosion. The IRRS spectral amplitude after 3 days corrosion was observed to fall in the medium range between the 5 minute treatment and the non-treated glass.

Thus, the importance of SO_2 treatments upon improving the durability of even a binary alkali-silicate glass has been demonstrated. This increase in durability occurs mainly because of the dealkalization of the glass surface caused by the diffusion of lithium ions to the glass surface and their resulting reaction with the hot SO_2 furnace gases (Li_2SO_4). This reaction results in the formation of a high silica surface film which exhibits a high resistance to dissolution over that observed for the non-treated glass surface. This observation is supported both by solution ion analysis and IRRS results.

B. SO_2 Surface Treatments - 100% Relative Humidity Weathering

The deterioration of glass surfaces due to their interaction with the atmosphere is generally referred to as "weathering." According to Clark et al.,[28] weathering may be classified into two types: type I weathering, condensation-runoff, in which moisture collects on the glass surface until natural runoff occurs, carrying away the reaction products; and, type II weathering, condensation-evaporation, in which a thin layer of "fog" forms on the glass surface but evaporates before droplets form. Type I weathering is the most similar to the aqueous corrosion process discussed in the previous section. In both aqueous corrosion and type I weathering, dealkalization of the glass surface increases in solution pH, and removal of the reaction products can occur; however, these processes in type I weathering depend upon the cyclic condition of water droplet formation and eventual runoff.

SO_2 surface treatments result in surface dealkalization by formation of Li_2SO_4 and development of a high silica surface film. Since dealkalization is the initial corrosion reaction (for pH $\geq$ 9) in the weathering process of alkali silicate glasses,[28] it was the objective of this

investigation to determine the effects of SO_2 treatments on the weathering process and to compare these results with those obtained from aqueous corrosion.

The effects of time of 100% relative humidity weathering on a $Li_2O \cdot 2SiO_2$ glass (LS-33, Table VIII) given various SO_2 treatments are shown in Figures 82-84. Bulk planar surfaces, polished with 600 grit dry SiC paper were exposed to various SO_2 treatments at 500°C and then weathered in 100% relative humidity (RH) at 25°C (Figure 3). This particular experiment led to type I weathering. IRRS spectra for the non-treated 5 minute treatment, and 30 minute SO_2 treated samples before weathering are shown in Figure 82. IRRS spectral results for 20 days of 100% RH weathering at 25°C are shown in Figure 83. The non-treated glass surface exhibits the greatest degree of surface attack, with the 30 minute treatment yielding the highest durability and the 5 minute treatment intermediate. At 60 days of 100% RH weathering (Figure 84), again the non-treated sample exhibits the highest degree of surface attack. The larger Si-O-Si stretch peak amplitude and the greatly reduced amplitude of the non-bridging oxygen peak (NSL) indicates a high degree of surface dealkalization and formation of a silica rich surface film.[14,25,37] The IRRS spectra of the samples with 5 and

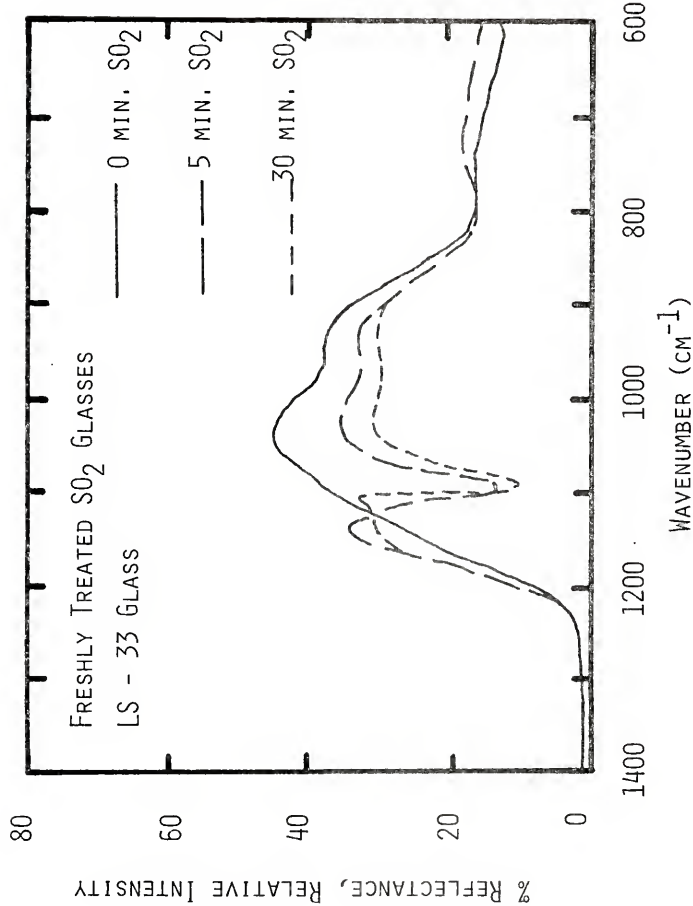

Figure 82. Infrared reflection spectra for bulk LS-33 glasses exposed to 0, 5 and 30 minute SO_2 treatment, prior to 100% relative humidity weathering.

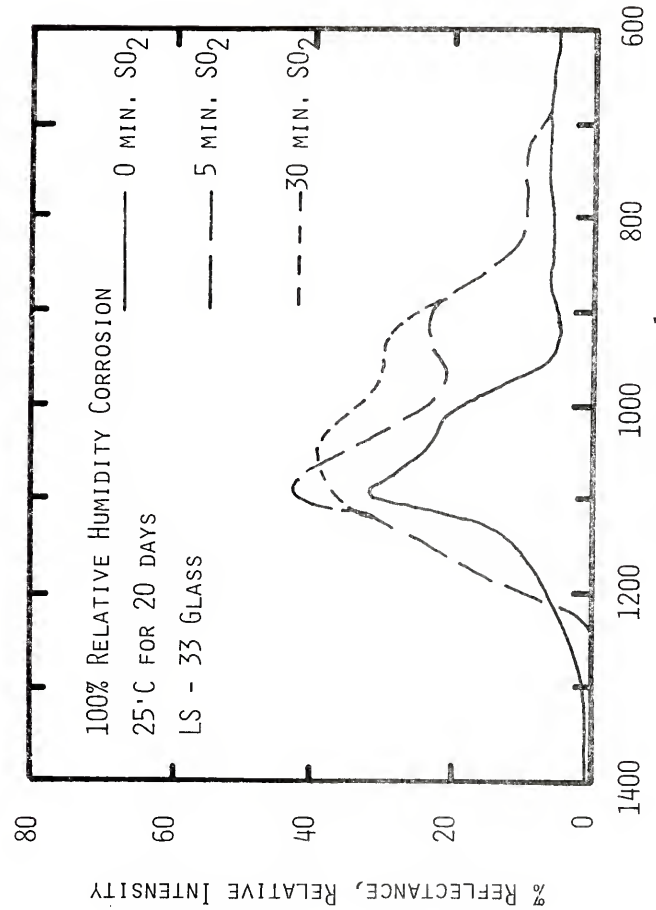

Figure 83. Infrared reflection spectra for bulk LS-33 glasses exposed to 0, 5 and 30 minute SO_2 treatments and weathered in a 100% relative humidity environment for 20 days.

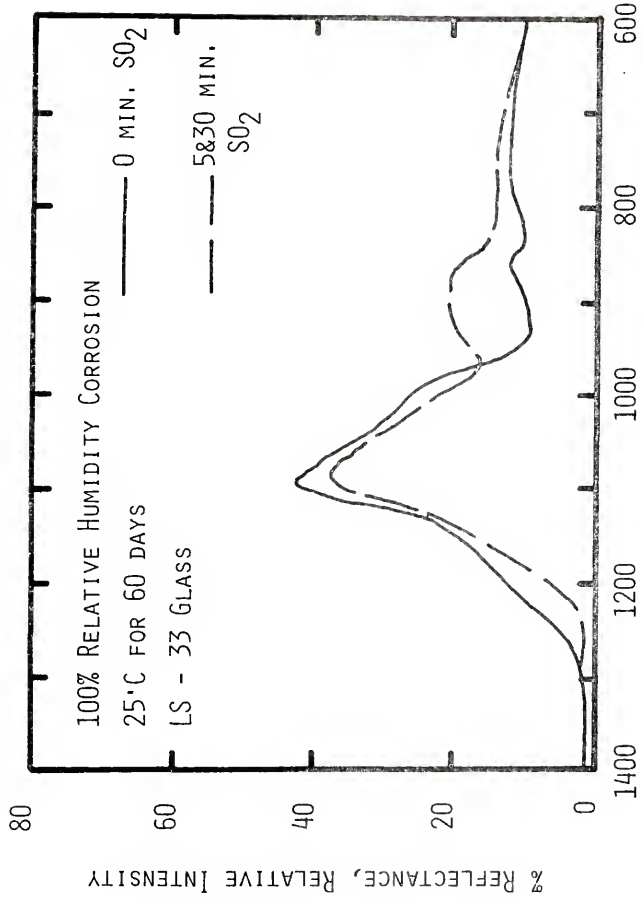

Figure 84. Infrared reflection spectra for bulk LS-33 glasses exposed to 0, 5 and 30 minute SO_2 treatments and weathered in a 100% relative humidity environment for 60 days.

30 minute treatments (Figure 84) indicate that the surface attack has not been as great as that observed for the non-treated sample. This is evidenced by the presence of a large NSL peak and the increasing Si-O-Si stretch peak.

Thus, the importance of SO_2 treatments on improving glass weathering characteristics has been shown from IRRS results. As was true in aqueous corrosion, this increase in durability is attributed to the dealkalization of the glass surface and the formation of a silica rich surface film. The 5 minute SO_2 treatment produced the largest increase in glass durability, the 30 minute SO_2 treatment improved durability, but to a lesser extent than that observed for the 5 minute treatment.

Conclusions

I. Time and Temperature

Two regions of corrosion were observed for the time and temperature "versus" alkali molarity plots, as evidenced by a change in the slope of the dissolution curves. The change-over from region I to region II occurs at approximately the same concentration of Na^+ regardless of the temperature utilized. In region I, selective leaching is the dominant form of glass corrosion ($pH \leq 9$). For region II, total dissolution is the dominant form of corrosion ($pH > 9$).

II. Glass Composition

Chemical durability is related to the degree of oxygen polarization (proportional to the percent of alkali ions). Therefore, as the size of the alkali ion present in the glass structure increases, the chemical durability decreases. Similarly, as the percent of alkali ions in the glass structure increases (increase in the overall polarization), the chemical durability decreases.

III. Effect of Glass Sample State on Corrosion

A rapid increase in glass dissolution was observed for glass powder corrosion (SA/V = 0.077, and 0.77 cm^{-1}) for periods of time less than 3 days. This was attributed to the following factors: (i) the dissolution of "fine" (<<100 mesh) particles attached to the -60+100 mesh particles; and, (ii) concentration cell effects which increase the corrosion kinetics of glass powders. For corrosion times of 3 to 14 days, both glass powder surface area to solution volume (0.077, 0.77 cm^{-1}) ratios and the bulk glass with a surface area to solution volume (0.77 cm^{-1}) ratio exhibit equal Si^{+4} dissolution rates. The equal dissolution rates observed for both bulk and powder surfaces is probably a result of the total dissolution of the "fine" particles associated with glass powders and attack of the abraded surface of the bulk glasses. From

glass powder corrosion, it was observed that as the SA/V ratio increases, the corrosion rate also increases. Also, the actual particle size utilized for evaluating glass corrosion does not appear to be important as long as the SA/V is held constant.

IV. Surface Roughness of Bulk Glasses

Comparison of the Si^{+4} solution data for the various SA/V ratios reveal that the extent of glass dissolution is directly proportional to the surface area of the glass exposed to the corrosion solution volume. The presence of cracks, scratches and sharp edges which can act as stress raisers have very little influence on the corrosion rate except to increase the SA/V ratio.

V. Effects of Solution Ions on Glass Durability

From α values (calculated from solution results), various salt compounds are listed in decreasing order of their ability to promote the ion-exchange reaction and prevent total dissolution: $CaCl_2$, $ZnCl_2$, $AlCl_3$, 3D-H_2O, and $CuCl_2$. Ca^{+2} ions in solution improve the corrosion resistance of $Li_2O{\cdot}2SiO_2$ glasses by a factor of 10 in comparison to 3D-H_2O.

VI. Buffered Corrosion Solutions

For buffered solutions of low pH (i.e., 5.4), selective leaching of a KS-25 glass is the primary mode of cor-

rosion. For buffered solutions of high pH (i.e., 9.4), total dissolution is the primary mode of corrosion. It was observed that for short periods of corrosion time, the 5.4 buffered solution slowed down the glass dissolution process. However, as the corrosion time increased (>9 hours), the 5.4 buffered solution was overridden and the total dissolution process therefore increased. For corrosion times >24 hours, the 3D-H_2O solution, the 5.4 buffered solution, and the 9.4 buffered solution all have equal total dissolution rates.

VII. SO_2 Surface Treatments

Comparison of aqueous corrosion and type I weathering indicate that SO_2 treatments improve the glass durability over non-treated LS-33 glass samples. This increase in durability has been attributed to the dealkalization of the glass surface and the formation of a silica-rich surface film. The 5 minute SO_2 treatment produces the largest increase in glass durability, and the 30 minute SO_2 treatment improved durability, but to a lesser extent than that observed for the 5 minute treatment.

REFERENCES

1. F. R. Bacon, "The Chemical Durability of Silicate Glass," Glass Industry, 49 (1968) 494-9, 554-9.

2. L. Holland, The Properties of Glass Surfaces, Chapman and Hall Co., London, England (1964).

3. W. A. Weyl and E. C. Marboe, The Constitution of Glasses: A Dynamic Interpretation, 3(2), John Wiley, Inc., New York (1967).

4. C. R. Das, "A Review of the Chemical Resistance of Glass," Trans. Indian Ceram. Soc., 24 (1965) 12-23, 34.

5. R. H. Doremus, Glass Science, John Wiley and Sons, New York, N.Y. (1973).

6. M. B. Volf, Technical Glasses, Sir Isaach Pitman and Sons, Ltd., London, England (1961).

7. G. W. Morey, The Properties of Glass, 2nd Ed., Reinhold Publishing Corp., New York, N.Y. (1954).

8. S. Tsuchihashi and E. Sekido, "On the Dissolution of Na_2O-CaO-SiO_2 Glass in Acid and in Water," Bull. Chem. Soc. Japan, 32(8) (1959) 868-872.

9. F. F. Wang and F. V. Tooley, "Influence of Reaction Products on Reaction Between Water and Soda-Lime-Silica Glass," J. Amer. Ceram. Soc., 91(12) (1958) 521-524.

10. F. R. Bacon and G. L. Calcamuggio, "Effect of Heat Treatment in Moist and Dry Atmospheres on Chemical Durability of Soda-Lime Glass Bottles," Amer. Ceram. Soc. Bull., 46(9) (1967) 850-855.

11. R. W. Douglas and T. M. M. El-Shamy, "Reaction of Glasses with Aqueous Solutions," J. Amer. Ceram. Soc., 50(1) (1967) 1-8.

12. Yu. A. Shmidt, "Structure of Glass," Consultants Bureau, New York, N.Y., 1 (1958) 253-254.

13. D. M. Sanders and L. L. Hench, "Mechanisms of Glass Corrosion," J. Amer. Ceram. Soc., 56(7) (1973) 373-377.

14. L. L. Hench, "Characterization of Glass Corrosion and Durability," J. Non-Crystalline Solids, 19 (1975) 27.39.

15. D. M. Sanders, "Structure and Kinetics of Glass Corrosion," Ph.D. Dissertation, University of Florida, Gainesville, Florida (1973).

16. C. G. Pantano, Jr., "Compositional Analysis of Glass Surfaces and Their Relation in Aqueous Environments," Ph.D. Dissertation, University of Florida, Gainesville, Florida (1976).

17. W. A. Weyl and E. C. Marboe, "The Constitution of Glasses: A Dynamic Interpretation," Vol. II, Part 1, John Wiley and Sons, New York, N.Y. (1967).

18. L. S. Yastrebova and N. L. Antonova, "Nature of the Two Alkali Effect in Silicate Glass," Izv. Acad. Nauk. SSSR, Neorganicheski Materialy, 3(2) (1967) 374-380.

19. C. J. Peddle, XVII. The Development of Various Types of Glasses, Part XI, "The Effect of the Joint Presence of Sodium and Potassium," J. Soc. Glass Technol., 4 (1920) 59-70T; Ceram. Abstracts, 3(8) (1920) 681-683.

20. C. J. Peddle, XX. The Development of Various Types of Glasses, Part XIV, "The Interaction of Silica, Barium Oxide, and the Oxides of Sodium and Potassium," J. Soc. Glass Technol., 4 (1920) 71-107T; Ceram. Abstracts, 3(8) (1920) 681-683.

21. S. Sen and F. V. Tooley, "Effect of Na_2O/K_2O Ratio on the Chemical Durability of Alkali-Lime Silica Glasses," J. Amer. Ceram. Soc., 38(5) (1955) 175-177.

22. J. O. Isard, "The Mixed Alkali Effect in Glass," J. of Non-Crystalline Solids, 1 (1969) 235-261.

23. R. J. Charles, "The Mixed Alkali Effect in Glasses," J. Amer. Ceram. Soc., 48(8) (1965) 432-434.

24. T. M. M. El-Shamy, J. Lewis and R. W. Douglas, "The Dependence on the pH of the Decomposition of Glasses by Aqueous Solutions," Glass Technol., 13(3) (1972) 81-87.

25. M. F. Dilmore, D. E. Clark and L. L. Hench, "Aqueous Corrosion of Mixed-Alkali Lime Silicate Glasses," to be published.

26. D. M. Sanders, W. B. Person and L. L. Hench., "New Methods for Studying Glass Corrosion Kinetics," Applied Spectroscopy, 26(5) (1972) 530-536.

27. Report of Committee on Chemical Durability of Glasses, Bull. Amer. Ceram. Soc., 14(5) (1935) 181-184.

28. D. E. Clark, "A Durability Evaluation of Soda-Lime-Silica Glasses Using Electron Microprobe Analysis, Infrared Reflection Spectroscopy and Other Techniques," Ph.D. Dissertation, University of Florida, Gainesville, Florida (1976).

29. J. R. Hendrickson and P. J. Bray, "A Theory for the Mixed-Alkali Effect in Glass: Part I," Phys. and Chem. of Glasses, 13(2) (1972) 43-49.

30. J. R. Hendrickson and P. J. Bray, "A Theory for the Mixed-Alkali Effect in Glass: Part II," Phys. and Chem. of Glasses," 13(4) (1972) 107-115.

31. R. M. Hakin and D. R. Uhlmann, "On the Mixed-Alkali Effect in Glasses," Phys. and Chem. of Glasses, 8(5) (1967) 174-177.

32. R. Hayami and R. Terai, "Diffusion of Alkali Ions in Na_2O-Cs_2O-SiO_2 Glasses," Phys. and Chem. of Glasses, 13(4) (1972) 102-106.

33. R. Terai, "The Mixed-Alkali Effect in the Na_2O-Cs_2O-SiO_2 Glasses," J. of Non-Crystalline Solids, 6 (1971) 121-135.

34. D. E. Day, "Mixed Alkali Glasses - Their Properties and Uses," to be published.

35. L. L. Hench and H. F. Schaake, "Electrical Properties of Glasses," Introduction in Glass Science (D. Dye and H. Simpson, eds.), Plenum Press, New York, N.Y., (1972) 583-661.

36. D. E. Clark, E. C. Ethridge, M. F. Dilmore and L. L. Hench, "Quantitative Analysis of Corroded Glass Using IRRS Frequency Shifts," accepted for publication in Glass Technol., Feb. 1977.

37. W. A. Weyl and E. C. Marboe, The Constitution of Glasses: A Dynamic Interpretation, Vol. II, Part 2, John Wiley and Sons, Inc., New York, N.Y. (1967).

38. M. A. Rana and R. W. Douglas, "The Reaction Between Glass and Water; Part 2 - Discussion of the Results," Phys. and Chem. of Glasses, 2(6) (1961) 196-205.

39. E. C. Ethridge, "Mechanisms and Kinetics of Binary Alkali Silicate Glass Corrosion," Ph.D. Dissertation, University of Florida, Gainesville, Florida (1977).

40. D. E. Clark, M. F. Dilmore, E. C. Ethridge and L. L. Hench, "Aqueous Corrosion of Soda-Silica and Soad-Lime-Silica Glass," J. Amer. Ceram. Soc., 59(1-2) (1976) 62-65.

41. V. Dimbleby and W. E. S. Turner, "The Relationship Between Chemical Composition and Resistance of Glasses to the Action of Chemical Reagents," Glass Technol., 10 (1926) 304-363.

42. J. Enss, "An Investigation of the Dependence of Water Attack of Glass on Its Chemical Composition," Glastechn., Ber. 5(10) (1928) 449; 5(11) (1928) 509.

43. Yu. A. Shmidt, "Reactions of Vitreous Lithium Alumino Silicates with Water," Zh. Prikl. Khim., 33(3) (1960) 536-540.

44. Yu. A. Shmidt, "Reactions with Water of Lithium Alumino Silicates and Comparison of them with Sodium Silicates," Zh. Prikl. Khim., 33(2) (1960) 266-273.

45. J. O. Isard, "Electrical Conduction in Aluminao Silicate Glasses," Glass Technol., 43(211) (1959) 113-T.

46. R. J. Charles, "Static Fatigue of Glass: I," J. Appl. Phys., 29(11) (1958) 1549-1553.

47. S. K. Dubrovo, "Decomposition by Aqueous Solutions of Nitreous Silicates and Sodium Alumina Silicates in Dependence on the State of the Silica in the Glass," Trudy Soveshch. Po Stroeniya Stekla (1953); Iz. Ak. Nauk. SSSR, (1955) 181-184.

48. T. M. M. El-Shamy and S. E. Morsi, "Chemical Durability of Na_2O-Al_2O_3-SiO_2 Glasses in Relation to Their Membrane Potentials," J. Non-Crystalline Solids, 19 (1975) 201-211.

49. S. K. Dubrove, "Reactions of Vitreous Silicates with Aqueous Solutions, Part IV - Reaction of Vitreous Sodium Alumino Silicates with Acid Solutions," Izv. Adac. Nauk. SSSR, Otd. Khim. Nauk., 5 (1954) 770-777.

50. B. E. Yoldos, "The Nature of the Co-existence of 4- and 6-fold Co-ordinated Al^{+3} in Glass," Phys. and Chem. of Glasses, 12(1) (1971) 28-32.

51. E. D. Lacy, "Aluminum in Glasses and in Melts," Phys. and Chem. of Glasses, 4(6) (1963) 234-238.

52. D. E. Day and G. E. Rindone, "Properties of Soda Aluminosilicate Glass: I. Refractive Index, Density, Molar Refractivity, and Infrared Absorption Spectra," J. Amer. Ceram. Soc., 45(10) (1962) 579-581.

53. M. A. Rana and R. W. Douglas, "The Reaction Between Glass and Water; Part 2 - Discussion of the Results," Phys. and Chem. of Glasses, 2(6) (1961) 196-205.

54. V. V. Vargin and V. E. Mishel, "Acid Resistance of Glasses in the High Silica Region of the System R_2O-Al_2O_3-SiO_2," Consultants Bureau, New York, N.Y. (1971).

55. J. A. Savage and J. O. Isard, "An Investigation of the Electrode Properties of Some Cation Sensitive Glasses," Phys. and Chem. of Glasses, 3(5) (1962) 147-156.

56. J. A. Savage and J. O. Isard, "Additional Studies of Cation Sensitive Glass Electrodes," Phys. and Chem. of Glasses, 7(2) (1966) 60-67.

57. S. K. Dubrovo, "Reaction of Nitreous Silicates and Sodium Aluminosilicates with Aqueous Solutions; Part III - Influence of the Silica and Alumina Content in the Composition of Sodium Silicates on Their Corrosion Ability in Acids," Izv. Akad. Nauk. SSSR, Otd. Khim. Nauk., 2 (1954) 244.

58. C. R. Das, "Theoretical Aspects of the Corrosion of Glass," The Glass Industry, 50 (1969) 422-427.

59. C. R. Das and R. W. Douglas, "Studies on the Reaction Between Water and Glass, Part 3," Phys. and Chem. of Glasses, 8(5) (1967) 178-184.

60. G. A. Hudson and F. R. Bacon, "Inhibition of Alkaline Attack on Soda-Lime Glass," Bull. Amer. Ceram. Soc., 37(4) (1958) 185-188.

61. V. S. Molchanov and N. E. Prikhid'ko, "Corrosion of Silicate Glasses by Alkaline Solution: Inhibitors of the Alkaline Corrosion of Glasses," Izv. Akad. Nauk. SSSR, Otd. Khim. Nauk., 7 (1958) 801-807.

62. K. C. Lyon, "Effect of Rinsing on Chemical Durability of a Container Glass," J. Amer. Ceram. Soc., 32(2) (1949) 46-48.

63. H. R. Persson, "Improvement of the Chemical Durability of Soda-Lime-Silicate Glass Bottles by Treating with Various Agents," Glass Technol., 3(1) (1962) 17-35.

64. R. K. Iller, "Effect of Adsorbed Alumina on the Solubility of Amorphous Silica in Water," J. Colloid and Interface Science, 43(2) (1973) 399-408.

65. W. Geffeken, "Chemical Attack of Glass by Alkaline Liquids and the Effect of Soluble Ions on its Action: I," Kolloid-Z., 8 (1939) 11-15; Ceram. Abstracts, 23(5) (1944) 86.

66. W. A. Weyl, "Some Practical Aspects of the Surface Chemistry of Glass: IV," Glass Industry, 28(8) (1947) 408-412, 428-432; Ceram. Abstracts, (1948) 127.

67. G. Y. Onoda, Personal Communication, University of Florida, Gainesville, Florida.

68. R. W. Douglas and J. O. Isard, "The Action of Water and Sulphur Dioxide on Glass Surfaces," J. Soc. Glass Tech., 33 (1949) 288-334.

69. T. M. M. El-Shamy and R. W. Douglas, "Kinetics of the Reaction of Water with Glass," Glass Technol., 13(3) (1972) 77-80.

70. R. J. Charles, "Dissolution Behavior of Microporous Glass," J. Amer. Ceram. Soc., 47(3) (1967) 154.

71. G. S. Khodakov, Uspeckhi Khim., 32(7) (1963) 860.

72. D. M. Sanders and L. L. Hench, "Surface Roughness and Glass Corrosion," Amer. Ceram. Soc. Bull., 52(9) (1973) 666-669.

73. R. E. Mould and R. D. Southwick, "Strength and Static Fatigue of Abraded Glass Under Controlled Ambient Condition: II," J. Amer. Ceram. Soc., 42(12) (1959) 582-592.

74. S. M. Wiederhorn, "Stress Corrosion and Static Fatigue of Glass," J. Amer. Ceram. Soc., 53(10) (1970) 543-548.

75. R. E. Mould, in Fundamental Phenomena in the Materials Sciences, Vol. 4 (L. J. Bonis, J. J. Duga, and J. J. Gilman, eds.), Plenum Publishing Corp., New York, N.Y. (1967).

76. S. P. Colowick and N. O. Kaplan, eds., Methods in Enzymology, Vol. 1, Academic Press, Inc., New York, N.Y. (1955).

77. A. E. Clark, Jr., "Solubility and Biocompatibility of Glass," Ph.D. Dissertation, University of Florida, Gainesville, Florida (1975).

78. H. Loeber, Sprechsaal, 61 (1928) 160-162, 181-183.

79. F. R. Bacon and S. W. Barber, "The Chemical Durability of Sulfur-Treated Bottles," Technical Bulletin, Owens-Illinois, Toledo, Ohio (1948).

80. J. N. Coward and W. E. S. Turner, Glass Technol., 22 (1938) 309.

81. H. S. Williams and W. A. Weyl, "Surface Dealkalization of Finished Glassware, Part I," Glass Industry, 26 (1945) 324-326, 339, 341-344.

BIOGRAPHICAL SKETCH

Morris Franklin Dilmore was born on January 9, 1948 in Crestview, Florida. He received his elementary education at Escambia Farms (High) School and graduated in 1966 from Baker High School. After receiving an Associates of Art Degree from Okaloosa Walton Junior College in 1968, he transferred to the Materials Science and Engineering Department of the University of Florida, earning a Bachelor of Science Degree in 1971 and a Master of Engineering Degree in 1975. Since then, he has been pursuing a Doctor of Philosophy Degree.

While at school, he married the former Katrina Yvonne Goodwin of Key West, Florida.

He is a member of the American Institute of Metallurgical Engineers (AIME), the American Society of Metals (ASM), the American Ceramic Society (ACS), and the Ceramic Honorary Society, Keramos.

I certify that I have read this study and that in my opinion it conforms to acceptable standards of scholarly presentation and is fully adequate, in scope and quality, as a dissertation for the degree of Doctor of Philosophy.

L. L. Hench, Chairman
Professor of Materials Science and Engineering

I certify that I have read this study and that in my opinion it conforms to acceptable standards of scholarly presentation and is fully adequate, in scope and quality, as a dissertation for the degree of Doctor of Philosophy.

G. Y. Onoda, Jr.
Associate Professor of Materials Science and Engineering

I certify that I have read this study and that in my opinion it conforms to acceptable standards of scholarly presentation and is fully adequate, in scope and quality, as a dissertation for the degree of Doctor of Philosophy.

R. E. Loehman
Associate Professor of Materials Science and Engineering

I certify that I have read this study and that in my opinion it conforms to acceptable standards of scholarly presentation and is fully adequate, in scope and quality, as a dissertation for the degree of Doctor of Philosophy.

D. O. Shah
Professor of Chemical Engineering

This dissertation was submitted to the Dean of the College of Engineering and to the Graduate Council, and was accepted as partial fulfillment of the requirements for the degree of Doctor of Philosophy.

March, 1977

Dean, College of Engineering

Dean, Graduate School